DISCLAIMER

This report was prepared as an account of work sponsored by an agency of the United States Government. Neither the United States Government nor any agency thereof, nor any of their employees, makes any warranty, express or implied, or assumes any legal liability or responsibility for the accuracy, completeness, or usefulness of any information, apparatus, product, or process disclosed, or represents that its use would not infringe privately owned rights. Reference herein to any specific commercial product, process, or service by trade name, trademark, manufacturer, or otherwise does not necessarily constitute or imply its endorsement, recommendation, or favoring by the United States Government or any agency thereof. The views and opinions of authors expressed herein do not necessarily state or reflect those of the United States Government or any agency thereof. Reference herein to any social initiative (including but not limited to Diversity, Equity, and Inclusion (DEI); Community Benefits Plans (CBP); Justice 40; etc.) is made by the Author independent of any current requirement by the United States Government and does not constitute or imply endorsement, recommendation, or support by the United States Government or any agency thereof.

Sandia National Laboratories

Operated for the U.S. Department of Energy by
National Technology and Engineering Solutions of Sandia, LLC
Albuquerque, New Mexico 87185-0405
Livermore, California 94551-0969

Date: 7 April 2025

To: Michelle Gallegos, Organization 02932
Michael Hansen, Organization 02932
Kevin Schafer, Organization 02932
Philip Wang, Organization 02932

From: Neal B. Hubbard, Organization 01554

Subject: Statistical Precision Intervals on Energy Required to Puncture AISI 304L VAR Steel Bar

Executive Summary

Specimens of AISI 304L VAR steel are punctured with AISI 4340 steel probes in a series of drop-table experiments. The times when the probe contacts the specimen and when it breaks through are indicated by the acceleration of the drop-table carriage. The change in the total energy of the carriage between these times is the energy mitigated by each specimen. Precision intervals bounding the energy mitigation provided by the specimens are derived by classical statistical inference. The lower bounds are reasonable because a sufficient number of replications are performed. The adequacy of making predictions about future observations from the population of all possible specimens of identical manufacture based on the normal, log-normal, Weibull, or gamma distribution are evaluated by standard techniques. The normal distribution is considered to fit the mitigated energy data, and the lower bounds in the table below are calculated with it. As an alternative to the statistics, a safety factor of 1.5 may be applied to the sample mean, resulting in a threshold mitigated energy of 21.7 ft-lb.

Table 1: Statistics of Energy Mitigated by 0.063-Inch-Thick Specimens of AISI 304L VAR Steel Punctured by 0.25-Inch-Diameter Flat-End Probe

Statistic	Mitigated Energy
Mean	32.5 ft-lb
Standard Deviation	1.8 ft-lb
Median, 50%	31.7 ft-lb
Lower Bound, 1%	25.9 ft-lb
Lower Bound, 1E-3	24.0 ft-lb
Lower Bound, 1E-6	19.8 ft-lb
Lower Bound, 1E-9	16.7 ft-lb

Introduction

Robert Waymel performed a series of experiments on a drop table to measure the energy mitigated by American Iron and Steel Institute (AISI) type 304L vacuum arc remelted (VAR) steel as a projectile passed through it (Ref. 1). Specimens were machined from bar stock that was sliced with the wire in an electrical discharge machine (EDM). The natural surface finish left by the EDM was preserved to give the specimens a texture representative of actual components. Cracks nucleate at flaws in the material, and a normal quantity of flaws produces characteristic performance. Polished specimens would likely have mitigated more energy but would have been unrealistic for comparison to cast or machined housings, covers, and containers. The interior features of the specimens were produced by milling operations, as many actual components are.

The disc specimen shown in Figure 1 has a pocket where the thickness is reduced to 1.60 mm (0.063 in) so that a projectile can easily penetrate. The thick rim constrains the thin portion, giving it a fixed boundary condition around the circular perimeter. The reaction forces at the boundary pull downward and radially inward on the rim and tend to curl it such that the outer edges lift off of the fixture. The rim is designed to minimize this deformation. The probes are straight cylinders turned from AISI 4340 steel bars and hardened to 42–48 Rockwell C hardness (HRC). Figure 2 gives the dimensions in inches.

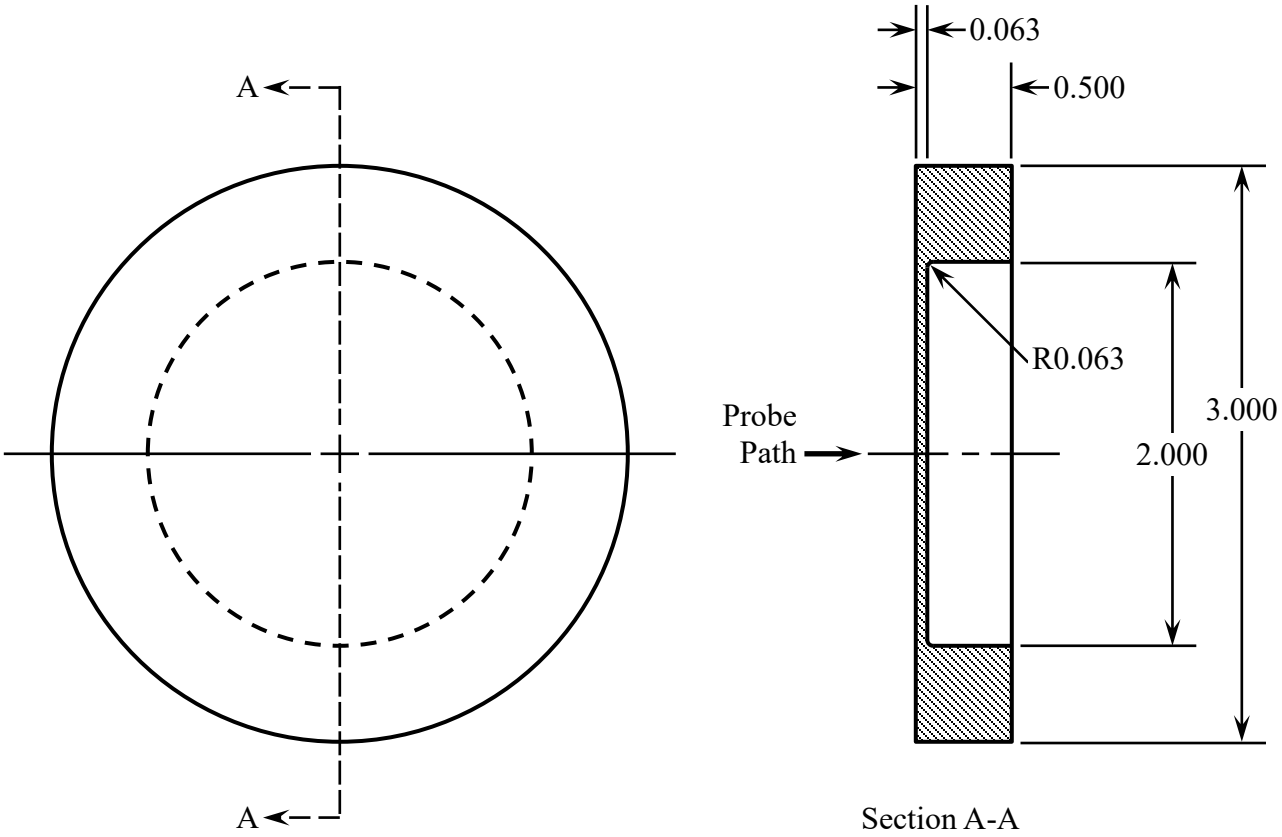

Figure 1: AISI 304L VAR Disc Specimen with Thickness of 0.063 Inch

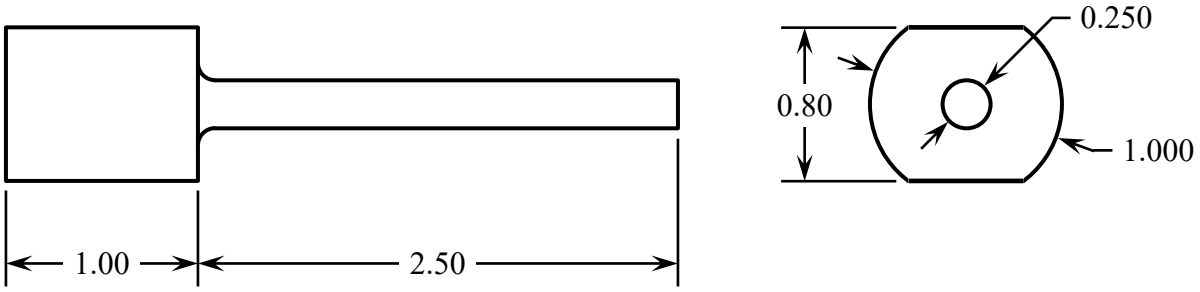

Figure 2: Cylindrical Probe with Diameter of 0.250 Inch and Flat End

The drop table has a 1370 N (308 lb) carriage that guides the probe along a straight path intersecting the specimen. The specimens are held in fixtures that constrain them against being pushed by the probe and resist lateral motion after a little clearance is removed. The specimens are free to lift off of the fixture and deform. Two laser interferometers measure the position of the carriage, and an accelerometer on the carriage measures the resistance to the falling mass. When the carriage is released from a planned height, the acceleration drops from 1 G to between 0.40 G and 0.70 G; friction in the guide rods prevents free-fall, and they are lubricated regularly to minimize it. Data collection begins as the probe approaches the specimen. Upon contact, an elastic wave travels through the probe to the carriage and registers an increase in the acceleration (resistance to gravity). The acceleration rises to about 8 G as the steel work hardens and drops off quickly after it reaches the ultimate stress and the specimen fractures. The peak acceleration indicates the maximum force required to puncture the specimen, after which the probe passes through a hole in the fixture, and the carriage settles onto felt programming rings. The data of interest are collected before the carriage contacts the rings.

As the probe punctured each specimen, it formed a circular plug. Many of the plugs adhered to the end of the probe. Following each test, the specimen clamped onto the probe and was lifted when the carriage raised to the reset position. A few broken specimens appear in the figures below.

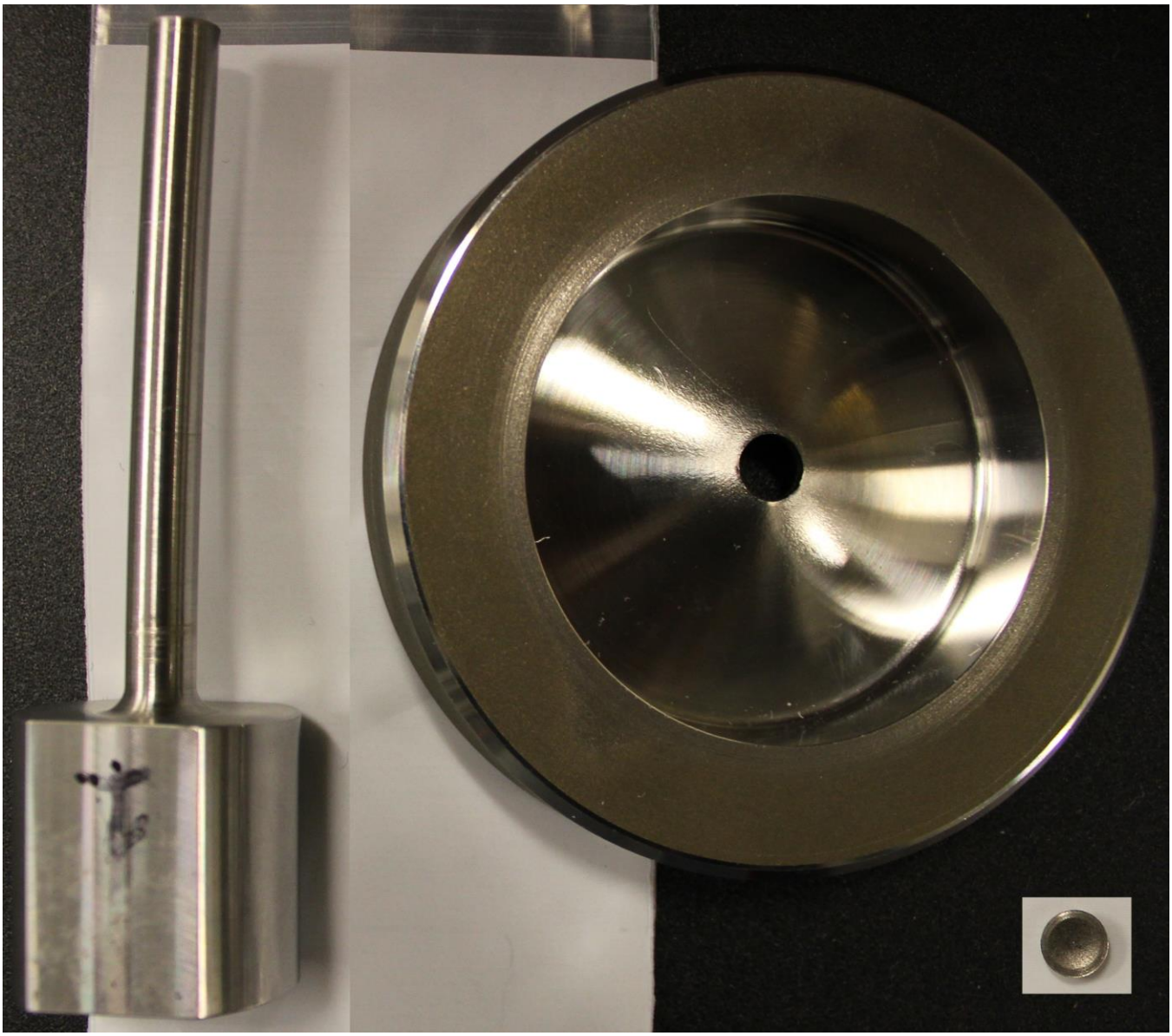

Figure 3: Probe, Specimen 1, and Ejected Plug After Test 7

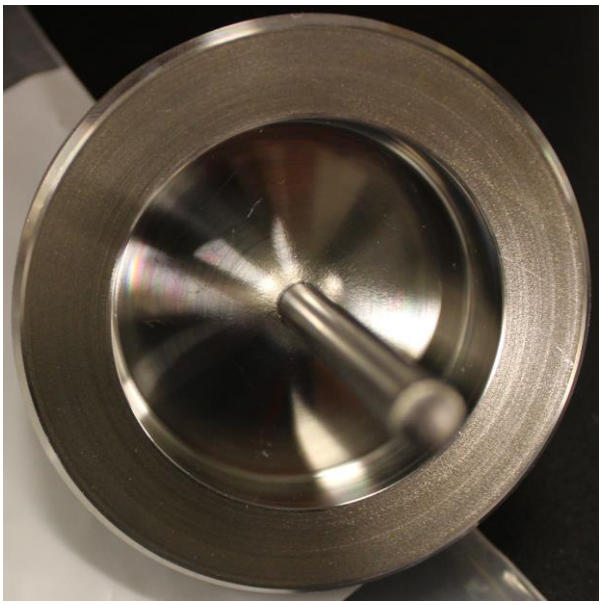

(a) Specimen 3 After Test 8, Plug Fused to Probe

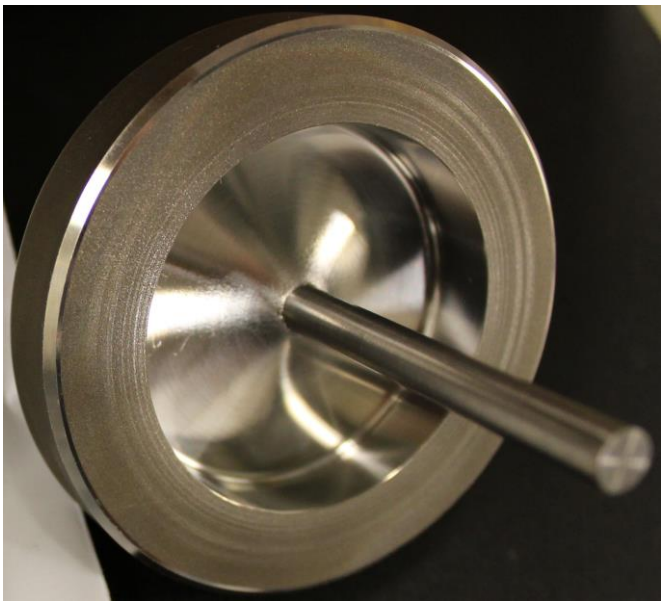

(b) Specimen 7 After Test 14, Plug Ejected

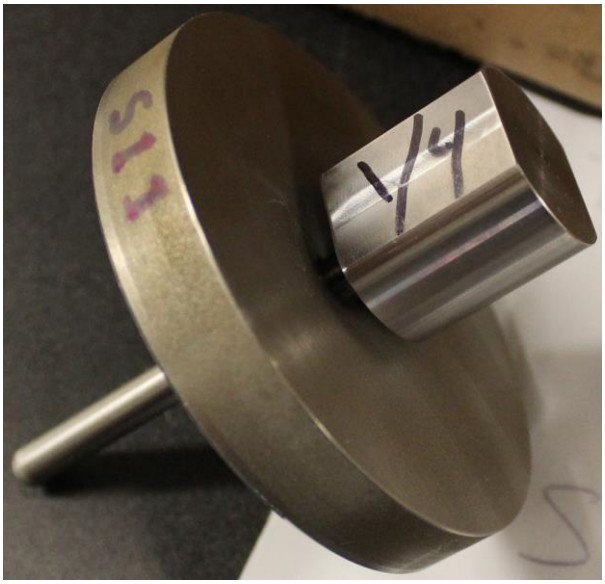

(c) Specimen 11 After Test 18, Top Surface

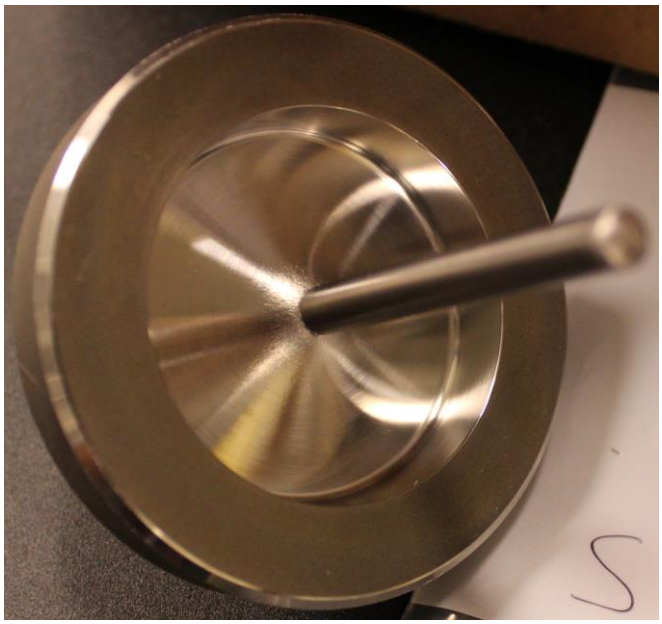

(d) Specimen 23 After Test 30, Bottom Surface

Figure 4: Probes Impaled In Specimens After Tests

The sample size is large enough to apply classical statistical inference techniques and obtain positive energy values at the customary 95% confidence. The Student's t distribution fits small samples from normally distributed populations. As the number of specimens in a sample approaches 30, the two-tailed Student's t distribution converges to the normal distribution within 5%. Given the available stock material and testing budget, a sample size of 24 was selected, for which the Student's t distribution only applies a slight penalty. All of the specimens were machined to the same specifications from the same stock material, and all were tested in the same fixtures and at approximately the same impact velocity. The specimens in the sample are considered independent but identically distributed.

Data Processing Method

The times when the probe contacts the specimen and penetrates it are determined from the acceleration data. A threshold acceleration (a_t) of 0.4 G is selected for all of the tests. Impact is considered to occur at the last time (t_i) when the acceleration is less than the threshold prior to the peak acceleration (a_p), and the puncture is considered complete at the last time (t_p) when the acceleration is greater than the threshold after the peak. Figure 5 illustrates these accelerations and times. The figures in Appendix A show the acceleration data for each test with the thresholds for impact and complete puncture.

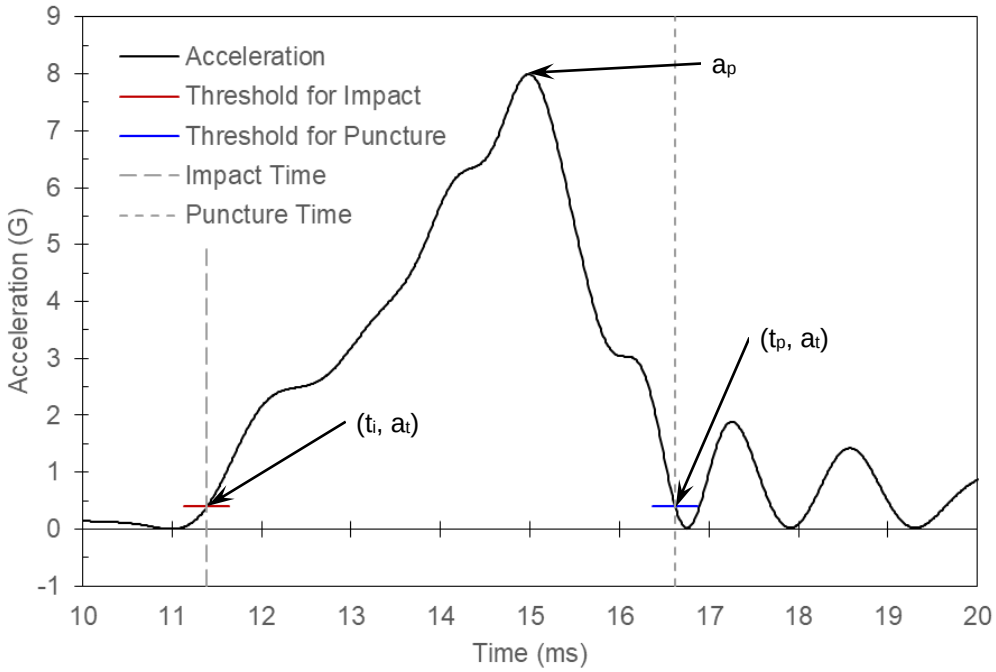

Figure 5: Representative Acceleration Curve with Impact and Puncture Times Identified

Although the threshold acceleration is constant, other processing parameters differ between tests. Table 2 lists these optimized parameters. Although consistency in the processing parameters has been preferred, these values are customized to the data and cannot be the same for every test.

Table 2: Data Processing Parameters

Test	Specimen	Acceleration		Puncture Time		Reference Position, p_r	
		Free-Fall, a_f (G)	Peak, a_p (G)	Offset, $\Delta t_{o,p}$ (ms)	Period, $\Delta t_{E,p}$ (ms)	(mm)	(in)
7	1	0.455	8.12	0.60	2.20	-7.55	-0.297
10	2	0.396	8.03	0.10	2.30	-7.62	-0.300
8	3	0.484	8.06	0.30	2.20	-7.61	-0.299
11	4	0.466	7.98	0.40	2.10	-8.02	-0.316
12	5	0.433	8.15	0.20	2.20	-7.66	-0.302
13	6	0.452	8.01	0.70	2.50	-8.59	-0.338
14	7	0.571	8.17	0.25	2.10	-8.02	-0.316
15	8	0.536	7.76	0.10	2.10	-7.55	-0.297
16	9	0.539	7.99	0.40	2.00	-8.17	-0.322
17	10	0.446	7.89	0.25	2.20	-7.77	-0.306
18	11	0.458	7.89	0.50	2.00	-8.35	-0.329
19	12	0.444	8.02	0.40	2.00	-8.05	-0.317
20	13	0.487	7.99	0.40	2.00	-8.14	-0.320
21	14	0.508	8.09	0.10	2.20	-7.62	-0.300
22	15	0.511	7.83	0.10	2.10	-7.54	-0.297
23	16	0.510	7.99	0.30	2.10	-8.01	-0.315
24	17	0.510	8.15	0.40	2.40	-7.21	-0.284
25	18	0.542	8.29	0.25	2.20	-8.10	-0.319
26	19	0.539	8.13	0.10	2.40	-7.58	-0.299
27	20	0.588	8.21	0.15	2.20	-7.63	-0.300
28	21	0.665	8.07	0.10	2.30	-7.58	-0.299
29	22	0.695	7.91	0.40	2.00	-8.26	-0.325
30	23	0.438	8.29	0.10	2.30	-7.84	-0.309
31	24	0.438	8.10	0.80	2.20	-9.40	-0.370

The position data from the two laser interferometers (p_L on the left and p_R on the right) are averaged and shifted with Equation 1. The reference position (p_r) is selected such that the position is zero when the puncture process is complete (t_p). The reference position also makes the potential energy (E_P, Eq. 2) positive when the probe contacts the specimen and zero when it breaks through. The mass (m) of the carriage with the attached mounting fixtures, accelerometer, and probe is 139.7 kg (9.57 slug). The free-fall acceleration of the carriage (a_f) is calibrated to correspond to a free-fall condition prior to the time of impact, accounting for friction in the guide rods, and is explained subsequently.

$$p = \frac{p_L + p_R}{2} - p_r \tag{1}$$

$$E_P = m\, a_f\, p \tag{2}$$

The average carriage position is differentiated to obtain the carriage velocity (v, Eq. 3). For each time in the data set, the velocity value (v_j) is given by Equation 4, where j is the index of the data points. The majority of the velocity values are computed with the second-order central finite difference formula; the first and last velocity values are evaluated with first-order finite difference formulas based on the available data points. The kinetic energy of the carriage and probe is defined by Equation 5 and the total energy by Equation 6.

$$v = \frac{dp}{dt} \tag{3}$$

$$v_j = \begin{cases} \dfrac{p_{j+1} - p_j}{t_{j+1} - t_j} & j = 1 \\ \dfrac{p_{j+1} - p_{j-1}}{t_{j+1} - t_{j-1}} & j = 2 \ldots n - 1 \\ \dfrac{p_j - p_{j-1}}{t_j - t_{j-1}} & j = n \end{cases} \tag{4}$$

$$E_K = \frac{m\, v^2}{2} \tag{5}$$

$$E_T = E_P + E_K \tag{6}$$

The free-fall acceleration of the carriage is optimized such that a linear fit to the total energy during a certain period of time prior to the probe contacting the specimen has zero slope. Table 2 gives the optimal values. This calibrates the data to a true free-fall condition prior to the time of impact. It correctly accounts for friction in the carriage guide rods and the increase in potential energy as the carriage falls through the specimen. The time period spans 10 ms ($\Delta t_{E,i}$) and ends 0.3 ms ($\Delta t_{o,i}$) before the impact time (t_i); during this period, several complete cycles of oscillation are observed in the total energy. The average of the total energy in this period is taken as the total energy before impact ($E_{T,i}$). The total energy after complete puncture ($E_{T,p}$) is the average value in a period of time beginning about 0.3 ms ($\Delta t_{o,p}$) after the puncture time (t_p) and lasting about 2 ms ($\Delta t_{E,p}$). Table 2 has the actual values of the time offset and period for each test. The total energy mitigated by the specimen is

$$E_M = E_{T,i} - E_{T,p} \tag{7}$$

Figure 6 illustrates the time periods over which the total energy is averaged and the difference between the averages. The figures in Appendix B plot the total energy as a function of time and bracket the time periods that are averaged before impact and after complete puncture.

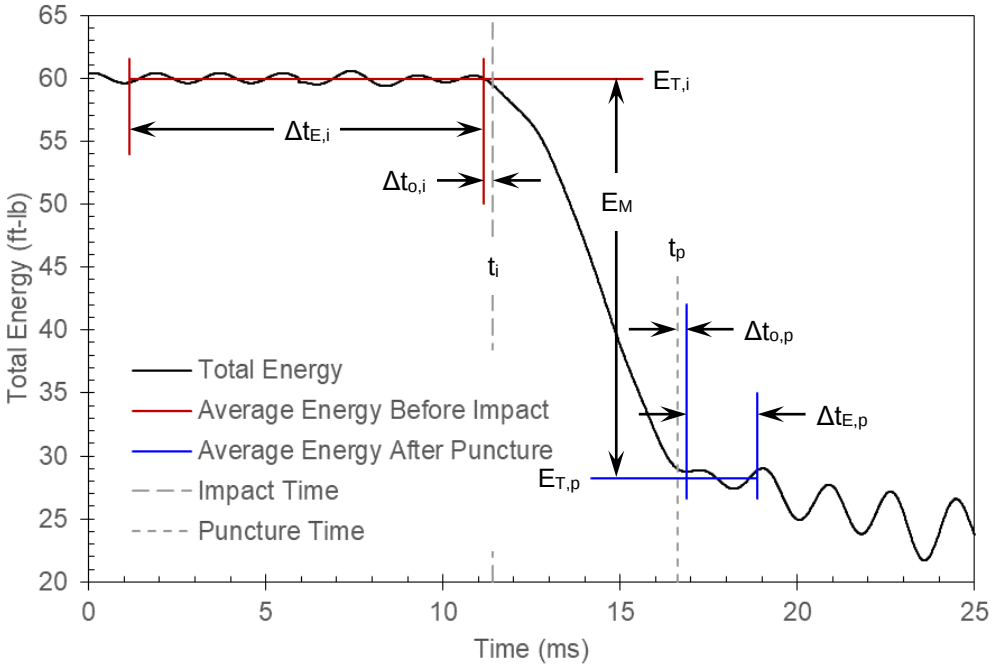

Figure 6: Representative Total Energy Curve and Time Periods for Averaging

The carriage velocity before impact (v_i) is found by averaging the velocity values over a time period of 0.5 ms ($\Delta t_{v,i}$) that ends 0.3 ms ($\Delta t_{o,i}$) before impact (t_i). The velocity after complete puncture (v_p) is the average value over a time period of 0.5 ms ($\Delta t_{v,p}$) that starts approximately 0.3 ms ($\Delta t_{o,p}$) after the penetration is complete (t_p). The time period and offset from the impact time are constant, but the offset from the puncture time is unique to each test (Table 2). Figure 7 illustrates the time periods over which the velocity is averaged. Appendix C has plots of the velocity data for each test and the time periods in which it is averaged.

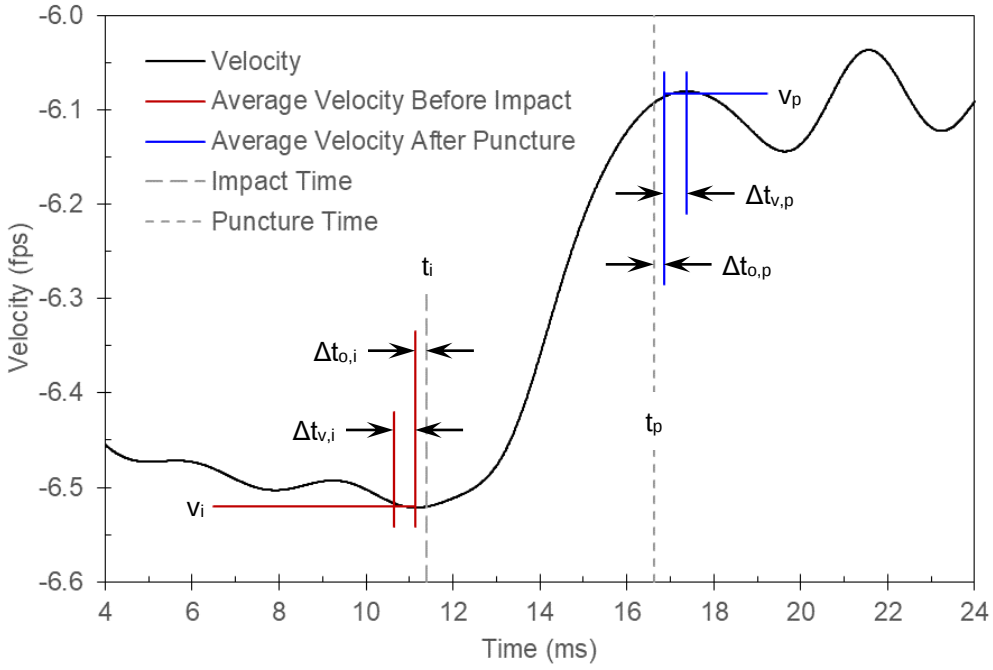

Figure 7: Representative Velocity Curve and Time Periods for Averaging

The distance traveled by the probe during the puncture process is the difference in the positions at the impact and puncture times (t_i, t_p). The results of the distance, velocity, and energy calculations are provided in Tables 3 and 4. The maximum deviation between the measured thickness in Table 3 (the average of several measurements) and the nominal thickness is 2.3%.

Table 3: Measurements and Results of Puncture Experiments on AISI 304L VAR Bar

		Thickness		Distance Traveled		Impact Velocity, v_i		Puncture Velocity, v_p	
Test	Specimen	(mm)	(in)	(mm)	(in)	(m/s)	(fps)	(m/s)	(fps)
7	1	1.636	0.0644	9.90	0.390	2.19	7.17	2.06	6.77
10	2	1.572	0.0619	9.79	0.386	2.04	6.68	1.89	6.20
8	3	1.609	0.0634	9.86	0.388	2.10	6.88	1.97	6.46
11	4	1.621	0.0638	10.08	0.397	2.02	6.62	1.87	6.14
12	5	1.617	0.0637	9.83	0.387	1.99	6.53	1.84	6.05
13	6	1.599	0.0630	10.68	0.421	2.02	6.61	1.88	6.16
14	7	1.634	0.0644	10.16	0.400	2.21	7.25	2.08	6.84
15	8	1.613	0.0635	9.75	0.384	2.17	7.13	2.06	6.74
16	9	1.632	0.0643	10.30	0.405	2.15	7.04	2.01	6.61
17	10	1.601	0.0631	9.84	0.387	2.11	6.92	1.98	6.48
18	11	1.617	0.0637	10.49	0.413	2.15	7.07	2.02	6.63
19	12	1.618	0.0637	10.12	0.398	2.10	6.89	1.97	6.48
20	13	1.629	0.0642	10.28	0.405	2.14	7.01	2.00	6.55
21	14	1.604	0.0632	9.81	0.386	2.16	7.09	2.04	6.68
22	15	1.613	0.0635	9.66	0.380	2.13	6.98	2.01	6.58
23	16	1.622	0.0639	10.31	0.406	2.23	7.30	2.10	6.89
24	17	1.626	0.0640	9.46	0.372	2.17	7.10	2.04	6.70
25	18	1.632	0.0643	10.24	0.403	2.21	7.26	2.08	6.82
26	19	1.617	0.0637	9.76	0.384	2.23	7.33	2.12	6.95
27	20	1.628	0.0641	9.91	0.390	2.24	7.35	2.12	6.94
28	21	1.637	0.0645	9.82	0.386	2.27	7.43	2.14	7.03
29	22	1.619	0.0638	10.46	0.412	2.29	7.51	2.18	7.14
30	23	1.619	0.0638	10.18	0.401	2.33	7.64	2.22	7.29
31	24	1.612	0.0635	11.77	0.463	2.40	7.88	2.29	7.50

Table 4: Total Energy in Puncture Experiments on AISI 304L VAR Bar

Test	Specimen	Total Energy Before Impact, $E_{T,i}$ (J)	(ft-lb)	After Puncture, $E_{T,p}$ (J)	(ft-lb)	Mitigated Energy, E_M (J)	(ft-lb)
7	1	341.3	251.7	298.8	220.4	42.5	31.4
10	2	295.5	218.0	250.6	184.8	44.9	33.1
8	3	313.8	231.5	272.1	200.7	41.7	30.7
11	4	291.7	215.2	246.3	181.7	45.4	33.5
12	5	283.1	208.8	237.8	175.4	45.3	33.4
13	6	291.0	214.6	247.2	182.3	43.8	32.3
14	7	350.0	258.1	303.9	224.2	46.1	34.0
15	8	337.3	248.7	295.6	218.0	41.7	30.7
16	9	330.4	243.7	283.7	209.2	46.7	34.4
17	10	317.3	234.0	273.5	201.8	43.7	32.3
18	11	330.8	244.0	284.9	210.2	45.8	33.8
19	12	314.9	232.3	272.5	201.0	42.4	31.3
20	13	326.5	240.8	279.6	206.2	46.9	34.6
21	14	333.0	245.6	290.9	214.5	42.1	31.0
22	15	323.2	238.4	282.6	208.4	40.6	30.0
23	16	353.9	261.0	308.7	227.7	45.2	33.3
24	17	334.2	246.5	292.3	215.6	41.9	30.9
25	18	349.9	258.1	302.3	223.0	47.6	35.1
26	19	356.3	262.8	315.0	232.3	41.3	30.5
27	20	360.4	265.8	314.1	231.7	46.3	34.2
28	21	368.8	272.0	322.8	238.1	46.0	33.9
29	22	376.8	277.9	331.2	244.3	45.6	33.6
30	23	384.4	283.5	346.5	255.5	38.0	28.0
31	24	412.0	303.9	366.7	270.5	45.3	33.4

Statistical Methods

The method for defining precision intervals on a data set is well known and available in many sources (*e.g.* Ref. 2–4); however, the equations are presented for the convenience of readers. The complete set of equations also facilitates explaining the methods.

Normal Probability Distribution

The goal is to use the information from the experiments to predict future observations of similar specimens under the same conditions. The entire population of specimens is assumed to be normally distributed with mean μ and standard deviation σ. These parameters are unknown but may be bounded by statistics of the sample that was tested. Each test result (the energy mitigated by a specific specimen, E_M) is x_i, for i = 1…n, where n is the sample size (24). The normal probability density function (PDF) is (Ref. 2, p. 117, Eq. 4.8; Ref. 3, p. 204; Ref. 4, p. 118, Eq. 3.3.27; Ref. 5)

$$f(x) = \frac{1}{\sigma\sqrt{2\pi e^{\left(\frac{x-\mu}{\sigma}\right)^2}}} = \frac{1}{\sigma\sqrt{2\pi}} e^{-\frac{1}{2}\left(\frac{x-\mu}{\sigma}\right)^2} \quad (8)$$

The probability (p) that a single measurement is less than a lower bound (b_L) is found by solving the normal cumulative distribution function (CDF; Ref. 3, p. 207; Ref. 4, p. 119, Eq. 3.3.29–30; Ref. 5):

$$p = \frac{1}{\sigma\sqrt{2\pi}} \int_{-\infty}^{b_L} e^{-\frac{1}{2}\left(\frac{x-\mu}{\sigma}\right)^2} dx \tag{9}$$

The maximum likelihood estimates (MLE) for the parameters of the normal distribution are (Ref. 4, p. 299)

$$\hat{\mu} = \frac{1}{n}\sum_{i=1}^{n} x_i \tag{10}$$

$$\hat{\sigma} = \sqrt{\frac{1}{n}\sum_{i=1}^{n}(x_i - \bar{x})^2} \tag{11}$$

The mean value of a data set x_i, for i = 1…n, is (Ref. 2, p. 121, Eq. 4.14a; Ref. 4, p. 264, Eq. 8.2.1)

$$\bar{x} = \hat{\mu} = \frac{1}{n}\sum_{i=1}^{n} x_i \tag{12}$$

The number of degrees of freedom (DoF) of the data relative to the mean is (Ref. 2, p. 121):

$$\nu = n - 1 \tag{13}$$

The standard deviation of the set is the square root of the variance between the data and the mean, which is normalized by the DoF (Ref. 2, p. 121, Eq. 4.14b; Ref. 4, p. 266, Eq. 8.2.7):

$$s_x = \hat{\sigma}\sqrt{\frac{n}{\nu}} = \sqrt{\frac{1}{\nu}\sum_{i=1}^{n}(x_i - \bar{x})^2} \tag{14}$$

The parameters of interest (μ, σ) are location-scale parameters; therefore, $\frac{\hat{\mu}-\mu}{\hat{\sigma}}$ and $\frac{\hat{\sigma}}{\sigma}$ are pivotal quantities suitable for deriving confidence intervals about the parameters of the entire population (μ, σ) based on the sample statistics ($\bar{x}$, s_x) (Ref. 4, p. 364). The confidence level (c) is the probability that confidence intervals developed from the statistics of a replicate sample will contain the true mean and standard deviation. The confidence level is also termed the frequentist coverage and has a customary value of 95%. Given a sample from a past test, the probability that the confidence intervals include the true parameters is either 0 or 1 but is unknown; therefore, the confidence level denotes the confidence in bounding the parameters of the distribution but not the probability of bounding a future test result. The significance level is (Ref. 2, p. 127; Ref. 4, p. 391)

$$s = 1 - c \tag{15}$$

For an infinite sample size equal to the entire population, the normal distribution defines the confidence interval about the true mean. The Student's t distribution accounts for additional uncertainty due to the finite number of specimens and converges to the normal distribution as the degrees of freedom increase. For 24 samples (23 DoF) and 95% confidence, the difference between the two-tailed bounds is 5.5%. The difference is less than 2% for 63 samples (62 DoF) and 1% for 124 samples (123 DoF) with 95% confidence.

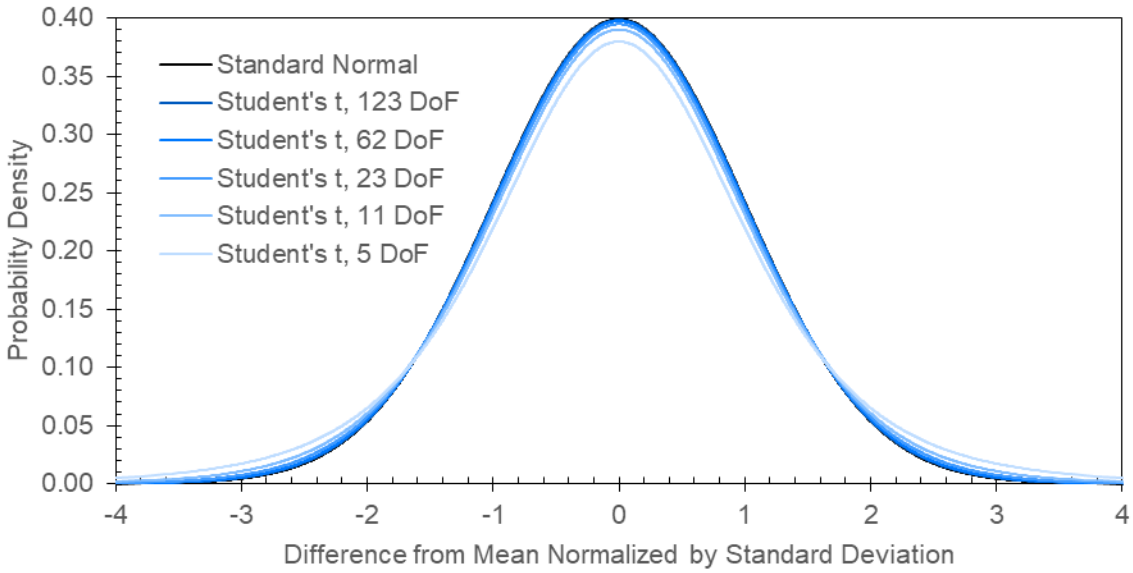

Figure 8: Convergence of Student's t and Normal Probability Density Functions

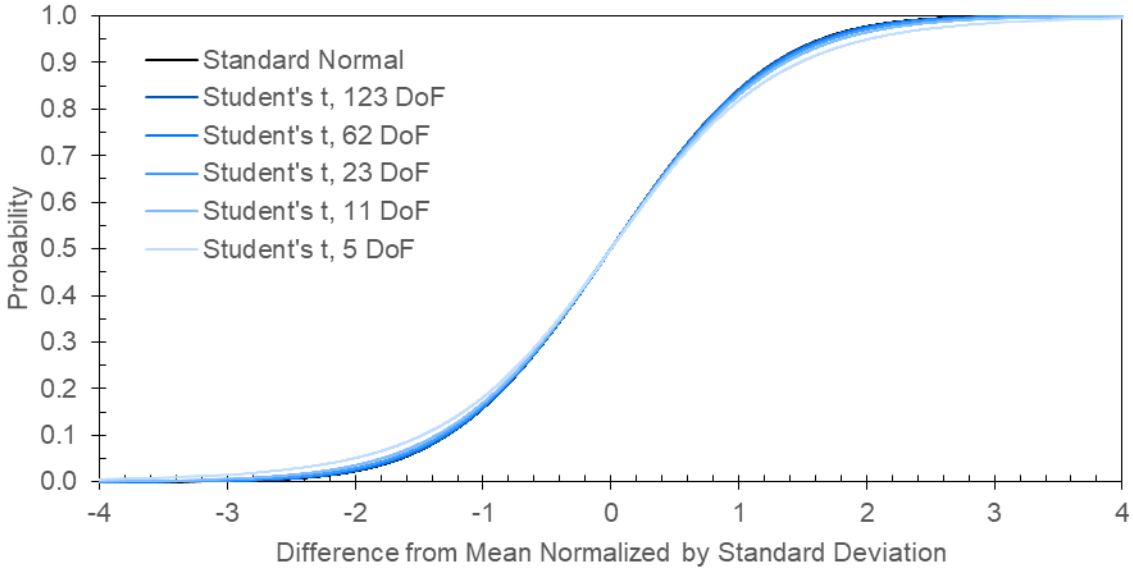

Figure 9: Convergence of Student's t and Normal Cumulative Distribution Functions

The Student's t PDF can be written (Ref. 4, p. 274, Eq. 8.4.2; Ref. 6)

$$f(x) = \frac{\Gamma\left(\frac{\nu+1}{2}\right)}{\Gamma\left(\frac{\nu}{2}\right)\sqrt{\pi\nu\left(1+\frac{x^2}{\nu}\right)^{\nu+1}}} = \frac{\Gamma\left(\frac{n}{2}\right)}{\sqrt{\pi\nu}\,\Gamma\left(\frac{\nu}{2}\right)}\left(1+\frac{x^2}{\nu}\right)^{-\frac{n}{2}} \tag{16}$$

or

$$f(x) = \frac{1}{B\left(\frac{1}{2},\frac{\nu}{2}\right)\sqrt{\nu\left(1+\frac{x^2}{\nu}\right)^{\nu+1}}} = \frac{1}{\sqrt{\nu}\,B\left(\frac{1}{2},\frac{\nu}{2}\right)}\left(1+\frac{x^2}{\nu}\right)^{-\frac{n}{2}} \tag{17}$$

The gamma function in Equation 16 is (Ref. 3, p. 222; Ref. 4, p. 111, Eq. 3.3.4; Ref. 7)

$$\Gamma(\gamma) = \int_0^\infty u^{\gamma-1} e^{-u} du \tag{18}$$

and the beta function in Equation 17 is (Ref. 3, pp. 226–227, Eq. 6.3; Ref. 3, p. 285; Ref. 6)

$$B(\beta_1, \beta_2) = \int_0^1 u^{\beta_1-1}(1-u)^{\beta_2-1} du = \frac{\Gamma(\beta_1)\,\Gamma(\beta_2)}{\Gamma(\beta_1+\beta_2)} \tag{19}$$

The CDF is the integral of the PDF from negative infinity to the non-dimensional limit parameter t and may be written in terms of gamma functions by placing Equation 16 in the integral or in terms of beta functions by substituting $u = \frac{\nu}{x^2+\nu}$ into Equation 17. Functions are available in many commercial software packages to solve these equations; the reason to include them here is to show what calculations are performed by those functions and explain the choice of the probability values based on the limits of integration. In Equations 16 and 17, the specific value that the probability equates to is computed from the significance such that the integral of the PDF over the interval {−t, t} equals the confidence; this requires that half of the significance be located in each tail of the distribution.

$$p = 1 - \frac{s}{2} = \frac{\Gamma\left(\frac{n}{2}\right)}{\sqrt{\pi\nu}\,\Gamma\left(\frac{\nu}{2}\right)} \int_{-\infty}^{t} \left(1 + \frac{x^2}{\nu}\right)^{-\frac{n}{2}} dx \tag{20}$$

or

$$p = 1 - \frac{s}{2} = \begin{cases} \dfrac{\int_0^{\frac{\nu}{t^2+\nu}} u^{\frac{\nu}{2}-1}(1-u)^{-\frac{1}{2}} du}{2\int_0^1 u^{\frac{\nu}{2}-1}(1-u)^{-\frac{1}{2}} du} & t < 0 \\ 1 - \dfrac{\int_0^{\frac{\nu}{t^2+\nu}} u^{\frac{\nu}{2}-1}(1-u)^{-\frac{1}{2}} du}{2\int_0^1 u^{\frac{\nu}{2}-1}(1-u)^{-\frac{1}{2}} du} & t \geq 0 \end{cases} \tag{21}$$

One of Equations 20 or 21 is solved for the parameter t. The confidence interval about the true mean is (Ref. 2, p. 124, Eq. 4.17; Ref. 4, p. 365, Eq. 11.3.5)

$$\mu_L = \bar{x} - \frac{t\,s_x}{\sqrt{n}} \leq \mu \leq \bar{x} + \frac{t\,s_x}{\sqrt{n}} = \mu_U \tag{22}$$

The chi-square distribution defines the confidence interval about the true variance. It is a specific gamma distribution (Ref. 4, p. 111, Eq. 3.3.8, and p. 268) with the PDF (Ref. 4, p. 597, Table B.2; Ref. 7)

$$f(x) = \frac{x^{\frac{\nu}{2}-1}}{\Gamma\left(\frac{\nu}{2}\right)\sqrt{2^\nu e^x}} \tag{23}$$

The CDF (Ref. 4, p. 112, Eq. 3.3.10, and p. 268; Ref. 7) may be expressed in two forms by substituting $x = 2u$ and the gamma function (Eq. 18) into the PDF.

$$p = \frac{1}{\sqrt{2^\nu}\,\Gamma\left(\frac{\nu}{2}\right)} \int_0^{\chi^2} x^{\frac{\nu}{2}-1} e^{-\frac{x}{2}} dx = \frac{\int_0^{\frac{\chi^2}{2}} u^{\frac{\nu}{2}-1} e^{-u} du}{\int_0^\infty u^{\frac{\nu}{2}-1} e^{-u} du} \tag{24}$$

The lower and upper bounds for the true variance are obtained by solving the CDF at different probabilities such that the total probability of being between the bounds equals the confidence, or half of the significance is in each tail of the distribution (Ref. 4, p. 365).

$$p_L = 1 - \frac{s}{2} = \frac{1}{\sqrt{2^\nu}\,\Gamma\left(\frac{\nu}{2}\right)} \int_0^{\chi_L^2} x^{\frac{\nu}{2}-1} e^{-\frac{x}{2}} dx = \frac{\int_0^{\frac{\chi_L^2}{2}} u^{\frac{\nu}{2}-1} e^{-u} du}{\int_0^{\infty} u^{\frac{\nu}{2}-1} e^{-u} du} \tag{25}$$

$$p_U = \frac{s}{2} = \frac{1}{\sqrt{2^\nu}\,\Gamma\left(\frac{\nu}{2}\right)} \int_0^{\chi_U^2} x^{\frac{\nu}{2}-1} e^{-\frac{x}{2}} dx = \frac{\int_0^{\frac{\chi_U^2}{2}} u^{\frac{\nu}{2}-1} e^{-u} du}{\int_0^{\infty} u^{\frac{\nu}{2}-1} e^{-u} du} \tag{26}$$

The confidence interval about the true variance is (Ref. 2, p. 127, Eq. 4.27; Ref. 4, p. 365, Eq. 11.3.6)

$$\frac{\nu\, s_x^2}{\chi_L^2} \le \sigma^2 \le \frac{\nu\, s_x^2}{\chi_U^2} \tag{27}$$

The bounds on the true standard deviation are

$$\sigma_L = s_x \sqrt{\frac{\nu}{\chi_L^2}} \tag{28}$$

$$\sigma_U = s_x \sqrt{\frac{\nu}{\chi_U^2}} \tag{29}$$

The precision interval bounds future observations b_i with probability p and confidence c.

$$b_L \le b_i \le b_U \tag{30}$$

The lower bound (b_L) is obtained by solving the normal CDF (Eq. 9) with the lower bound for the true mean (μ_L, Eq. 22) and the upper bound for the true standard deviation (σ_U, Eq. 29); Equation 31 encapsulates this combination of inputs to the CDF. The upper bound (b_U) is calculated by solving the normal CDF with the upper bounds for both parameters (μ_U, Eq. 22; σ_U, Eq. 29) and the complement of the probability; Equation 32 expresses this relation.

$$p = \frac{1}{\sigma_U\sqrt{2\pi}} \int_{-\infty}^{b_L} e^{-\frac{1}{2}\left(\frac{x-\mu_L}{\sigma_U}\right)^2} dx \tag{31}$$

$$1 - p = \frac{1}{\sigma_U\sqrt{2\pi}} \int_{-\infty}^{b_U} e^{-\frac{1}{2}\left(\frac{x-\mu_U}{\sigma_U}\right)^2} dx \tag{32}$$

Log-Normal Probability Distribution

Up to this point, the mitigated energy has been assumed to fit a normal distribution, but it physically cannot be negative, and the normal distribution does admit negative input values. Therefore, the log-normal distribution is also considered for establishing bounds on future observations. The PDF (Ref. 4, p. 199, Eq. 6.3.3; Ref. 8) is

$$f(x) = \frac{1}{x\sigma\sqrt{2\pi e^{\left[\frac{\ln(x)-\mu}{\sigma}\right]^2}}} = \frac{1}{x\sigma\sqrt{2\pi}} e^{-\frac{1}{2}\left[\frac{\ln(x)-\mu}{\sigma}\right]^2} \tag{33}$$

The data set x_i, for i = 1…n, is transformed with

$$y_i = \ln(x_i) \tag{34}$$

The natural logarithm function ensures that the input x_i does not take on negative values when the log-normal distribution is solved for specific probabilities. Equations 35 and 36 are evaluated to find the sample mean ($\bar{y}$) and standard deviation (s_y); these are simply Equations 12 and 14 with y_i substituted for x_i. The precision interval about a future observation may be computed by the same method as for the normal distribution but with the substitution of Equation 34; then the reverse substitution (antilogarithm function) must be applied to the bounds of the interval.

$$\bar{y} = \frac{1}{n}\sum_{i=1}^{n} y_i \tag{35}$$

$$s_y = \sqrt{\frac{1}{\nu}\sum_{i=1}^{n}\left(y_i - \bar{y}\right)^2} \tag{36}$$

Equations 37 and 38 (Ref. 4, p. 597, Table B.2) map the sample statistics through the logarithmic transformation and express them in terms of the measured random variable (x). The random variable y is normally distributed and x is lognormally distributed. The results of Equations 37 and 38 differ from those of Equations 12 and 14 by 0.009% and 2%, respectively.

$$\bar{x} = e^{\left(\bar{y}+\frac{s_y^2}{2}\right)} \tag{37}$$

$$s_x = \sqrt{e^{(2\bar{y}+s_y^2)}\left(e^{s_y^2} - 1\right)} \tag{38}$$

Equations 22 and 29 are evaluated to place bounds on the true mean (μ_L, μ_U) and standard deviation (σ_L, σ_U) of the transformed random variable (y), which is normally distributed. Then the log-normal CDF (Ref. 4, p. 119, Eq. 3.3.29–30, and p. 199, Eq. 6.3.5; Ref. 8) is solved for the bounds on the mitigated energy (b_L, b_U), given the probability (p).

$$p = \frac{1}{\sigma_U\sqrt{2\pi}} \int_{-\infty}^{\ln(b_L)} e^{-\frac{1}{2}\left(\frac{x-\mu_L}{\sigma_U}\right)^2} dx \tag{39}$$

$$1 - p = \frac{1}{\sigma_U\sqrt{2\pi}} \int_{-\infty}^{\ln(b_U)} e^{-\frac{1}{2}\left(\frac{x-\mu_U}{\sigma_U}\right)^2} dx \tag{40}$$

The bounds (Eq. 22, 28, and 29) on the parameters of the log-normal distribution are denoted $\mu_{L,y}$, $\mu_{U,y}$, $\sigma_{L,y}$, and $\sigma_{U,y}$. These are transformed back to the original units with Equations 41 through 44, which are derived from Equations 37 and 38.

$$\mu_{L,x} = e^{\left(\mu_{L,y}+\frac{\sigma_{L,y}^2}{2}\right)} \tag{41}$$

$$\mu_{U,x} = e^{\left(\mu_{U,y}+\frac{\sigma_{U,y}^2}{2}\right)} \tag{42}$$

$$\sigma_{L,x} = \sqrt{e^{\left(2\mu_{L,y}+\sigma_{L,y}^2\right)}\left(e^{\sigma_{L,y}^2}-1\right)} \tag{43}$$

$$\sigma_{U,x} = \sqrt{e^{\left(2\mu_{U,y}+\sigma_{U,y}^2\right)}\left(e^{\sigma_{U,y}^2}-1\right)} \tag{44}$$

Weibull Probability Distribution

The Weibull distribution does not assume negative values when it is solved for specific probabilities, so it is also a good option for predicting precision intervals on the mitigated energy. The PDF is (Ref. 3, p. 225; Ref. 4, p. 116, Eq. 3.3.20; Ref. 9)

$$f(x) = \frac{\alpha}{\beta}\left(\frac{x}{\beta}\right)^{\alpha-1} e^{-\left(\frac{x}{\beta}\right)^{\alpha}} = \frac{\alpha}{\beta^{\alpha}} x^{\alpha-1} e^{-\left(\frac{x}{\beta}\right)^{\alpha}} \tag{45}$$

where α is the shape parameter and β is the scale parameter. The mean and standard deviation are (Ref. 4, p. 117)

$$\mu_w = \beta\,\Gamma\left(1+\frac{1}{\alpha}\right) \tag{46}$$

$$\sigma_w = \beta\sqrt{\Gamma\left(1+\frac{2}{\alpha}\right) - \left[\Gamma\left(1+\frac{1}{\alpha}\right)\right]^2} \tag{47}$$

The MLE of the parameters (α, β) for a data set x_i are $\hat{\alpha}$, which is the solution of (Ref. 4, p. 591, Eq. 16.4.4, 16.4.5)

$$\frac{\sum_{i=1}^{n}\left[x_i^{\hat{\alpha}}\ln(x_i)\right]}{\sum_{i=1}^{n} x_i^{\hat{\alpha}}} - \frac{1}{\hat{\alpha}} = \frac{1}{n}\sum_{i=1}^{n}\ln(x_i) \tag{48}$$

and

$$\hat{\beta} = \left(\frac{1}{n}\sum_{i=1}^{n} x_i^{\hat{\alpha}}\right)^{\frac{1}{\hat{\alpha}}} \tag{49}$$

There is not a closed-form solution of Equation 48 (Ref. 4, p. 591), so the values of $\hat{\alpha}$ and $\hat{\beta}$ are found by non-linear optimization. The 95% confidence bounds on the parameters are returned by the same software tools, but the details of the optimization and bounding methods are too lengthy to present here. Selecting the lower bound on each MLE ($\hat{\alpha}_L$, $\hat{\beta}_L$) minimizes the lower bounds on the mitigated energy (b_L), which are found by solving the CDF (Ref. 3, p. 224, Eq. 6.2; Ref. 4, p. 116, Eq. 3.3.22) at specific probability values (p).

$$p = 1 - e^{-\left(\frac{x}{\hat{\beta}_L}\right)^{\hat{\alpha}_L}} \tag{50}$$

The closed-form solution of Equation 50 is

$$x = \hat{\beta}_L \left[\ln\left(\frac{1}{1-p}\right) \right]^{\frac{1}{\hat{\alpha}_L}} \tag{51}$$

Gamma Probability Distribution

The gamma distribution does not take on negative values when it is solved for specific probabilities, so it is another good option for predicting the energy mitigated by future specimens. The PDF is (Ref. 3, p. 222; Ref. 4, p. 111, Eq. 3.3.8; Ref. 10)

$$f(x) = \frac{\left(\frac{x}{\beta}\right)^{\alpha-1} e^{-\frac{x}{\beta}}}{\beta\,\Gamma(\alpha)} = \frac{x^{\alpha-1} e^{-\frac{x}{\beta}}}{\beta^{\alpha}\,\Gamma(\alpha)} \tag{52}$$

where α is the shape parameter and β is the scale parameter. The mean and standard deviation are (Ref. 3, p. 360, Table 7.2; Ref. 4, pp. 113–114)

$$\mu_g = \alpha\beta \tag{53}$$

$$\sigma_g = \sqrt{\alpha}\beta \tag{54}$$

There is not a closed-form solution for the MLE of the parameters, so the values are found by multi-variate non-linear optimization. The 95% confidence bounds on the parameters are returned by the same software tools, but no details of the optimization or bounding methods are presented here.

The lower bounds on the parameter values ($\hat{\alpha}_L$, $\hat{\beta}_L$) minimize the lower bounds on the mitigated energy (b_L), which are found by solving the CDF (Ref. 4, p. 112, Eq. 3.3.10) at specific probability values (p).

$$p = \frac{1}{\hat{\beta}_L^{\,\hat{\alpha}_L}\,\Gamma(\hat{\alpha}_L)} \int_{-\infty}^{b_L} x^{\hat{\alpha}_L - 1} e^{-\frac{x}{\hat{\beta}_L}}\, dx \tag{55}$$

Results of Statistical Inference and Safety Factor Method

The sample size is known, and the population is considered to be infinite. Four probability distributions are hypothesized to fit the data set for the purpose of predicting the energy mitigated by future specimens from the population. The parameters of each distribution are either calculated with explicit equations or optimized by numerical methods. The MLE of the parameters for all of the probability distributions are bounded at the same confidence and significance levels, so half of the significance (Eq. 26) and the one-tail probability (Eq. 20, 21, 25) are also the same. The parameters in Table 5 are common to all the distributions.

Table 5: General Parameters for Bounding the MLE of Probability Distributions

Parameter	Value
Sample Size, n	24
Degrees of Freedom, ν	23
Confidence Level, C	0.950
Significance Level, s	0.050
Half Significance	0.025
One Tail Probability	0.975
Student's t Parameter	2.069

Summary statistics for the energy mitigated by the specimens are presented in Tables 6 and 7. The differences between the normal and log-normal distributions are almost negligible with the appropriate number of significant digits in the results. The means and standard deviations of the Weibull and gamma distributions are computed with either the MLE or the lower bounds of both parameters: the statistics based on the MLE show that the optimized parameters are correct because they agree closely with the sample statistics, and the statistics based on the lower bounds relate to the precision intervals. The shape parameter of the Weibull distribution is moderately large because the sample standard deviation is small relative to the sample mean; the resulting shape concentrates most of the probability from Equation 45 far from the origin. The Weibull scale parameter is comparable to the upper bounds on the mean values of the normal and log-normal distributions. The gamma distribution has a very large shape parameter, considering that it is an exponent in Equation 52, and a relatively small scale parameter (less than 1 ft-lb). This combination of optimal parameter values could produce numerical instability in evaluating Equation 55.

Table 6: Mitigated Energy Statistics for the Normal and Log-Normal Distributions

Statistic	Normal Distribution		Log-Normal Distribution	
Sample Mean	44.0 J	32.5 ft-lb	44.0 J	32.5 ft-lb
Sample Standard Deviation	2.42 J	1.784 ft-lb	2.47 J	1.822 ft-lb
Lower Bound on Mean	43.0 J	31.7 ft-lb	43.0 J	31.7 ft-lb
Upper Bound on Mean	45.1 J	33.2 ft-lb	45.2 J	33.3 ft-lb
Lower Bound on Standard Deviation	1.880 J	1.387 ft-lb	1.874 J	1.382 ft-lb
Upper Bound on Standard Deviation	3.39 J	2.50 ft-lb	3.56 J	2.62 ft-lb

Table 7: Mitigated Energy Statistics for the Weibull and Gamma Distributions

Statistic	Weibull Distribution		Gamma Distribution	
MLE of Shape Parameter, α	23.7	23.7	337	337
MLE of Scale Parameter, β	45.1 J	33.3 ft-lb	130.7E-3 J	96.4E-3 ft-lb
Mean Based on MLE	44.1 J	32.5 ft-lb	44.0 J	32.5 ft-lb
Standard Deviation Based on MLE	2.32 J	1.710 ft-lb	2.40 J	1.770 ft-lb
Lower Bound on α	17.09	17.09	191.3	191.3
Upper Bound on α	32.8	32.8	593	593
Lower Bound on β	44.3 J	32.7 ft-lb	74.2E-3 J	54.8E-3 ft-lb
Upper Bound on β	45.9 J	33.9 ft-lb	230E-3 J	169.8E-3 ft-lb
Mean Based on Lower Bounds	42.9 J	31.7 ft-lb	14.20 J	10.48 ft-lb
Standard Deviation Based on Lower Bounds	3.10 J	2.28 ft-lb	1.027 J	757E-3 ft-lb

The lower bounds of the precision intervals for the mitigated energy are listed in Table 8 at several probability values of interest, including those that define screening thresholds in Reference 11, page 2 (1E-6, 1E-9). The normal distribution yields positive lower bounds for the mitigated energy at the screening probabilities, although they are extremely small, and the other hypothetical distributions always produce positive energy values. The lower bounds for the normal and log-normal distributions are based on the lower bound for the

mean and the upper bound for the standard deviation. The lower bounds for the Weibull and gamma distributions are based on the lower bounds for both the shape and scale parameters. Predicting a lower bound for the energy mitigated by future test specimens depends on the assumptions that the sample data come from the selected probability distribution and that the parameters of the distribution are known when, in fact, they are only estimated. The adequacy of each distribution for making these predictions is considered subsequently.

Table 8: Lower Bounds for Energy Mitigated by Disc Specimens of AISI 304L VAR Bar

Probability of Lower Future Observation		Normal Distribution (J)	Normal Distribution (ft-lb)	Log-Normal Distribution (J)	Log-Normal Distribution (ft-lb)	Weibull Distribution (J)	Weibull Distribution (ft-lb)	Gamma Distribution (J)	Gamma Distribution (ft-lb)
50%	500E-3	43.0	31.7	42.9	31.7	43.4	32.0	14.2	10.5
10%	100E-3	38.7	28.5	38.8	28.6	38.8	28.6	12.9	9.5
5%	50E-3	37.4	27.6	37.7	27.8	37.2	27.5	12.6	9.3
1%	10E-3	35.1	25.9	35.8	26.4	33.8	25.0	11.9	8.8
0.1%	1E-3	32.5	24.0	33.7	24.8	29.6	21.8	11.2	8.3
0.0001%	1E-6	26.9	19.8	29.5	21.8	19.7	14.6	9.8	7.3
0.0000001%	1E-9	22.7	16.7	26.8	19.8	13.2	9.7	8.9	6.6

With n specimens (24), the Student's t parameter (2.069) is close enough to the inverse standard normal cumulative distribution function (1.960) at the customary 95% confidence that the relative difference is small—5.5%. The effect of the finite sample size on the lower bounds is not severe (-23% at 1E-9) but it could be diminished by testing more specimens.

An alternative to classical statistical inference is to divide the sample mean by a safety factor of 1.5 (Ref. 12, p. 7).

$$b_L = \frac{\bar{x}}{1.5} \tag{56}$$

The result, 29.4 J (21.7 ft-lb), happens to be above the lower bounds predicted by the normal, Weibull, and gamma distributions at a probability of 1E-6 and below the prediction of the lognormal distribution at the same probability, but this is a consequence of the variance in the sample. The safety factor does not correlate to any probability or confidence level; it expresses engineering judgement regarding the reliability of specimens made to the same material specifications, dimensional tolerances, and surface finishes.

Adequacy of Probability Distributions for Predicting Future Observations

The data are arranged into a histogram (Fig. 10) for evaluating the adequacy of the hypothetical probability distributions as predictors for future outcomes. The shaded area of the histogram equals the integrals of the PDF curves that are overlaid on it. The bins of the histogram are coarse with an interval of 2.71 J (2.00 ft-lb). The normal, log-normal, and gamma distributions are remarkably similar when plotted with the MLE of the parameters. The shape of the Weibull distribution based on the MLE of the parameters is distinct but compatible with the data set. The large left tail causes it to predict lower energy thresholds at small probabilities of not bounding future observations.

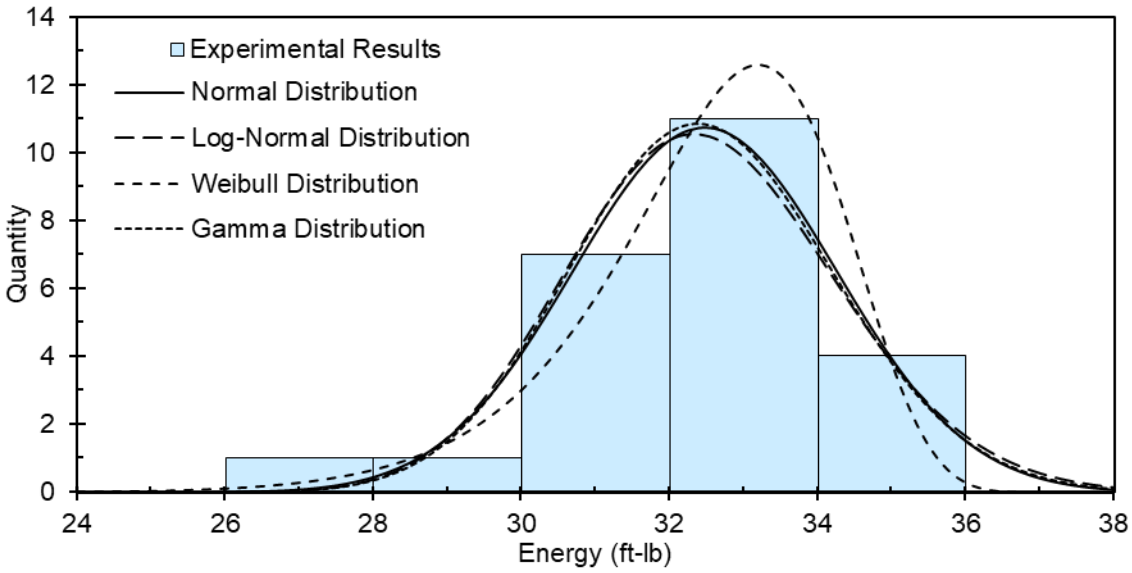

Figure 10: Histogram of Experimental Results and Probability Distributions

The data set (x_i) is sorted in ascending order. The measurement quantile (r_i) is the number of specimens with an equal or lesser result. The theoretical quantile (q_i) is defined by Equations 57 through 60 for the standard normal, log-normal, Weibull, and gamma distributions, respectively. The measurement and theoretical quantiles are co-plotted in Figures 11 and 12, which show similar trends. A line is fitted to each quantile plot by minimizing the sum of the squares of the residuals between the measurement and theoretical quantiles, $\sum_{i=1}^{n}(r_i - q_i)^2$. Equations 61 through 63 define the lines that are overlaid on the quantile plots to make the variance visible. The proximity of the points to the line indicates how well the probability distribution fits the data. Equation 64 calculates the coefficient of determination, which is 0.920 for the normal, Weibull, and gamma distributions and 0.905 for the log-normal distribution.

$$q_i = \frac{x_i - \bar{x}}{s_x} \tag{57}$$

$$q_i = \frac{y_i - \bar{y}}{s_y} \tag{58}$$

$$q_i = \frac{x_i - \mu_w}{\sigma_w} \tag{59}$$

$$q_i = \frac{x_i - \mu_g}{\sigma_g} \tag{60}$$

$$L_i = a_0 + a_1 q_i \tag{61}$$

$$a_0 = \frac{\sum_{i=1}^{n} q_i \sum_{i=1}^{n}(q_i r_i) - \sum_{i=1}^{n} q_i^2 \sum_{i=1}^{n} r_i}{\left(\sum_{i=1}^{n} q_i\right)^2 - n\sum_{i=1}^{n} q_i^2} \tag{62}$$

$$a_1 = \frac{\sum_{i=1}^{n} q_i \sum_{i=1}^{n} r_i - n\sum_{i=1}^{n}(q_i r_i)}{\left(\sum_{i=1}^{n} q_i\right)^2 - n\sum_{i=1}^{n} q_i^2} \tag{63}$$

$$R^2 = 1 - \frac{(n-1)\sum_{i=1}^{n}(L_i - r_i)^2}{(n-2)\sum_{i=1}^{n}\left(r_i - \frac{n+1}{2}\right)^2} \quad (64)$$

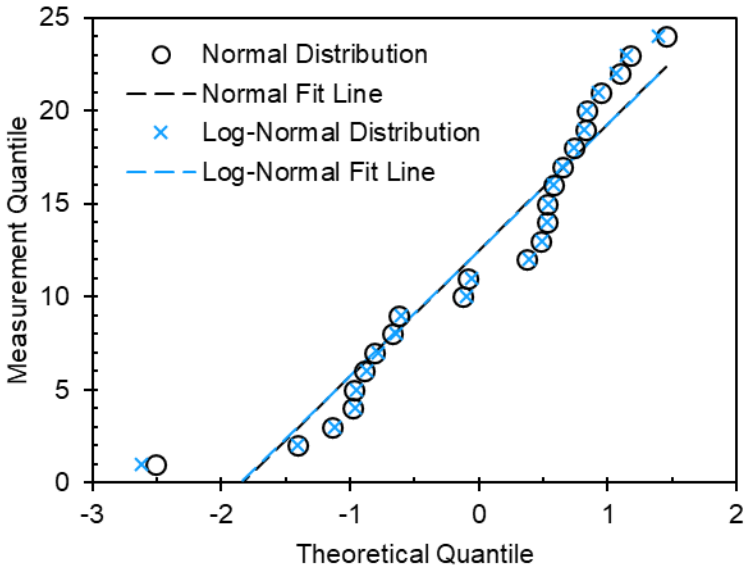

Figure 11: Quantile Plots of Normal and Log-Normal Probability Distributions

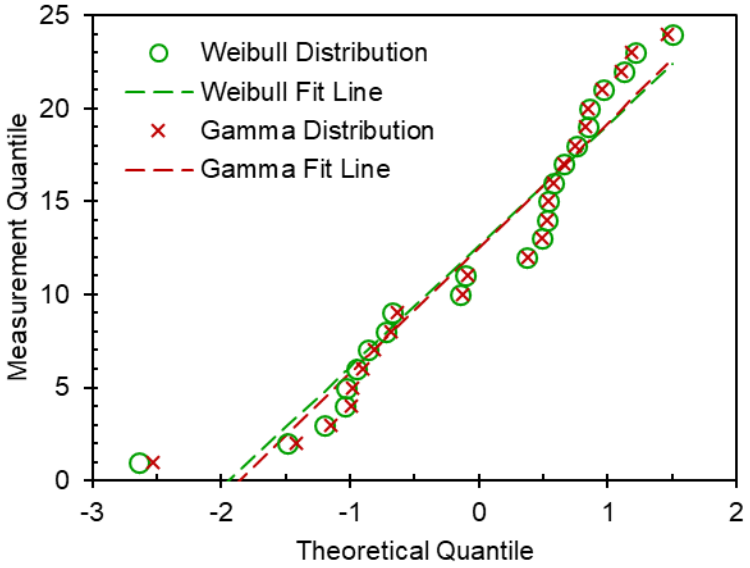

Figure 12: Quantile Plots of Weibull and Gamma Probability Distributions

Another method for investigating the possibility that a probability distribution fits a data set is the Anderson-Darling test (Ref. 13–23). The probability (p) of each data point occurring if the data were from the normal or log-normal distribution is computed with the CDF based on the sample mean and standard deviation. Equation 65 applies to the normal distribution (compare Eq. 9) and Equation 66 to the log-normal distribution (compare Eq. 33 and 34). The probability (p) of the data coming from the Weibull or gamma distribution is computed with the CDF based on the MLE of the parameters. Equation 67 applies to the Weibull distribution (compare Eq. 50) and Equation 68 to the gamma distribution (compare Eq. 55).

$$p(x_i) = \frac{1}{s_x\sqrt{2\pi}} \int_{-\infty}^{x_i} e^{-\frac{1}{2}\left(\frac{u-\bar{x}}{s_x}\right)^2} du \tag{65}$$

$$p(y_i) = \frac{1}{s_y\sqrt{2\pi}} \int_{-\infty}^{y_i} e^{-\frac{1}{2}\left(\frac{u-\bar{y}}{s_y}\right)^2} du \tag{66}$$

$$p(x_i) = 1 - e^{-\left(\frac{x_i}{\hat{\beta}}\right)^{\hat{\alpha}}} \tag{67}$$

$$p(x_i) = \frac{1}{\hat{\beta}^{\hat{\alpha}}\,\Gamma(\hat{\alpha})} \int_{-\infty}^{x_i} u^{\hat{\alpha}-1} e^{-\frac{u}{\hat{\beta}}} du \tag{68}$$

The Anderson-Darling statistic is given by Equation 69 for the normal distribution (Ref. 14, p. 9-82; Ref. 15; Ref. 16, p. 731; Ref. 18, p. 2, Eq. 1; Ref. 19; Ref. 21; Ref. 22; Ref. 23, p. 24, Eq. 4), or Equation 70 for the log-normal distribution. References 15, 18, and 19 also apply Equation 69 to the Weibull distribution, but Reference 14 (p. 9-91) specifies Equation 71 for the Weibull distribution and uncensored data. Reference 18 (p. 4, Eq. 2) combines Equations 67 and 69 to obtain the simplified form of Equation 72. Reference 19 applies Equation 69 to the gamma distribution.

$$A^2 = -n - \frac{1}{n}\sum_{i=1}^{n} (2i-1)\left(\ln[p(x_i)] + \ln[1 - p(x_{n-i+1})]\right) \tag{69}$$

$$A^2 = -n - \frac{1}{n}\sum_{i=1}^{n} (2i-1)\left(\ln\left[p(y_i)\right] + \ln\left[1 - p(y_{n-i+1})\right]\right) \tag{70}$$

$$A^2 = -\frac{n}{2}(3 + [p(x_1)]^2) - \frac{1}{n}\sum_{i=1}^{n} (2i-1)\ln[p(x_i)] - 2p(x_i) \tag{71}$$

$$A^2 = -n - \frac{1}{n}\sum_{i=1}^{n} (2i-1)\left(\ln\left[1 - e^{-\left(\frac{x_i}{\hat{\beta}}\right)^{\hat{\alpha}}}\right] - \left[\frac{x_{n-i+1}}{\hat{\beta}}\right]^{\hat{\alpha}}\right) \tag{72}$$

The Anderson-Darling statistics from Equations 69 and 70 are adjusted because the sample statistics serve as estimates for the parameters of the distributions in Equations 65 through 68. The adjusted statistic for both the normal and log-normal distributions is either Equation 73 (Ref. 16, page 732, Table 1A, case 3) or Equation 74 (Ref. 19; Ref. 21; Ref. 23, p. 24, Eq. 5), depending on the source of the critical values it is compared to. The adjusted statistic for the Weibull distribution is evaluated with Equation 75 (Ref. 18, p. 4, Eq. 2; Ref. 19, Fig. 2), and the adjusted statistic for the gamma distribution is given by Equation 76 (Ref. 19, Fig. 2, $\hat{\alpha} \geq 2$).

$$AD = A^2\left(1 + \frac{4}{n} - \frac{25}{n^2}\right) \tag{73}$$

$$AD = A^2\left(1 + \frac{3}{4n} + \frac{9}{4n^2}\right) \tag{74}$$

$$AD = A^2\left(1 + \frac{1}{5\sqrt{n}}\right) \tag{75}$$

$$AD = A^2 + \frac{1}{n}\left(\frac{1}{5} + \frac{3}{10\hat{\alpha}}\right) \tag{76}$$

The probability (p) that it would be incorrect to reject a normal or log-normal distribution as a fit for the data is Equation 77 (Ref. 19, 21), which is a piece-wise-defined function of the adjusted statistic in Equation 74. For the Weibull distribution, the probability is given by Equation 78 (Ref. 18, p. 4).

$$p = \begin{cases} 1 - e^{-13.436 + 101.14\,AD - 223.73\,AD^2} & AD \leq 0.2 \\ 1 - e^{-8.318 + 42.796\,AD - 59.938\,AD^2} & 0.2 < AD \leq 0.34 \\ e^{0.9177 - 4.279\,AD - 1.38\,AD^2} & 0.34 < AD < 0.6 \\ e^{1.2937 - 5.709\,AD + 0.0186\,AD^2} & AD \geq 0.6 \end{cases} \tag{77}$$

$$p = \frac{1}{1 + e^{-0.1 + 1.24\,\ln(AD) + 4.48\,AD}} \tag{78}$$

A probability of at least 5% is recommended to infer that the selected distribution fits the data and has the correct parameters (Ref. 18, p. 4; Ref. 21). This inference is considered valid if neither the distribution nor the parameters are refuted, so it is termed the null hypothesis (H_0; Ref. 18, p. 2; Ref. 21). The alternative hypothesis (H_1) is that the either the distribution or the parameters are incorrect (Ref. 18, p. 2; Ref. 21).

The more general test criterion is to compare either the Anderson-Darling statistic to an adjusted critical value (Ref. 14; 18, p. 2) or the adjusted Anderson-Darling statistic to a critical value (Ref. 15; 16; 18, p. 4). Reference 19 adjusts both the statistic and the critical value. The customary significance level (s) is 5%, and the most frequently quoted critical value for a normal or log-normal distribution at this significance is 0.752 (Ref. 14, p. 9-82; Ref. 15; Ref. 18, p. 2). References 16 (p. 732, Table 1A, case 3) and 17 (p. 367, Table 4, case 3) also provide values for AD_c, which are quoted in Table 9; these apply to normal and log-normal distributions. Reference 17 states on page 368 that it corrects the values published in Reference 16 but follows the same method for the Anderson-Darling test.

Table 9: Critical Values of Adjusted Anderson-Darling Statistic for Normal and Log-Normal Distributions

Significance, s	Critical Adjusted Statistic, AD_c (Ref. 16)	(Ref. 17)
1.0%	1.092	1.029
2.5%	0.918	0.870
5.0%	0.787	0.751
10.0%	0.656	0.632
15.0%	0.576	0.560

The critical values of the adjusted Anderson-Darling statistic for the Weibull and gamma distributions are obtained from Reference 20 and listed in Table 10.

Table 10: Critical Values of Adjusted Anderson-Darling Statistic for Weibull and Gamma Distributions

Significance, s	Critical Adjusted Statistic, AD_c	
	Weibull	Gamma
0.5%		1.159
1.0%	1.038	1.035
2.5%	0.877	0.873
5.0%	0.757	0.752
10.0%	0.637	0.631
25.0%	0.474	0.470

References 14 (p. 9-82) and 18 (p. 2) adjust the critical value of the Anderson-Darling statistic for a normal or log-normal distribution in a manner analogous to Equation 74:

$$A_c^2 = \frac{AD_c}{1 + \frac{3}{4n} + \frac{9}{4n^2}} \tag{79}$$

Reference 14 compares the result of Equation 71 directly to the critical value defined by Equation 80 (p. 9-91, Eq. 9.5.4.7.3, uncensored) to determine if the Weibull distribution is adequate ($A^2 < A_c^2$).

$$A_c^2 = 0.3951 + 41.86\text{E-}6\ n \tag{80}$$

With a significance of s (5%) and n specimens (24), the adjusted critical value from References 14 and 18 is 0.726. If the Anderson-Darling statistic does not exceed this value $\left(A^2 \le A_c^2\right)$, the null hypothesis is not rejected at the selected significance level and the proposed distribution might fit the data (Ref. 14, 18, 22). If Equation 79 with n equal to 24 specimens is applied to the values from Reference 17 in Table 9, Table 11 results.

Table 11: Adjusted Critical Values of Anderson-Darling Statistic

Significance, s	Adjusted Critical Statistic, A_c^2
1.0%	0.994
2.5%	0.840
5.0%	0.725
10.0%	0.611
15.0%	0.541

Reference 19 calculates the critical value of the adjusted statistic (AD_c) with Equation 81. The parameters a, b, and d are tabulated in Reference 20 and Table 12. The results of Equation 81 with n equal to 24 specimens are also included in Table 12.

$$AD_c = a\left(1 - \frac{b}{n} - \frac{d}{n^2}\right) \tag{81}$$

Table 12: Parameters and Critical Values of Adjusted Anderson-Darling Statistic

Significance, s	Parameter a	b	d	Critical Adjusted Statistic, AD_c (n = 24)
0.5%	1.1578	1.063	1.34	1.104
1.0%	1.0348	1.013	0.93	0.989
2.5%	0.8728	0.881	0.94	0.839
5.0%	0.7514	0.795	0.89	0.725
10.0%	0.6305	0.750	0.80	0.610
20.0%	0.5091	0.756	0.39	0.493

The values of parameter a are similar to the values of AD_c from Reference 17 in Table 9, and the values of AD_c in Table 12 are similar to the values of A_c^2 in Table 11 at the same significance levels. Equations 79 and 81 appear to have a similar effect over a range of significance levels, but the adjustment is already accomplished with Equation 74 in the method of Reference 19. The possibility that the distribution fits the data is not rejected if the adjusted statistic is less than or equal to the critical value ($AD \leq AD_c$; Ref. 15, 16, 19). Consequently, the method of Reference 19 is more stringent than the method of References 14 and 18.

The Anderson-Darling test can only disprove that a particular probability distribution fits a data set with a specified significance. The test is designed such that a false rejection will only occur with probability less than the significance level; otherwise, it may be reasonable to assert that the distribution fits. The nature of the test biases it in favor of admitting (not rejecting) the hypothesis that the distribution fits the data, but it is never conclusive. Tables 9 through 12 demonstrate that low significance corresponds to a lenient test criterion and high significance corresponds to a strict criterion.

In contrast to the precision interval, where the confidence in the result is negatively correlated to the significance by Equation 15, the complement of the significance is not the confidence in the conclusion of the Anderson-Darling test. With a precision interval, the significance level is the probability that a future observation is unbounded. In a fit quality test, it is the probability of error if the null hypothesis is rejected, but no conclusion can be made about the likelihood that the distribution fits the data.

Clearly, there are many ways to approach the Anderson-Darling test and adjust the criterion for uncertainty in the parameters of the proposed probability distribution. Table 13 summarizes four methods for applying the test to normal and log-normal distributions. The general rows apply to all four methods. When the inference is to admit the fit (methods 1 and 2 for the normal distribution), the null hypothesis is not rejected at the selected significance. An inference that the null hypothesis should be rejected at the specified significance (methods 3 and 4 for the normal distribution and all methods for the log-normal distribution) means that the distribution is less likely to fit the data because there would be less probability of error in rejecting the fit than the stated significance.

Table 13: Results of Anderson-Darling Tests for the Normal and Log-Normal Distributions

Method	External References	Internal Reference	Parameter	Normal Distribution	Log-Normal Distribution
General	14–16, 18, 19, 21–23	Eq. 69	A^2	0.701	0.747
	14–22	p. 24	s	5.0%	5.0%
1	19, 21, 23	Eq. 74	AD	0.726	0.773
	19, 21	Eq. 77	p	5.8%	4.5%
	19		Inference	Admit	Reject
2	14, 18	Eq. 79	A_c^2	0.726	0.726
	14, 18		Inference	Admit	Reject
3	16	Eq. 73	AD	0.787	0.839
	17	Table 9	AD_c	0.751	0.751
	15, 16		Inference	Reject	Reject
4	19, 21, 23	Eq. 74	AD	0.726	0.773
	19, 20	Eq. 81	AD_c	0.725	0.725
	15, 19		Inference	Reject	Reject

The first two methods support the hypothesis that the experimental data are normally distributed and reject the hypothesis that they are log-normally distributed. The third and fourth methods reject the null hypothesis for both probability distributions. Although the margin is small, engineering judgement suggests that the normal distribution is suitable for calculating the precision intervals in Table 8. The second method is preferred because it is simple and published in an industry standard (Ref. 14).

Three methods of applying the Anderson-Darling test to a Weibull distribution are summarized in Table 14, and all three admit the possibility that it fits the data set. The method from Reference 19 that applies to the gamma distribution is also included, but it rejects the null hypothesis, so this is not a good probability distribution for establishing precision intervals.

Table 14: Results of Anderson-Darling Tests for the Weibull and Gamma Distributions

Method	External References	Internal References	Parameter	Weibull Distribution	Gamma Distribution
General	14, 15, 18, 19	p. 24	s	5.0%	5.0%
1	15, 18, 19	Eq. 69	A^2	0.560	
	18, 19	Eq. 75	AD	0.583	
	18	Eq. 78	p	13.7%	
	18		Inference	Admit	
2	14	Eq. 71	A^2	0.316	
	14	Eq. 80	A_c^2	0.396	
	14		Inference	Admit	
3	15, 18, 19	Eq. 69	A^2	0.560	0.756
	18, 19	Eq. 75, 76	AD	0.583	0.765
	20	Table 10	AD_c	0.757	0.752
	15, 19		Inference	Admit	Reject

The Shapiro-Wilk test (Ref. 23–26) is another option for evaluating the possibility that the normal and log-normal distributions fit the data set. The Shapiro-Wilk statistic is calculated with Equation 82 or 83 for the normal or log-normal distribution, respectively (Ref. 23, p. 25, Eq. 8; Ref. 25). It depends on the sample size (n), the number of data points below the median (d), and the coefficients in Tables 15 through 20 (Ref. 26). The number of points below the median is half of the sample size truncated to an integer. For a sample size of 24, there are 12 points below the median, and the 12 coefficients are obtained from Table 17.

$$W = \frac{\left[\sum_{i=1}^{d} a_i (x_{n-i+1} - x_i)\right]^2}{\sum_{i=1}^{n} (x_i - \bar{x})^2} \tag{82}$$

$$W = \frac{\left[\sum_{i=1}^{d} a_i \left(y_{n-i+1} - y_i\right)\right]^2}{\sum_{i=1}^{n} \left(y_i - \bar{y}\right)^2} \tag{83}$$

Table 15: Shapiro-Wilk Coefficients for Sample Sizes from 3 to 10

	Sample Size							
Coefficient	3	4	5	6	7	8	9	10
a_1	0.7071	0.6872	0.6646	0.6431	0.6233	0.6052	0.5888	0.5739
a_2		0.1677	0.2413	0.2806	0.3031	0.3164	0.3244	0.3291
a_3				0.0875	0.1401	0.1743	0.1976	0.2141
a_4						0.0561	0.0947	0.1224
a_5								0.0399

Table 16: Shapiro-Wilk Coefficients for Sample Sizes from 11 to 18

	Sample Size							
Coefficient	11	12	13	14	15	16	17	18
a_1	0.5601	0.5475	0.5359	0.5251	0.5150	0.5056	0.4968	0.4886
a_2	0.3315	0.3325	0.3325	0.3318	0.3306	0.3290	0.3273	0.3253
a_3	0.2260	0.2347	0.2412	0.2460	0.2495	0.2521	0.2540	0.2553
a_4	0.1429	0.1586	0.1707	0.1802	0.1878	0.1939	0.1988	0.2027
a_5	0.0695	0.0922	0.1099	0.1240	0.1353	0.1447	0.1524	0.1587
a_6		0.0303	0.0539	0.0727	0.0880	0.1005	0.1109	0.1197
a_7				0.0240	0.0433	0.0593	0.0725	0.0837
a_8						0.0196	0.0359	0.0496
a_9								0.0163

Table 17: Shapiro-Wilk Coefficients for Sample Sizes from 19 to 26

	Sample Size							
Coefficient	19	20	21	22	23	24	25	26
a_1	0.4808	0.4734	0.4643	0.4590	0.4542	0.4493	0.4450	0.4407
a_2	0.3232	0.3211	0.3185	0.3156	0.3126	0.3098	0.3069	0.3043
a_3	0.2561	0.2565	0.2578	0.2571	0.2563	0.2554	0.2543	0.2533
a_4	0.2059	0.2085	0.2119	0.2131	0.2139	0.2145	0.2148	0.2151
a_5	0.1641	0.1686	0.1736	0.1764	0.1787	0.1807	0.1822	0.1836
a_6	0.1271	0.1334	0.1399	0.1443	0.1480	0.1512	0.1539	0.1563
a_7	0.0932	0.1013	0.1092	0.1150	0.1201	0.1245	0.1283	0.1316
a_8	0.0612	0.0711	0.0804	0.0878	0.0941	0.0997	0.1046	0.1089
a_9	0.0303	0.0422	0.0530	0.0618	0.0696	0.0764	0.0823	0.0876
a_{10}		0.0140	0.0263	0.0368	0.0459	0.0539	0.0610	0.0672
a_{11}				0.0122	0.0228	0.0321	0.0403	0.0476
a_{12}						0.0107	0.0200	0.0284
a_{13}								0.0094

Table 18: Shapiro-Wilk Coefficients for Sample Sizes from 27 to 34

	Sample Size							
Coefficient	27	28	29	30	31	32	33	34
a_1	0.4366	0.4328	0.4291	0.4254	0.4220	0.4188	0.4156	0.4127
a_2	0.3018	0.2992	0.2968	0.2944	0.2921	0.2898	0.2876	0.2854
a_3	0.2522	0.2510	0.2499	0.2487	0.2475	0.2463	0.2451	0.2439
a_4	0.2152	0.2151	0.2150	0.2148	0.2145	0.2141	0.2137	0.2132
a_5	0.1848	0.1857	0.1864	0.1870	0.1874	0.1878	0.1880	0.1882
a_6	0.1584	0.1601	0.1616	0.1630	0.1641	0.1651	0.1660	0.1667
a_7	0.1346	0.1372	0.1395	0.1415	0.1433	0.1449	0.1463	0.1475
a_8	0.1128	0.1162	0.1192	0.1219	0.1243	0.1265	0.1284	0.1301
a_9	0.0923	0.0965	0.1002	0.1036	0.1066	0.1093	0.1118	0.1140
a_{10}	0.0728	0.0778	0.0822	0.0862	0.0899	0.0931	0.0961	0.0988
a_{11}	0.0540	0.0598	0.0650	0.0697	0.0739	0.0777	0.0812	0.0844
a_{12}	0.0358	0.0424	0.0483	0.0537	0.0585	0.0629	0.0669	0.0706
a_{13}	0.0178	0.0253	0.0320	0.0381	0.0435	0.0485	0.0530	0.0572
a_{14}		0.0084	0.0159	0.0227	0.0289	0.0344	0.0395	0.0441
a_{15}				0.0076	0.0144	0.0206	0.0262	0.0314
a_{16}						0.0068	0.0131	0.0187
a_{17}								0.0062

Table 19: Shapiro-Wilk Coefficients for Sample Sizes from 35 to 42

	Sample Size							
Coefficient	35	36	37	38	39	40	41	42
a_1	0.4096	0.4068	0.4040	0.4015	0.3989	0.3964	0.3940	0.3917
a_2	0.2834	0.2813	0.2794	0.2774	0.2755	0.2737	0.2719	0.2701
a_3	0.2427	0.2415	0.2403	0.2391	0.2380	0.2368	0.2357	0.2345
a_4	0.2127	0.2121	0.2116	0.2110	0.2104	0.2098	0.2091	0.2085
a_5	0.1883	0.1883	0.1883	0.1881	0.1880	0.1878	0.1876	0.1874
a_6	0.1673	0.1678	0.1683	0.1686	0.1689	0.1691	0.1693	0.1694
a_7	0.1487	0.1496	0.1505	0.1513	0.1520	0.1526	0.1531	0.1535
a_8	0.1317	0.1331	0.1344	0.1356	0.1366	0.1376	0.1384	0.1392
a_9	0.1160	0.1179	0.1196	0.1211	0.1225	0.1237	0.1249	0.1259
a_{10}	0.1013	0.1036	0.1056	0.1075	0.1092	0.1108	0.1123	0.1136
a_{11}	0.0873	0.0900	0.0924	0.0947	0.0967	0.0986	0.1004	0.1020
a_{12}	0.0739	0.0770	0.0798	0.0824	0.0848	0.0870	0.0891	0.0909
a_{13}	0.0610	0.0645	0.0677	0.0706	0.0733	0.0759	0.0782	0.0804
a_{14}	0.0484	0.0523	0.0559	0.0592	0.0622	0.0651	0.0677	0.0701
a_{15}	0.0361	0.0404	0.0444	0.0481	0.0515	0.0546	0.0575	0.0602
a_{16}	0.0239	0.0287	0.0331	0.0372	0.0409	0.0444	0.0476	0.0506
a_{17}	0.0119	0.0172	0.0220	0.0264	0.0305	0.0343	0.0379	0.0411
a_{18}		0.0057	0.0110	0.0158	0.0203	0.0244	0.0283	0.0318
a_{19}				0.0053	0.0101	0.0146	0.0188	0.0227
a_{20}						0.0049	0.0094	0.0136
a_{21}								0.0045

Table 20: Shapiro-Wilk Coefficients for Sample Sizes from 43 to 50

	Sample Size							
Coefficient	43	44	45	46	47	48	49	50
a_1	0.3894	0.3872	0.3850	0.3830	0.3808	0.3789	0.3770	0.3751
a_2	0.2684	0.2667	0.2651	0.2635	0.2620	0.2604	0.2589	0.2574
a_3	0.2334	0.2323	0.2313	0.2302	0.2291	0.2281	0.2271	0.2260
a_4	0.2078	0.2072	0.2065	0.2058	0.2052	0.2045	0.2038	0.2032
a_5	0.1871	0.1868	0.1865	0.1862	0.1859	0.1855	0.1851	0.1847
a_6	0.1695	0.1695	0.1695	0.1695	0.1695	0.1693	0.1692	0.1691
a_7	0.1539	0.1542	0.1545	0.1548	0.1550	0.1551	0.1553	0.1554
a_8	0.1398	0.1405	0.1410	0.1415	0.1420	0.1423	0.1427	0.1430
a_9	0.1269	0.1278	0.1286	0.1293	0.1300	0.1306	0.1312	0.1317
a_{10}	0.1149	0.1160	0.1170	0.1180	0.1189	0.1197	0.1205	0.1212
a_{11}	0.1035	0.1049	0.1062	0.1073	0.1085	0.1095	0.1105	0.1113
a_{12}	0.0927	0.0943	0.0959	0.0972	0.0986	0.0998	0.1010	0.1020
a_{13}	0.0824	0.0842	0.0860	0.0876	0.0892	0.0906	0.0919	0.0932
a_{14}	0.0724	0.0745	0.0765	0.0783	0.0801	0.0817	0.0832	0.0846
a_{15}	0.0628	0.0651	0.0673	0.0694	0.0713	0.0731	0.0748	0.0764
a_{16}	0.0534	0.0560	0.0584	0.0607	0.0628	0.0648	0.0667	0.0685
a_{17}	0.0442	0.0471	0.0497	0.0522	0.0546	0.0568	0.0588	0.0608
a_{18}	0.0352	0.0383	0.0412	0.0439	0.0465	0.0489	0.0511	0.0532
a_{19}	0.0263	0.0296	0.0328	0.0357	0.0385	0.0411	0.0436	0.0459
a_{20}	0.0175	0.0211	0.0245	0.0277	0.0307	0.0335	0.0361	0.0386
a_{21}	0.0087	0.0126	0.0163	0.0197	0.0229	0.0259	0.0288	0.0314
a_{22}		0.0042	0.0081	0.0118	0.0153	0.0185	0.0215	0.0244
a_{23}				0.0039	0.0076	0.0111	0.0143	0.0174
a_{24}						0.0037	0.0071	0.0104
a_{25}								0.0035

The Shapiro-Wilk statistic is tabulated in Reference 26 with respect to the sample size (n) and the probability (p) of erroneously rejecting the null hypothesis (H_0). The statistic may be interpolated between the values in Table 21 on the row corresponding to the sample size to obtain the probability from the table heading, as recommended by Reference 25. Letting j be the index of the last column that is less than or equal to the statistic, limited so as to prevent extrapolating beyond the provided values, Equation 84 performs the interpolation.

Table 21: Shapiro-Wilk Statistic

Sample	Probability or Significance Level								
Size	1%	2%	5%	10%	50%	90%	95%	98%	99%
3	0.753	0.756	0.767	0.789	0.959	0.998	0.999	1.000	1.000
4	0.687	0.707	0.748	0.792	0.935	0.987	0.992	0.996	0.997
5	0.686	0.715	0.762	0.806	0.927	0.979	0.986	0.991	0.993
6	0.713	0.743	0.788	0.826	0.927	0.974	0.981	0.986	0.989
7	0.730	0.760	0.803	0.838	0.928	0.972	0.979	0.985	0.988
8	0.749	0.778	0.818	0.851	0.932	0.972	0.978	0.984	0.987
9	0.764	0.791	0.829	0.859	0.935	0.972	0.978	0.984	0.986
10	0.781	0.806	0.842	0.869	0.938	0.972	0.978	0.983	0.986

Table 21: Shapiro-Wilk Statistic, Continued

Sample Size	Probability or Significance Level								
	1%	2%	5%	10%	50%	90%	95%	98%	99%
11	0.792	0.817	0.850	0.876	0.940	0.973	0.979	0.984	0.986
12	0.805	0.828	0.859	0.883	0.943	0.973	0.979	0.984	0.986
13	0.814	0.837	0.866	0.889	0.945	0.974	0.979	0.984	0.986
14	0.825	0.846	0.874	0.895	0.947	0.975	0.980	0.984	0.986
15	0.835	0.855	0.881	0.901	0.950	0.975	0.980	0.984	0.987
16	0.844	0.863	0.887	0.906	0.952	0.976	0.981	0.985	0.987
17	0.851	0.869	0.892	0.910	0.954	0.977	0.981	0.985	0.987
18	0.858	0.874	0.897	0.914	0.956	0.978	0.982	0.986	0.988
19	0.863	0.879	0.901	0.917	0.957	0.978	0.982	0.986	0.988
20	0.868	0.884	0.905	0.920	0.959	0.979	0.983	0.986	0.988
21	0.873	0.888	0.908	0.923	0.960	0.980	0.983	0.987	0.989
22	0.878	0.892	0.911	0.926	0.961	0.980	0.984	0.987	0.989
23	0.881	0.895	0.914	0.928	0.962	0.981	0.984	0.987	0.989
24	0.884	0.898	0.916	0.930	0.963	0.981	0.984	0.987	0.989
25	0.888	0.901	0.918	0.931	0.964	0.981	0.985	0.988	0.989
26	0.891	0.904	0.920	0.933	0.965	0.982	0.985	0.988	0.989
27	0.894	0.906	0.923	0.935	0.965	0.982	0.985	0.988	0.990
28	0.896	0.908	0.924	0.936	0.966	0.982	0.985	0.988	0.990
29	0.898	0.910	0.926	0.937	0.966	0.982	0.985	0.988	0.990
30	0.900	0.912	0.927	0.939	0.967	0.983	0.985	0.988	0.990
31	0.902	0.914	0.929	0.940	0.967	0.983	0.986	0.988	0.990
32	0.904	0.915	0.930	0.941	0.968	0.983	0.986	0.988	0.990
33	0.906	0.917	0.931	0.942	0.968	0.983	0.986	0.989	0.990
34	0.908	0.919	0.933	0.943	0.969	0.983	0.986	0.989	0.990
35	0.910	0.920	0.934	0.944	0.969	0.984	0.986	0.989	0.990
36	0.912	0.922	0.935	0.945	0.970	0.984	0.986	0.989	0.990
37	0.914	0.924	0.936	0.946	0.970	0.984	0.987	0.989	0.990
38	0.916	0.925	0.938	0.947	0.971	0.984	0.987	0.989	0.990
39	0.917	0.927	0.939	0.948	0.971	0.984	0.987	0.989	0.991
40	0.919	0.928	0.940	0.949	0.972	0.985	0.987	0.989	0.991
41	0.920	0.929	0.941	0.950	0.972	0.985	0.987	0.989	0.991
42	0.922	0.930	0.942	0.951	0.972	0.985	0.987	0.989	0.991
43	0.923	0.932	0.943	0.951	0.973	0.985	0.987	0.990	0.991
44	0.924	0.933	0.944	0.952	0.973	0.985	0.987	0.990	0.991
45	0.926	0.934	0.945	0.953	0.973	0.985	0.988	0.990	0.991
46	0.927	0.935	0.945	0.953	0.974	0.985	0.988	0.990	0.991
47	0.928	0.936	0.946	0.954	0.974	0.985	0.988	0.990	0.991
48	0.929	0.937	0.947	0.954	0.974	0.985	0.988	0.990	0.991
49	0.929	0.938	0.947	0.955	0.974	0.985	0.988	0.990	0.991
50	0.930	0.939	0.947	0.955	0.974	0.985	0.988	0.990	0.991

$$p = p_j + \left(p_{j+1} - p_j\right)\frac{W - W_j}{W_{j+1} - W_j} \tag{84}$$

Alternately, the desired significance level (s) may be selected from the values in the heading of Table 21 to obtain the critical value of the Shapiro-Wilk statistic (W_c) from the same column and the appropriate row for the sample size (n). The criterion for the probability is to admit the possibility that a normal or log-normal distribution fits the data if $p \geq s$. The distribution is also considered a possible fit if $W \geq W_c$. These two methods are equivalent because the same statistic is evaluated with respect to the same tabular values. Table 22 summarizes the results of the Shapiro-Wilk tests for the normal and log-normal distributions. The Shapiro-Wilk test is more lenient than the Anderson-Darling test for this data set because it admits both distributions with sufficient margin. Reference 22 states that the Anderson-Darling test is more sensitive to variance between the data and the tails of the distribution, whereas the Shapiro-Wilk test is more sensitive to outliers. References 16 and 23 consider the Shapiro-Wilk test to be slightly more accurate than the Anderson-Darling test for admitting normal distributions and rejecting others. All of these sources concur that the two tests are comparable (Ref. 16, 22, 23).

Table 22: Results of Shapiro-Wilk Tests for the Normal and Log-Normal Distributions

Method	External References	Internal References	Parameter	Normal Distribution	Log-Normal Distribution
General		p. 11	n	24	24
	25	p. 28	d	12	12
	25, 26	Eq. 82, 83; Table 17	W	0.930	0.921
	25	p. 24	s	5.0%	5.0%
1	25, 26	Table 21	p	9.8%	6.6%
	25		Inference	Admit	Admit
2	26	Table 21	W_c	0.916	0.916
			Inference	Admit	Admit

Conclusion

Experiments were performed to measure the energy mitigated by specimens of AISI 304L VAR bar as a cylindrical bar of AISI 4340 steel punctured them. The 24 specimens were cut from the same stock material with the same processes and nominal dimensions. The initial and boundary conditions were kept as similar as possible for all of the tests. These data are amenable to classical statistical inference because there are enough specimens to achieve low variance and positive lower bounds for precision intervals with 95% confidence. The median mitigated energy is within 3% of the sample mean. Given the large sample size (24) and low ratio of the standard deviation to the mean (5.5%), this data set appears adequate for setting precision intervals with bounding probabilities as low as 1% (10E-3) but not lower.

The data are assumed to be normally distributed, though the Weibull distribution might also fit. The parameters of both distributions are conservatively bounded at 95% confidence and used to calculate the lower bounds on the energy mitigated by the AISI 304L steel disc specimens for a range of probabilities (Table 23). Probabilities of one per thousand, million, and billion are included for reference; however, these lower bounds are considered uncertain because they would change significantly if more independent but identically distributed specimens were tested. The probabilities that define the screening thresholds in Reference 11, page 2, are extremely small, but the normal and Weibull distributions yield positive lower bounds for the precision intervals on mitigated energy.

Table 23: Lower Bounds for Mitigated Energy Based on Normal and Weibull Distributions

Bounding Probability	Probability of Lower Future Observation		Normal Distribution (J)	Normal Distribution (ft-lb)	Weibull Distribution (J)	Weibull Distribution (ft-lb)
Median	50%	500E-3	43.0	31.7	43.4	32.0
One in One Hundred	1%	10E-3	35.1	25.9	33.8	25.0
One in One Thousand	0.1%	1E-3	32.5	24.0	29.6	21.8
One in One Million	0.0001%	1E-6	26.9	19.8	19.7	14.6
One in One Billion	0.0000001%	1E-9	22.7	16.7	13.2	9.7

Anderson-Darling and Shapiro-Wilk tests are performed to evaluate the assumption that a normal distribution fits the data. The methods of comparing a probability value to a significance level (Ref. 19, 21, 25) and comparing a statistic to an adjusted critical value (Ref. 14, 18) support the possibility of using the normal distribution to predict future observations similar to the experimental measurements. The methods of comparing an adjusted statistic to a critical value in References 15, 16, and 19 refute this hypothesis. The log-normal, Weibull, and gamma distributions are also considered for bounding future observations because they only predict positive lower bounds for the energy values. The Shapiro-Wilk test supports using both the normal and log-normal distributions, and the Anderson-Darling test admits the Weibull distribution as a possible fit, although the PDF differs visibly from the other proposed distributions (Fig. 10). However, the hypotheses that the log-normal and gamma distributions fit this data set are rejected by all of the Anderson-Darling test methods that were applied. The Shapiro-Wilk and Anderson-Darling tests both confirm that the normal distribution is admissible for setting the lower bounds on the precision intervals of the mitigated energy.

The data set may be improved by increasing the number of specimens. The variance might increase or decrease depending on how consistent the new specimens are with those that have already been tested, but the Student's t parameter would decrease, which would tend to raise the lower bounds. Any additional experiments should be performed according to the same test procedure (Ref. 27) to minimize the variance in the augmented data set. The experiments were performed with specimens from the same stock material, so they experienced the same heat treatments. This minimized the variance and maximized the lower bounds on the mitigated energy at each probability; however, it also neglected differences between heat treatment lots and material production batches. Testing specimens from multiple manufacturers would reduce this unconservative bias.

Uncertainty in the measurements of the energy mitigated by each specimen is due to the accuracy of the laser interferometers, machining tolerances, spatial variation in material properties (non-homogeneity), and the stochastic nature of ductile fracture. The acceleration data serves as a trigger for selecting the time ranges over which to average the total energy, but the energy is calculated solely from the position data, and the trigger times are adjusted such that the intervals appear reasonable on the total energy plot. Therefore, error in the accelerometer has no influence on the test results. The specimens are manufactured with reasonable tolerances and surface roughness limits for milling operations. The variation in thickness can be as much as 3% and remain within the tolerance limits. The hardness of 304L VAR steel has been shown to vary by 5% over a cross-section of a bar (Ref. 28). Ductile fracture occurs when voids form in the material and coalesce into cracks. The locations of voids and the reduction in the engineering strength as they grow and combine depend on the microstructure, which is not known before a component fractures and is,

therefore, assumed to be homogeneous. Uncertainty about the microstructure makes the crack paths appear random although they follow patterns based on the boundary conditions.

The methods described in this memorandum may be applied to setting energy thresholds based on experiments with continuous results (real numbers). Logistic regression (Ref. 29, 30) applies to experiments that have binary results, such as those that measure the mechanical impact energy that causes a pyrotechnic material to react.

Considering the assumptions and limitations of statistics, the simpler method of applying a safety factor may be preferred. Dividing by a safety factor of 1.5, the sample mean of the mitigated energy is reduced to 29.4 J (21.7 ft-lb). This method credits engineering judgement that a future test of a specimen made to the same specifications would mitigate at least two-thirds as much energy as the average of the specimens in the sample.

References

1. Waymel, R., "MIP Puncture Disc Results," Sandia National Laboratories, 15 July 2020.
2. Figliola, R. S., and Beasley, D. E., *Theory and Design for Mechanical Measurements*, 3rd ed., John Wiley & Sons, 2000.
3. Ross, S., *A First Course in Probability*, 5th ed., Prentice Hall, 1998.
4. Bain, L. J., and Engelhardt, M., *Introduction to Probability and Mathematical Statistics*, 2nd ed., Duxbury Press, 1992.
5. National Institute of Standards and Technology with Semiconductor Manufacturing Technology, "Engineering Statistics Handbook: §1.3.6.6.1. Normal Distribution," U.S. Department of Commerce, https://www.itl.nist.gov/div898/handbook/eda/section3/eda3661.htm, Accessed 30 September 2024.
6. National Institute of Standards and Technology with Semiconductor Manufacturing Technology, "Engineering Statistics Handbook: §1.3.6.6.4. t Distribution," U.S. Department of Commerce, https://www.itl.nist.gov/div898/handbook/eda/section3/eda3664.htm, Accessed 30 September 2024.
7. National Institute of Standards and Technology with Semiconductor Manufacturing Technology, "Engineering Statistics Handbook: §1.3.6.6.6. Chi-Square Distribution," U.S. Department of Commerce, https://www.itl.nist.gov/div898/handbook/eda/section3/eda3666.htm, Accessed 30 September 2024.
8. National Institute of Standards and Technology with Semiconductor Manufacturing Technology, "Engineering Statistics Handbook: §1.3.6.6.9. Lognormal Distribution," U.S. Department of Commerce, https://www.itl.nist.gov/div898/handbook/eda/section3/eda3669.htm, Accessed 30 September 2024.
9. National Institute of Standards and Technology with Semiconductor Manufacturing Technology, "Engineering Statistics Handbook: §1.3.6.6.8. Weibull Distribution," U.S. Department of Commerce, , Accessed 3 February 2025.
10. National Institute of Standards and Technology with Semiconductor Manufacturing Technology, "Engineering Statistics Handbook: §1.3.6.6.11. Gamma Distribution," U.S. Department of Commerce, , Accessed 3 February 2025.
11. Department of Energy, DOE-NA-STD-3016-2023, "Hazard Analysis Reports for Nuclear Explosive Operations," 2023.
12. Weapon Response Analysis Department, "Use of Safety Factors in Weapon Response Technical Basis," Sandia National Laboratories, 28 February 2024.

13. Anderson, T. W., and Darling, D. A., "Asymptotic Theory of Certain 'Goodness of Fit' Criteria Based on Stochastic Processes," *Annals of Mathematical Statistics*, Vol. 23, No. 2, pp. 193–212, June 1952.
14. Department of Defense, MIL-HDBK-5J, "Metallic Materials and Elements for Aerospace Vehicle Structures," 31 January 2003.
15. National Institute of Standards and Technology with Semiconductor Manufacturing Technology, "Engineering Statistics Handbook: §1.3.5.14. Anderson-Darling Test," U.S. Department of Commerce, https://www.itl.nist.gov/div898/handbook/eda/section3/eda35e.htm, Accessed 8 November 2023.
16. Stephens, M. A., "EDF Statistics for Goodness of Fit and Some Comparisons," *Journal of the American Statistical Association*, Vol. 69, No. 347, pp. 730–737, September 1974.
17. Stephens, M. A., "Asymptotic Results for Goodness-of-Fit Statistics with Unknown Parameters," *The Annals of Statistics*, Vol. 4, No. 2, pp. 357–369, 1976.
18. Romeu, J. L., "Anderson-Darling: A Goodness of Fit Test for Small Samples Assumptions," *Selected Topics in Assurance Related Technologies*, Vol. 10, No. 5, Department of Defense, Reliability Analysis Center, https://web.cortland.edu/matresearch/AndrsDarlSTART.pdf, Accessed 8 November 2023.
19. Zaiontz, C., "One-Sample Anderson-Darling Test," https://real-statistics.com/non-parametric-tests/goodness-of-fit-tests/anderson-darling-test, Accessed 8 November 2023.
20. Zaiontz, C., "One-Sample Anderson-Darling Test Table," https://real-statistics.com/statistics-tables/anderson-darling-test-table, Accessed 8 November 2023.
21. SPC for Excel Software, "Anderson-Darling Test for Normality," https://www.spcforexcel.com/knowledge/basic-statistics/anderson-darling-test-for-normality, Accessed 8 November 2023.
22. SixSigma, "A Complete Guide to the Anderson-Darling Normality Test," https://www.6sigma.us/six-sigma-in-focus/anderson-darling-normality-test, 31 July 2024, Accessed 3 October 2024.
23. Razali, N. M., and Wah, Y. B., "Power Comparisons of Shapiro-Wilk, Kolmogorov-Smirnov, Lilliefors and Anderson-Darling Tests," *Journal of Statistical Modeling and Analytics*, Vol. 2, No. 1, pp. 21–33, 2011.
24. Shapiro, S. S., and Wilk, M. B., "An Analysis of Variance Test for Normality (Complete Samples)," *Biometrika*, Vol. 52, Nos. 3–4, pp. 591–611, 1 December 1965.
25. Zaiontz, C., "Shapiro-Wilk Original Test," https://real-statistics.com/tests-normality-and-symmetry/statistical-tests-normality-symmetry/shapiro-wilk-test, Accessed 30 January 2025.
26. Zaiontz, C., "Shapiro-Wilk Tables," https://real-statistics.com/statistics-tables/shapiro-wilk-table, Accessed 30 January 2025.
27. Hubbard, N., "Test Plan for 304L Steel Puncture Specimens," Sandia National Laboratories, 6 April 2020.
28. Kramer, S., Antoun, B., Lu, W., Jones, A., Sanborn, B., Song, B., Jin, H., and Deibler, L., SAND2019-10152PE, "DE L2 Milestone Presentation: Ductile Failure," Sandia National Laboratories, 21 August 2019.
29. Kleinbaum, D. G., and Klein, M., *Logistic Regression: A Self-Learning Text*, 3rd ed., Springer, 2010, https://link.springer.com/book/10.1007/978-1-4419-1742-3, Accessed 12 March 2025.
30. Neyer, B. T., "A D-Optimality-Based Sensitivity Test," *Technometrics*, Vol. 36, No. 1, pp. 61–70, February 1994.

Appendix A: Acceleration

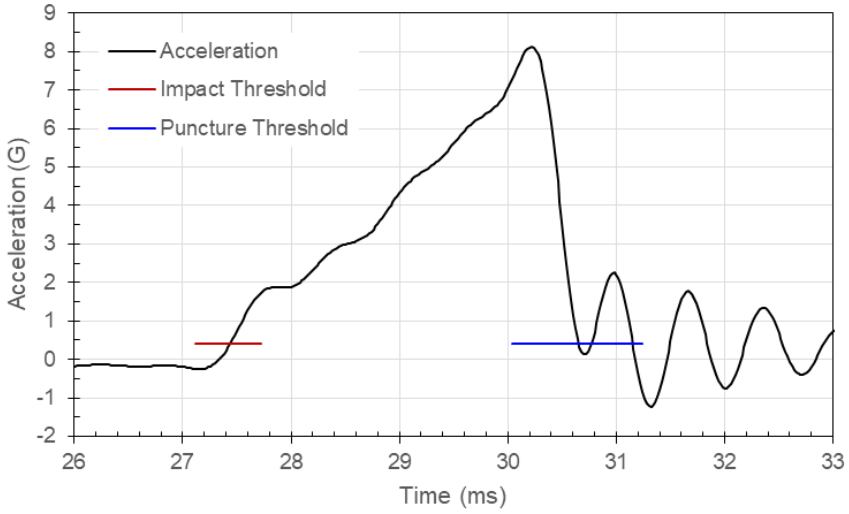

Figure 13: Carriage Acceleration in Test 7 with Specimen 1

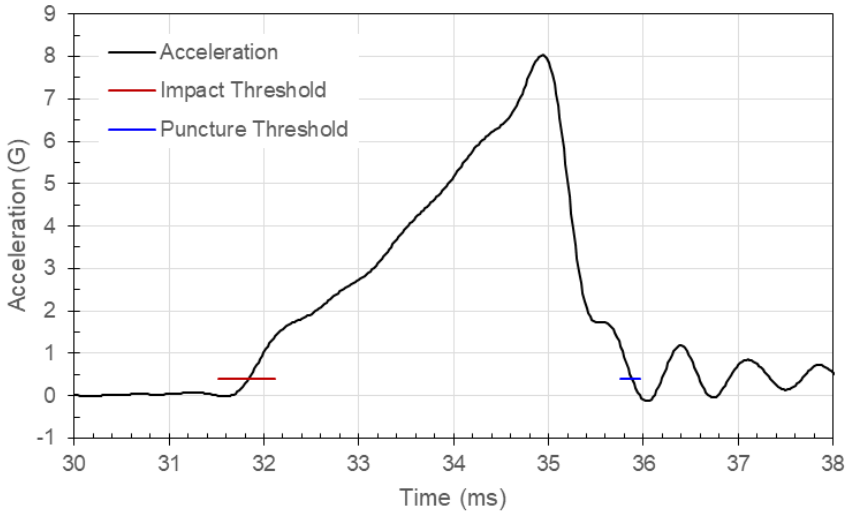

Figure 14: Carriage Acceleration in Test 10 with Specimen 2

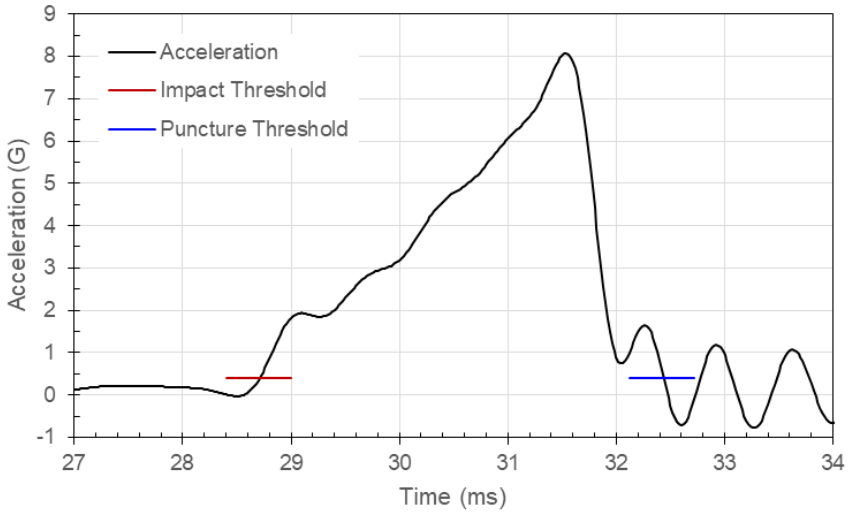

Figure 15: Carriage Acceleration in Test 8 with Specimen 3

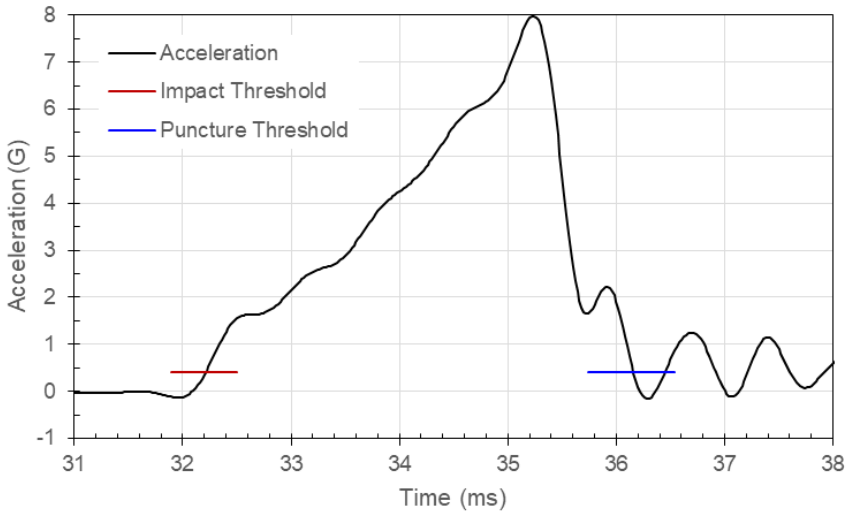

Figure 16: Carriage Acceleration in Test 11 with Specimen 4

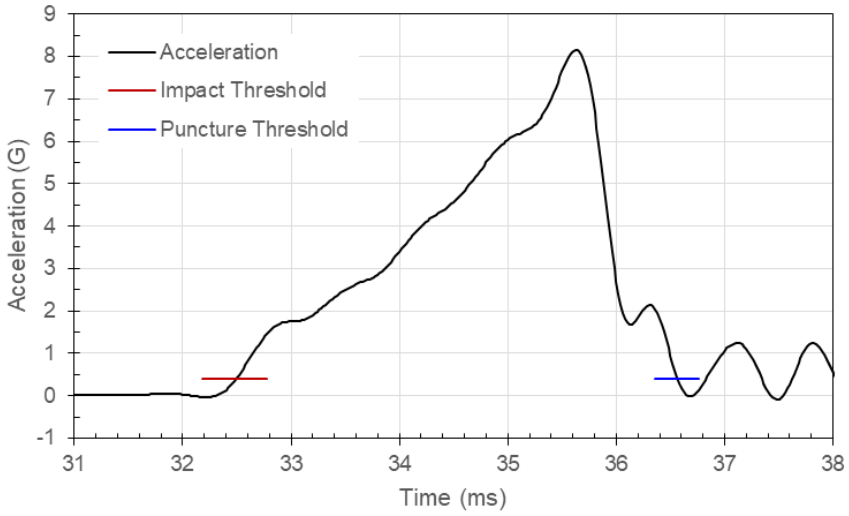

Figure 17: Carriage Acceleration in Test 12 with Specimen 5

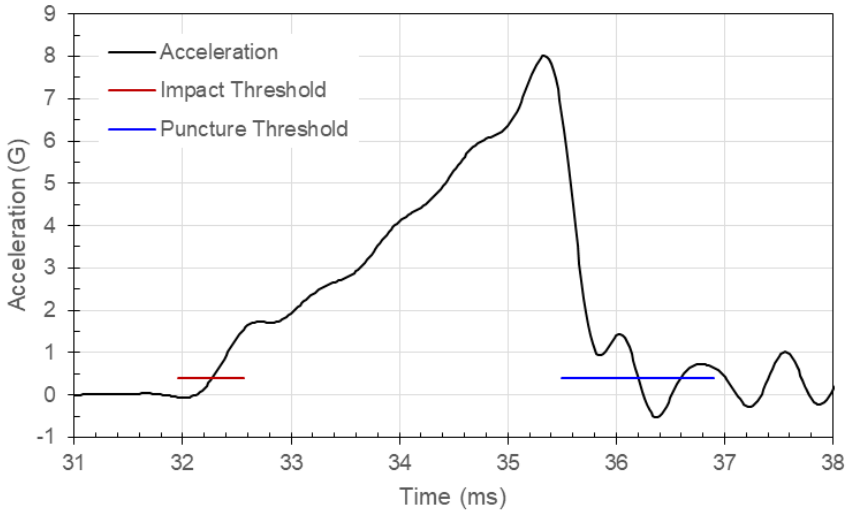

Figure 18: Carriage Acceleration in Test 13 with Specimen 6

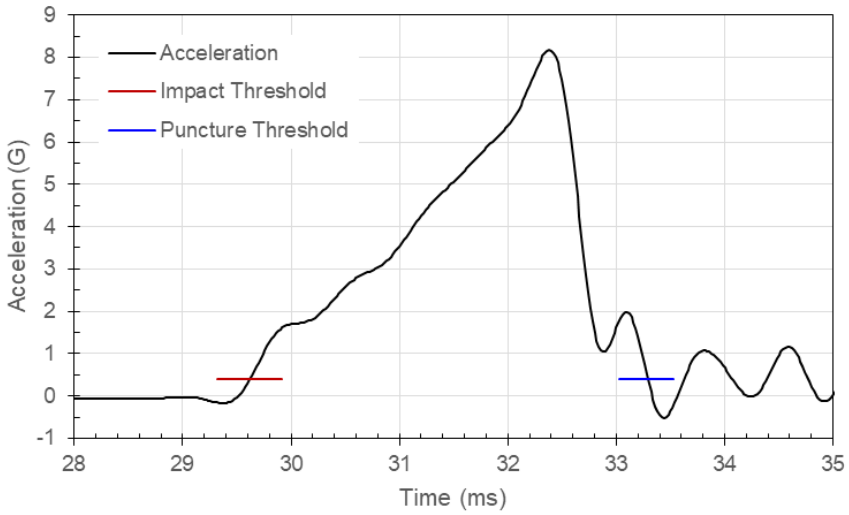

Figure 19: Carriage Acceleration in Test 14 with Specimen 7

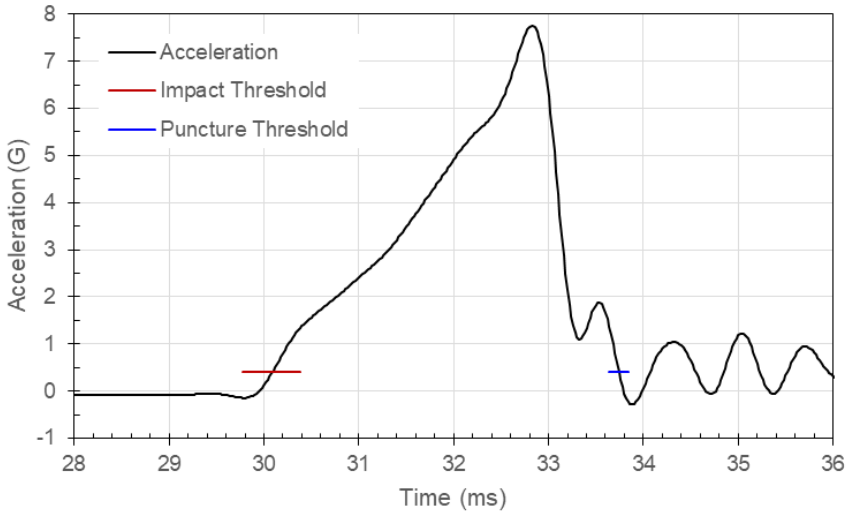

Figure 20: Carriage Acceleration in Test 15 with Specimen 8

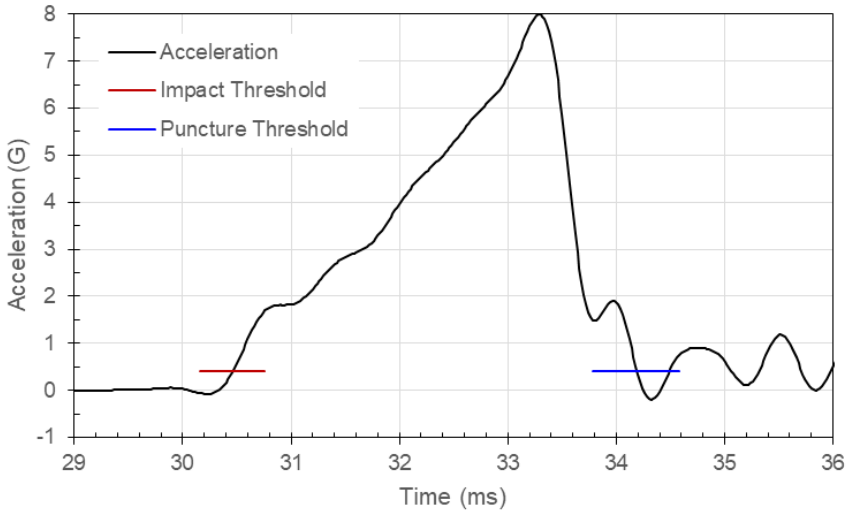

Figure 21: Carriage Acceleration in Test 16 with Specimen 9

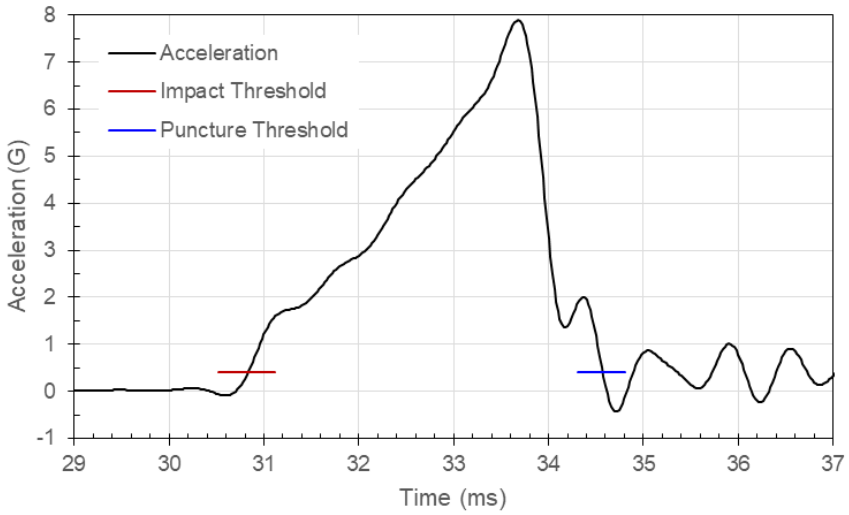

Figure 22: Carriage Acceleration in Test 17 with Specimen 10

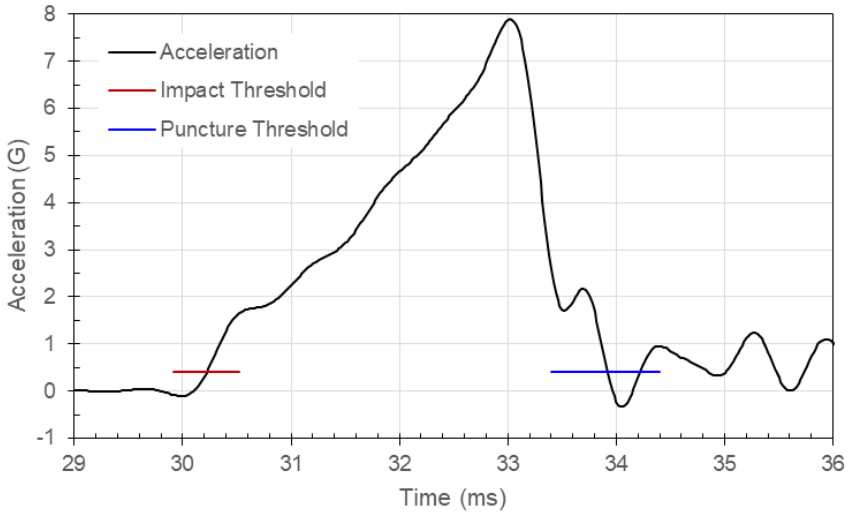

Figure 23: Carriage Acceleration in Test 18 with Specimen 11

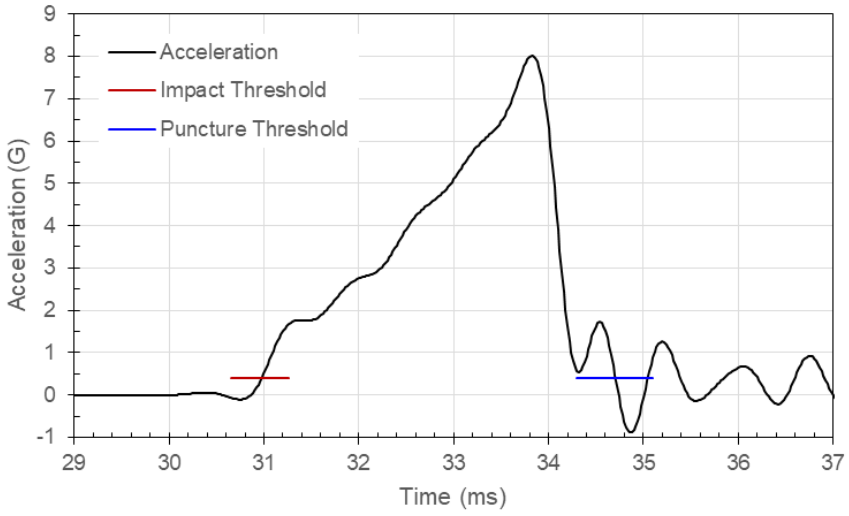

Figure 24: Carriage Acceleration in Test 19 with Specimen 12

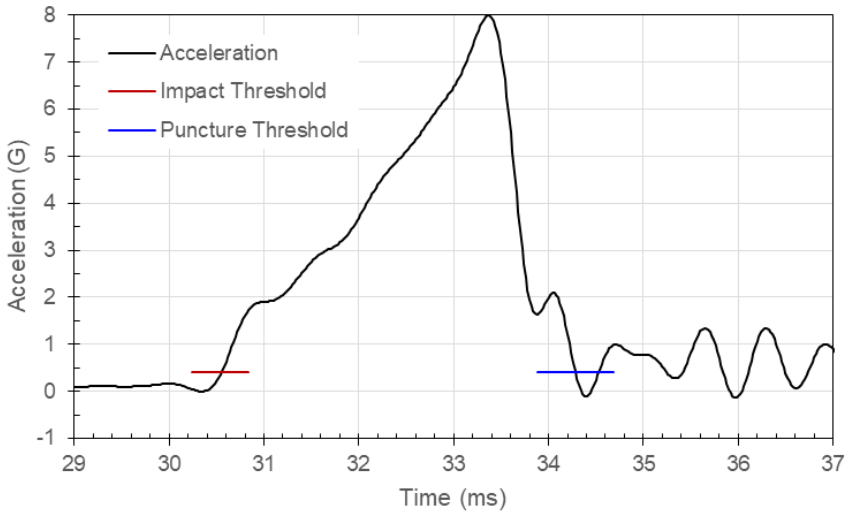

Figure 25: Carriage Acceleration in Test 20 with Specimen 13

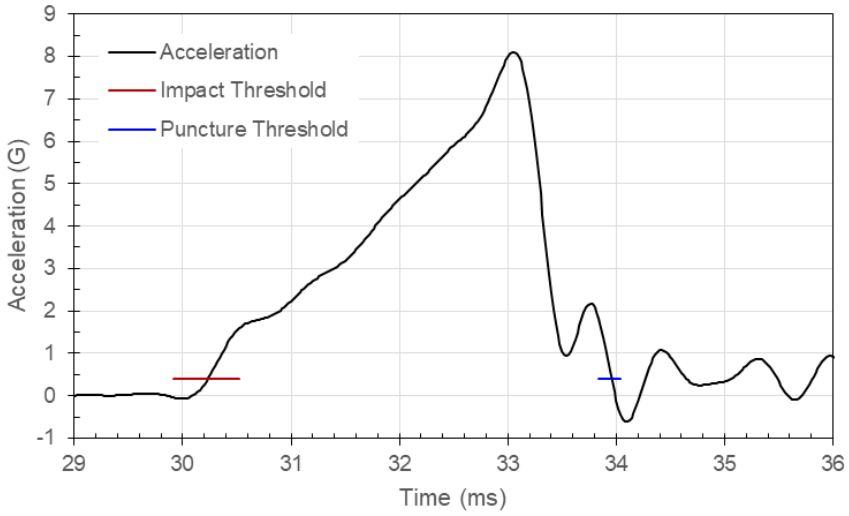

Figure 26: Carriage Acceleration in Test 21 with Specimen 14

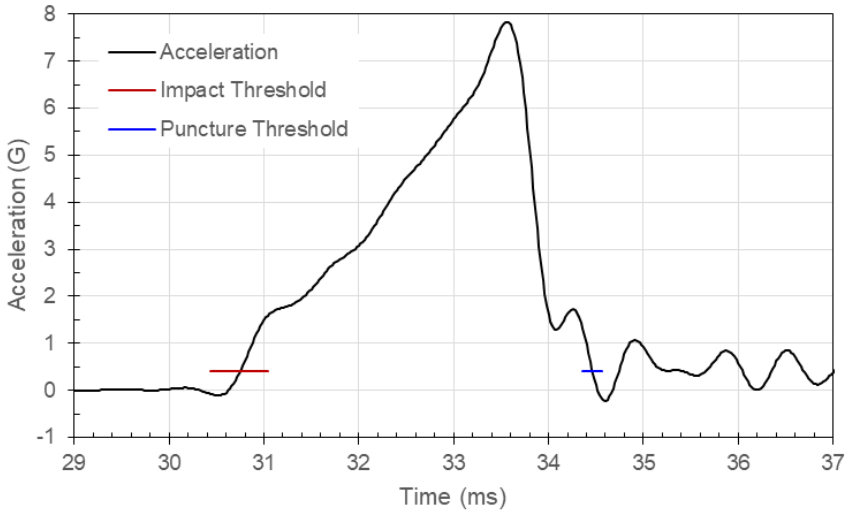

Figure 27: Carriage Acceleration in Test 22 with Specimen 15

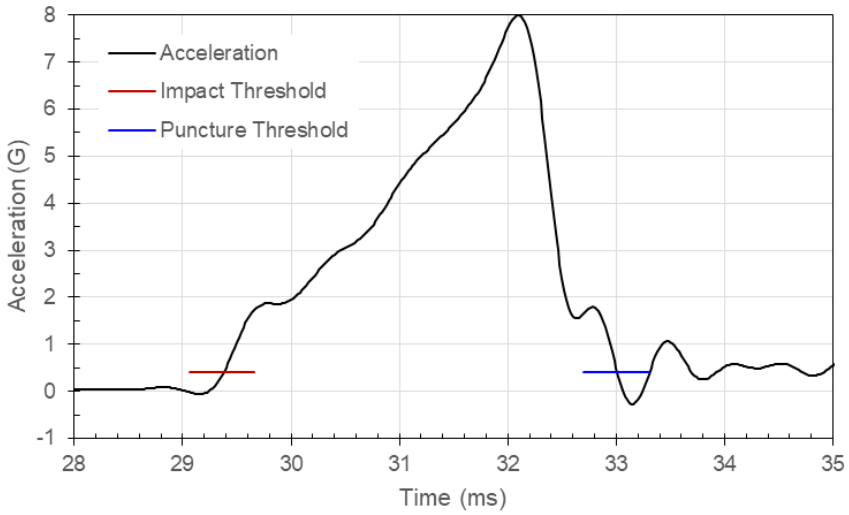

Figure 28: Carriage Acceleration in Test 23 with Specimen 16

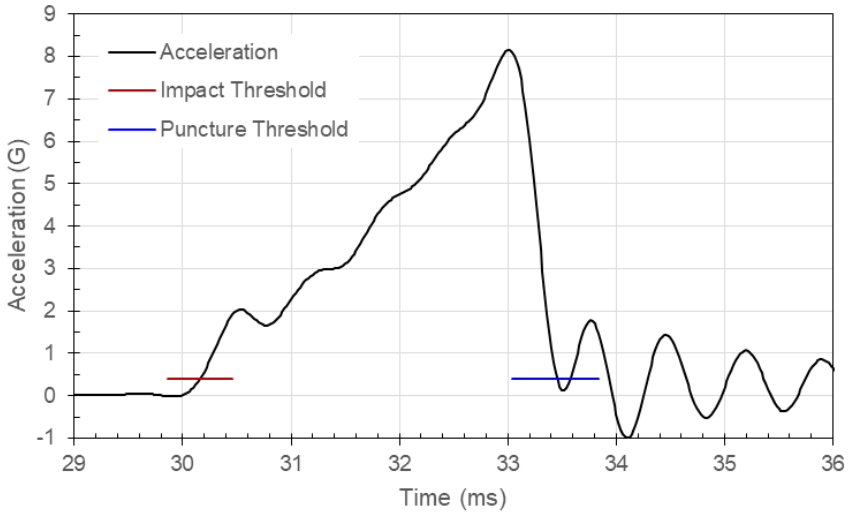

Figure 29: Carriage Acceleration in Test 24 with Specimen 17

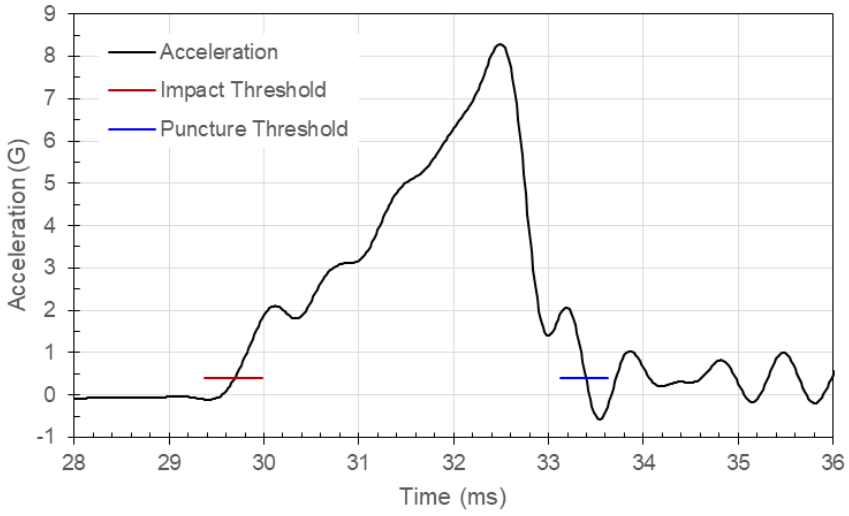

Figure 30: Carriage Acceleration in Test 25 with Specimen 18

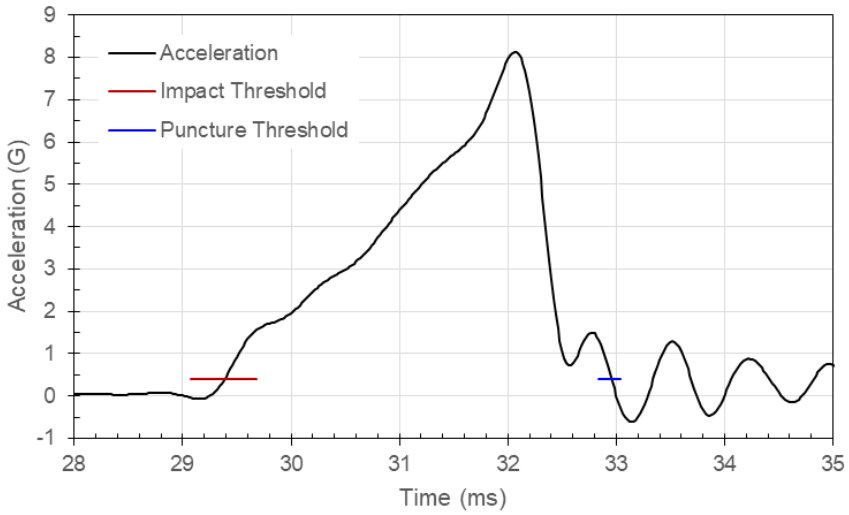

Figure 31: Carriage Acceleration in Test 26 with Specimen 19

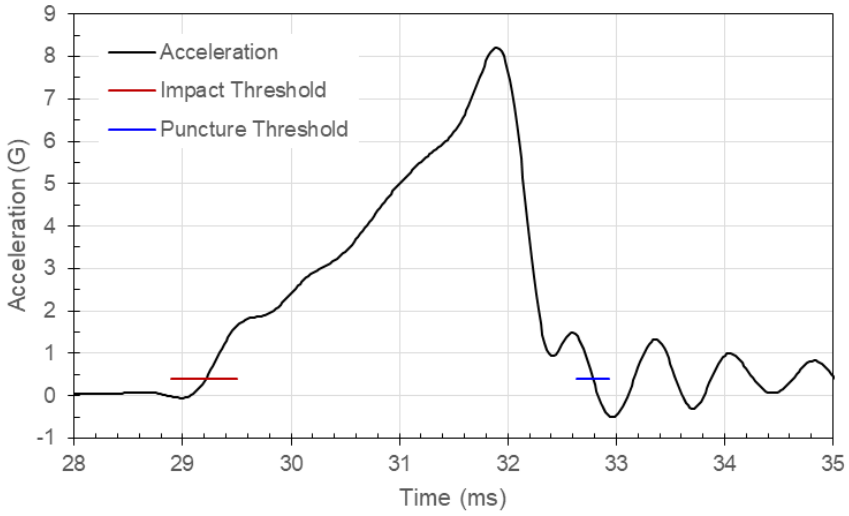

Figure 32: Carriage Acceleration in Test 27 with Specimen 20

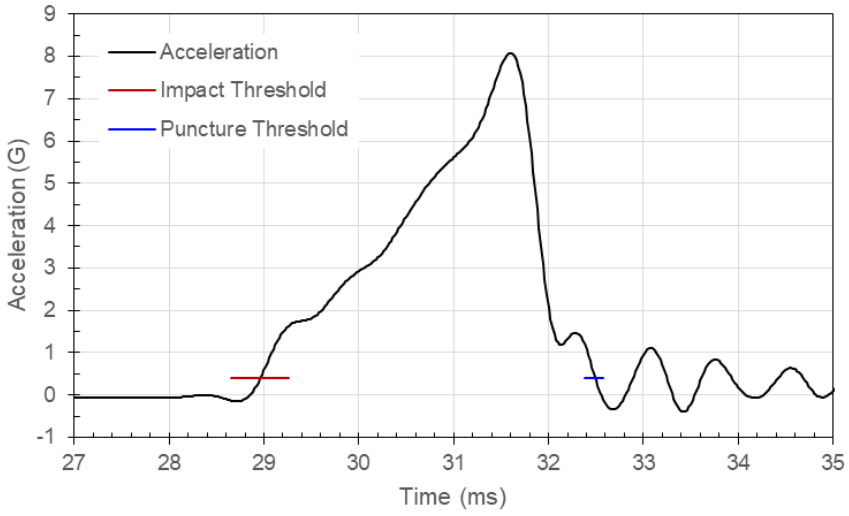

Figure 33: Carriage Acceleration in Test 28 with Specimen 21

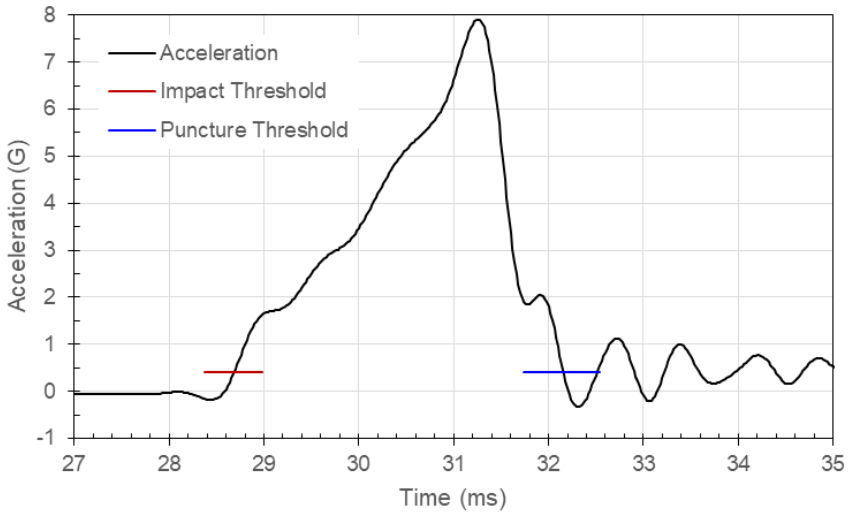

Figure 34: Carriage Acceleration in Test 29 with Specimen 22

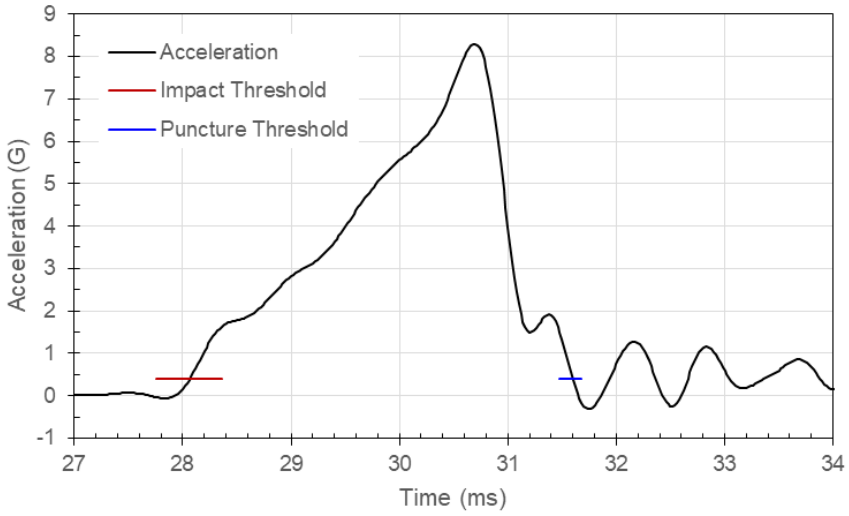

Figure 35: Carriage Acceleration in Test 30 with Specimen 23

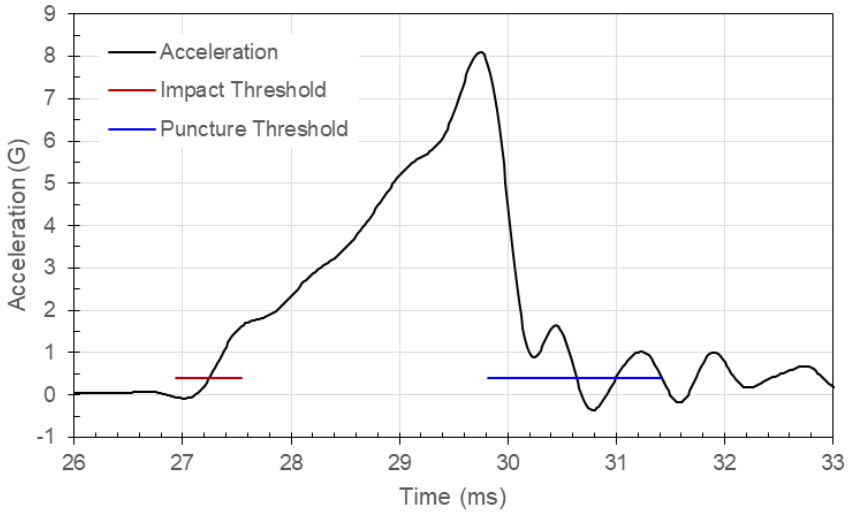

Figure 36: Carriage Acceleration in Test 31 with Specimen 24

Appendix B: Total Energy

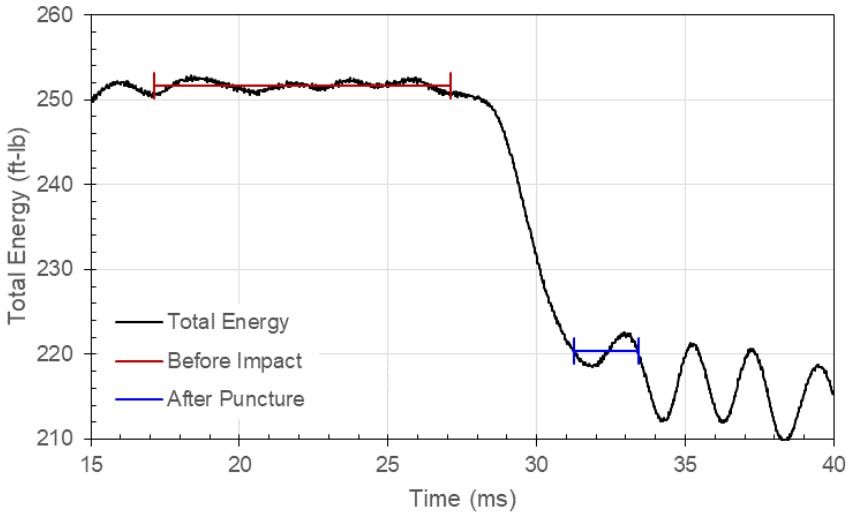

Figure 37: Total Energy in Test 7 with Specimen 1

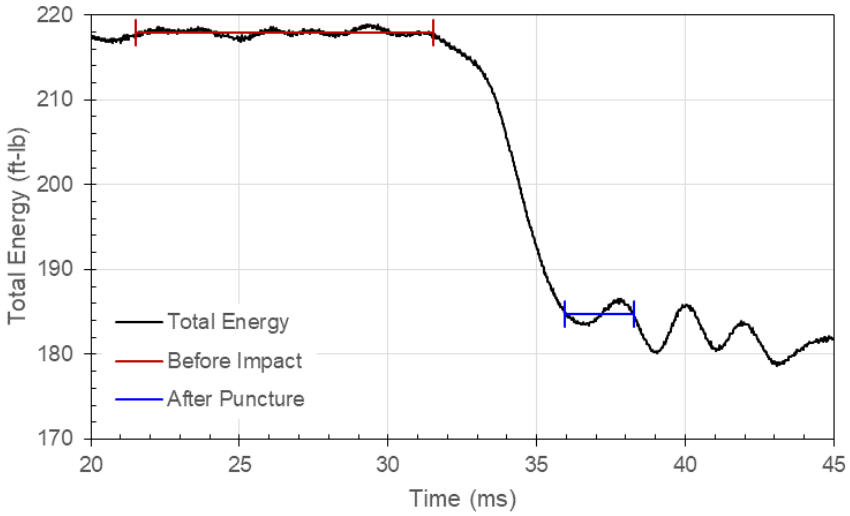

Figure 38: Total Energy in Test 10 with Specimen 2

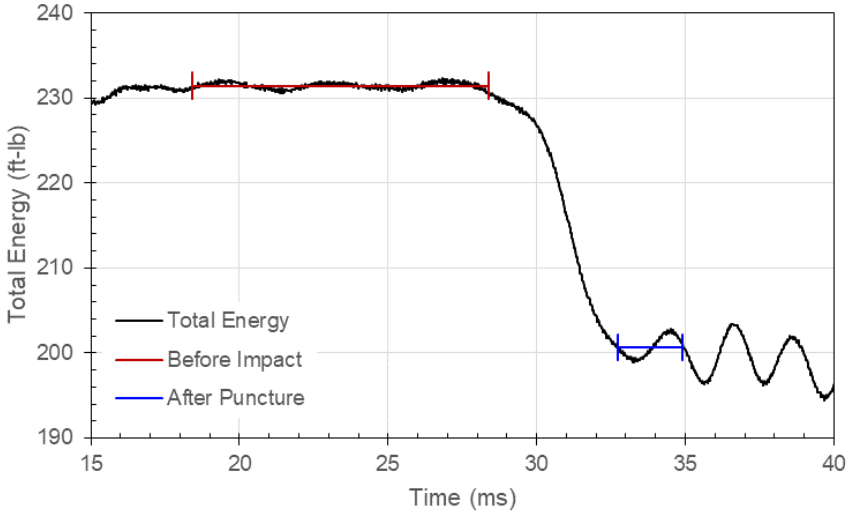

Figure 39: Total Energy in Test 8 with Specimen 3

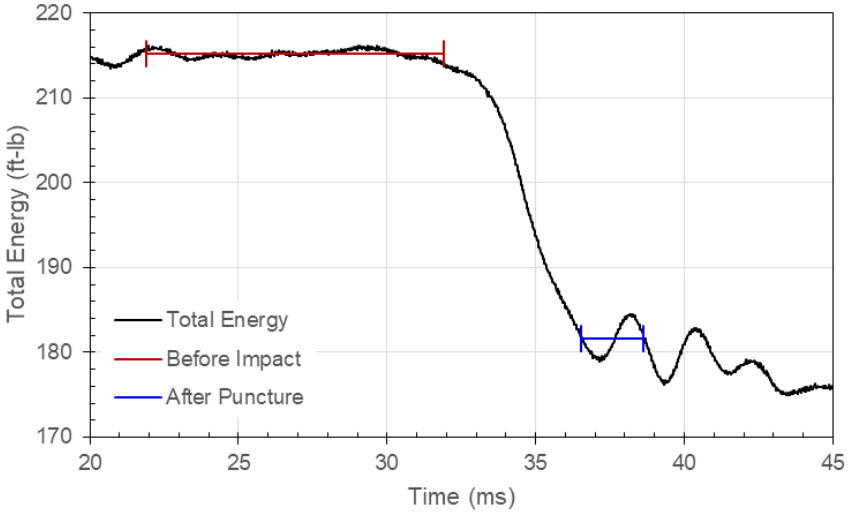

Figure 40: Total Energy in Test 11 with Specimen 4

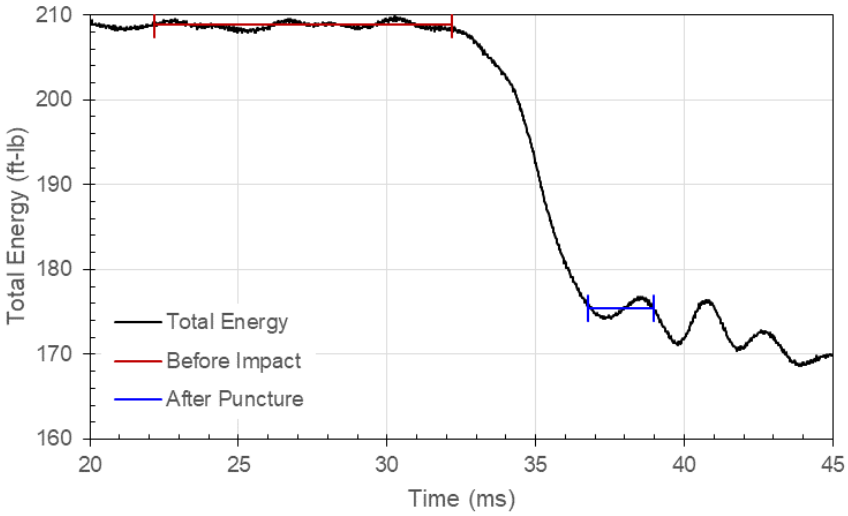

Figure 41: Total Energy in Test 12 with Specimen 5

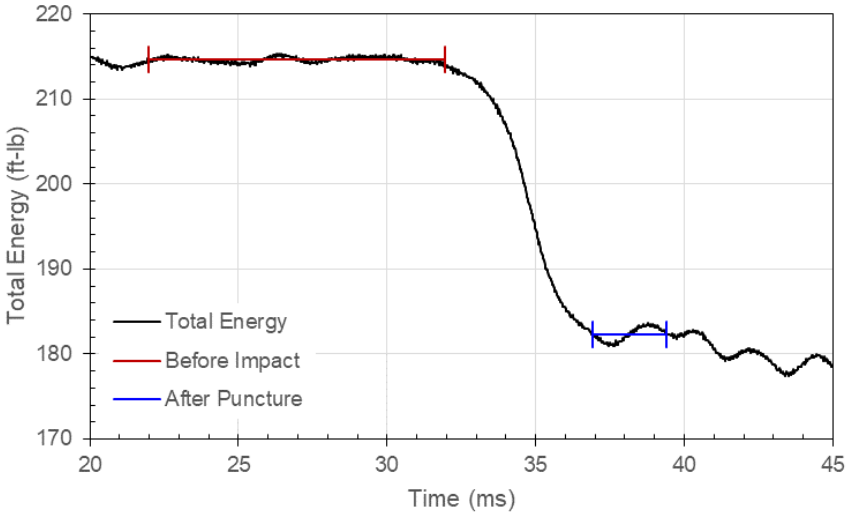

Figure 42: Total Energy in Test 13 with Specimen 6

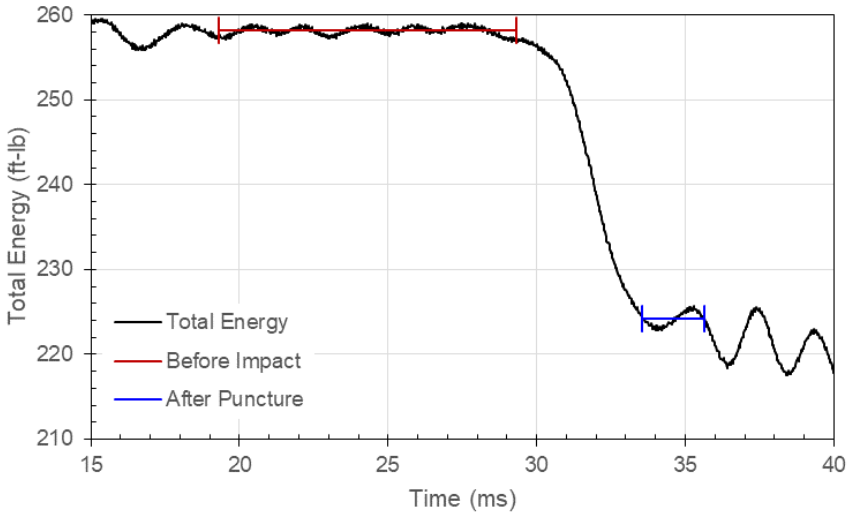

Figure 43: Total Energy in Test 14 with Specimen 7

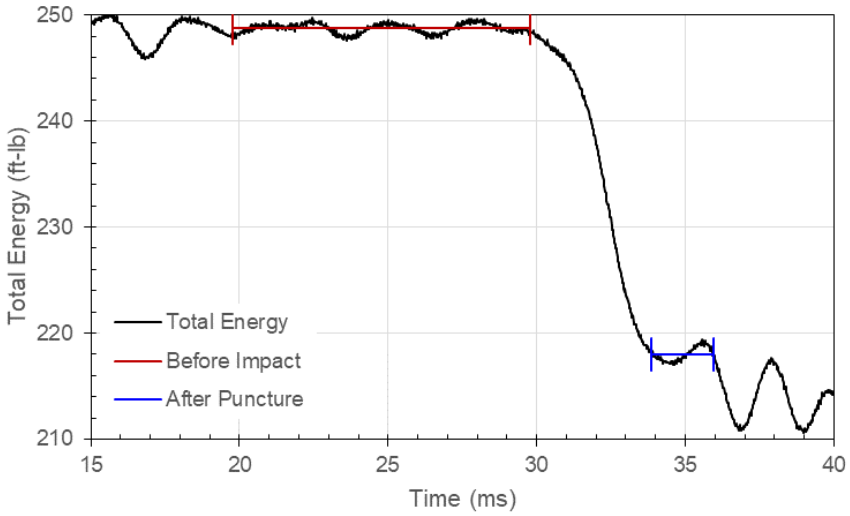

Figure 44: Total Energy in Test 15 with Specimen 8

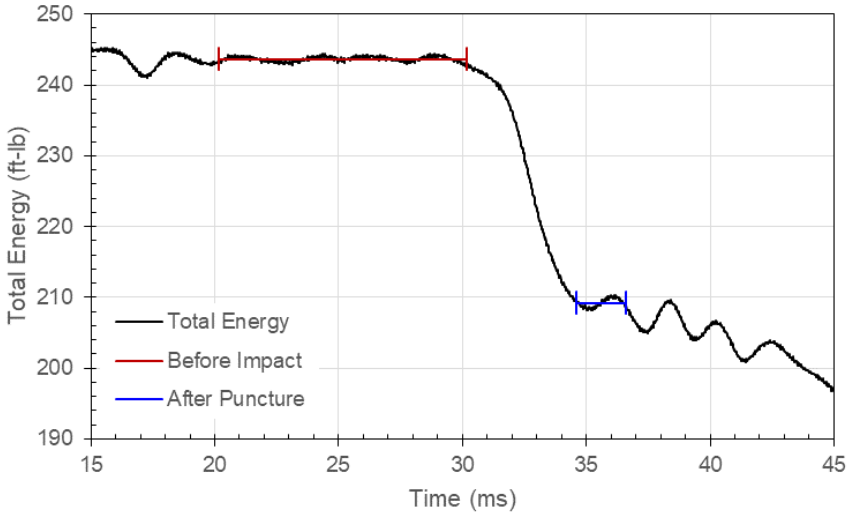

Figure 45: Total Energy in Test 16 with Specimen 9

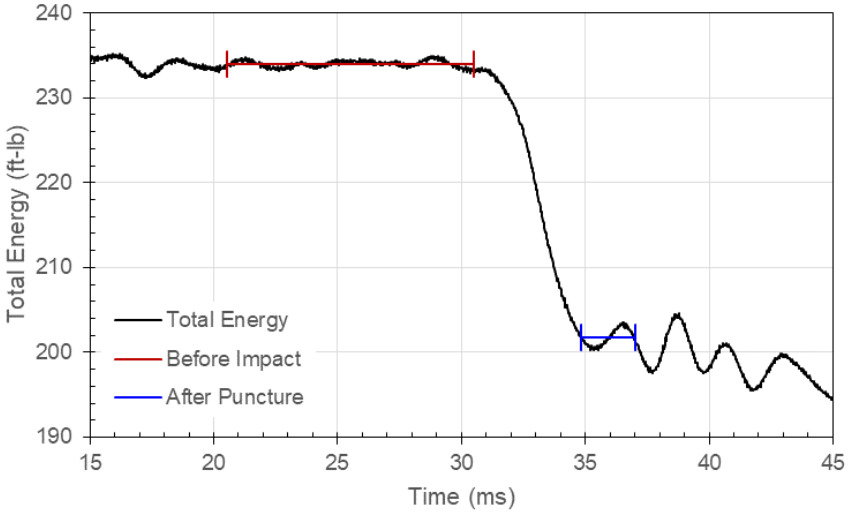

Figure 46: Total Energy in Test 17 with Specimen 10

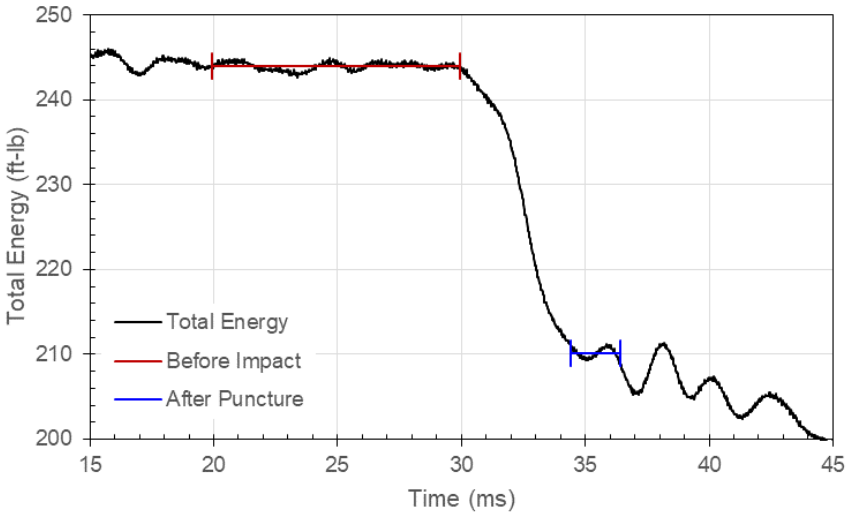

Figure 47: Total Energy in Test 18 with Specimen 11

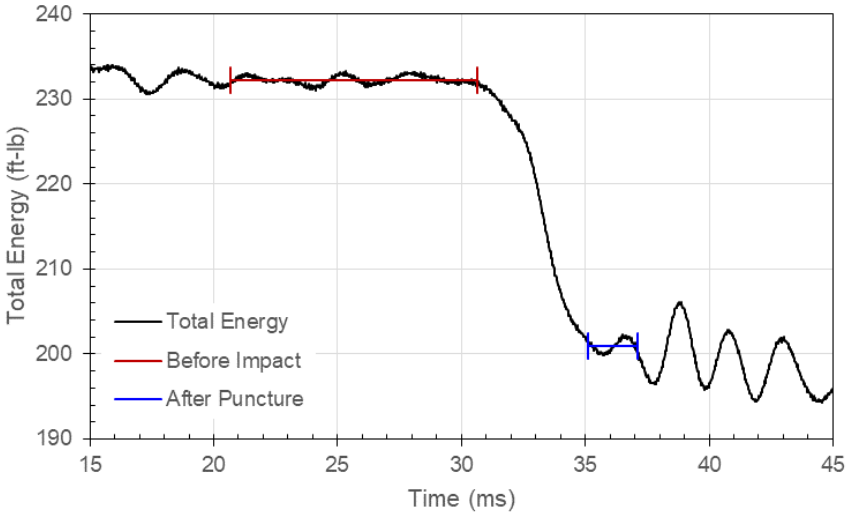

Figure 48: Total Energy in Test 19 with Specimen 12

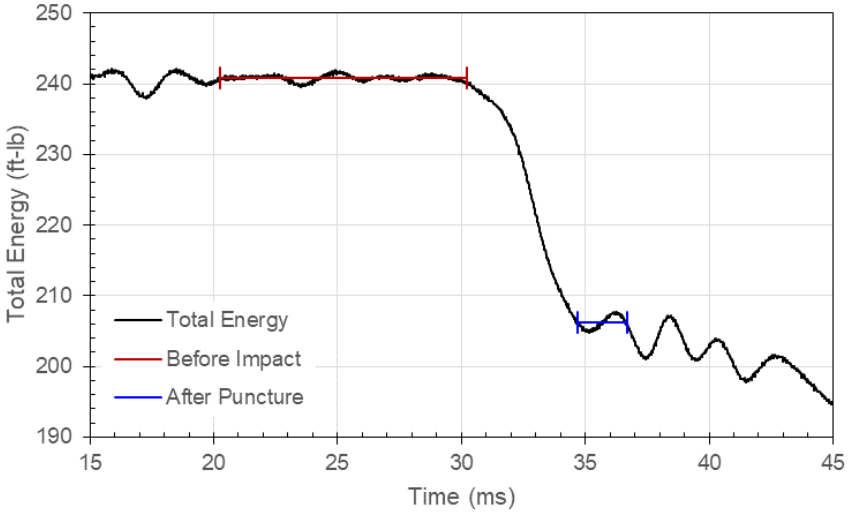

Figure 49: Total Energy in Test 20 with Specimen 13

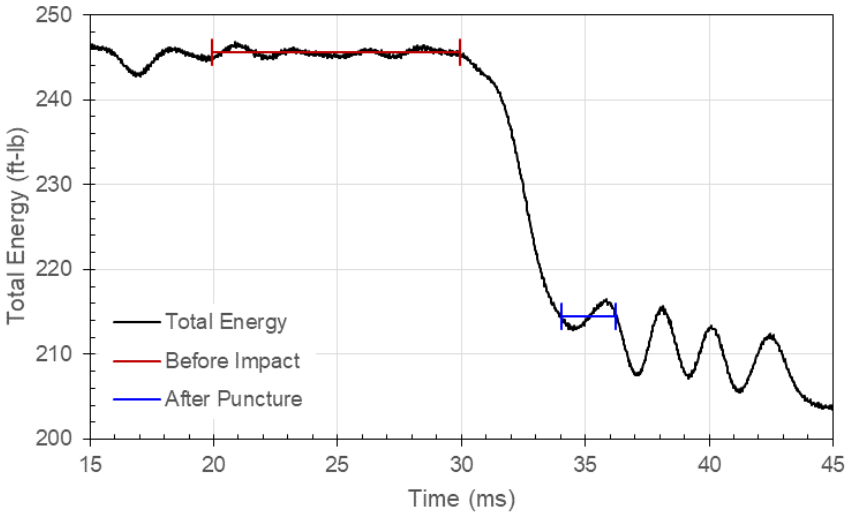

Figure 50: Total Energy in Test 21 with Specimen 14

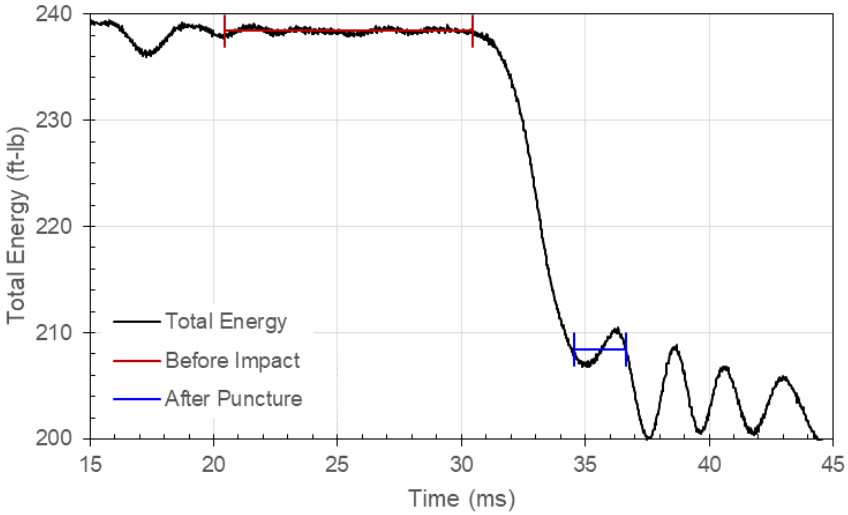

Figure 51: Total Energy in Test 22 with Specimen 15

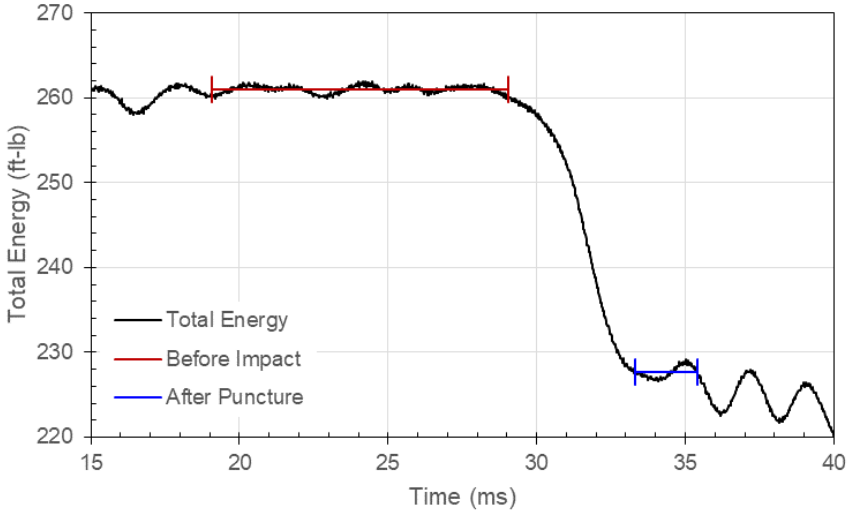

Figure 52: Total Energy in Test 23 with Specimen 16

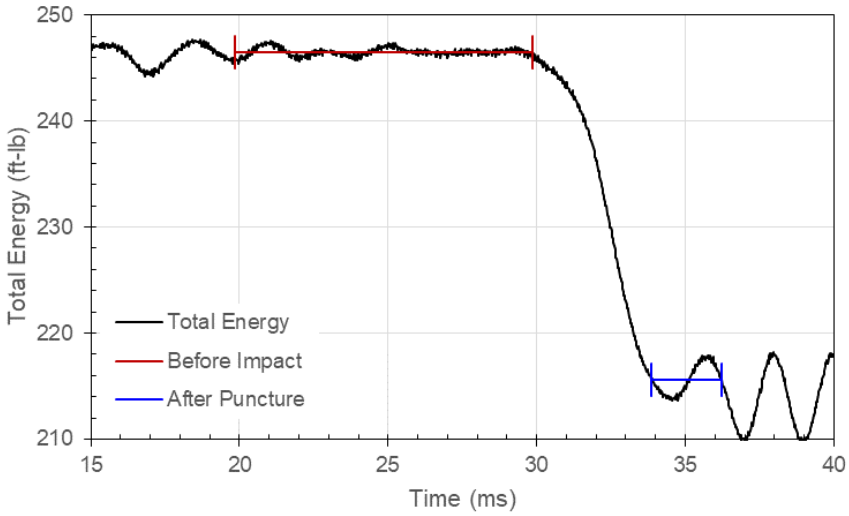

Figure 53: Total Energy in Test 24 with Specimen 17

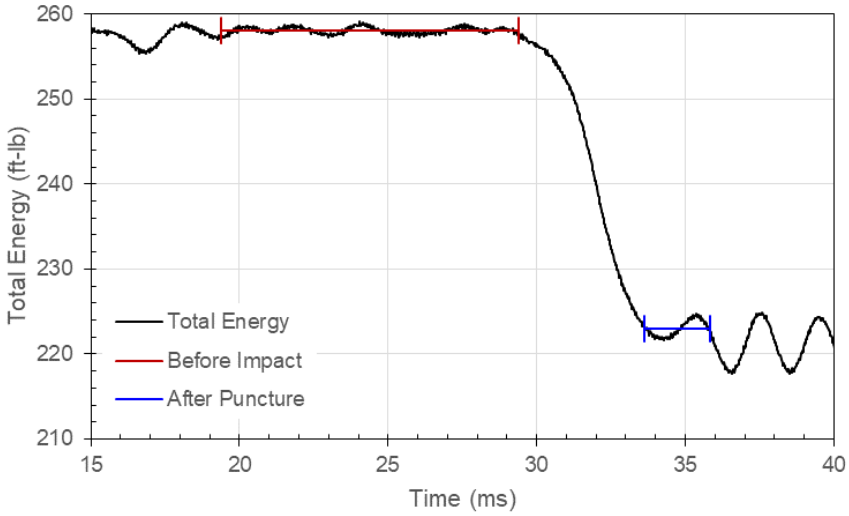

Figure 54: Total Energy in Test 25 with Specimen 18

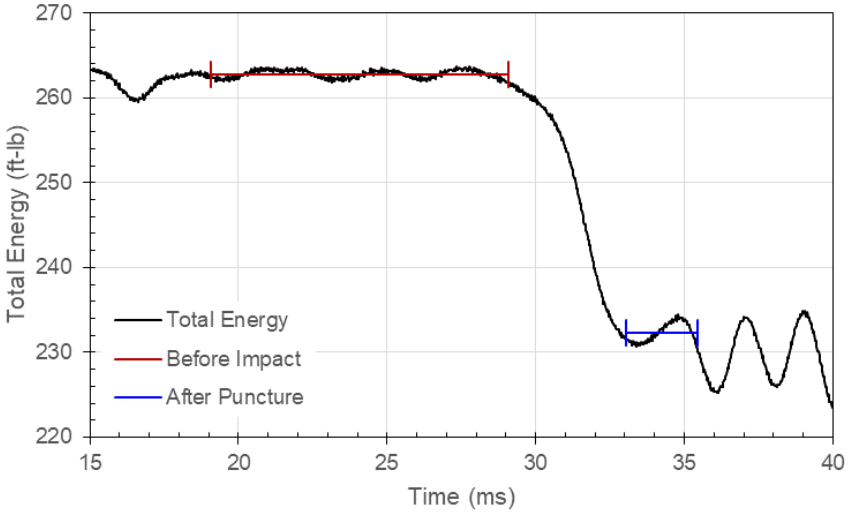

Figure 55: Total Energy in Test 26 with Specimen 19

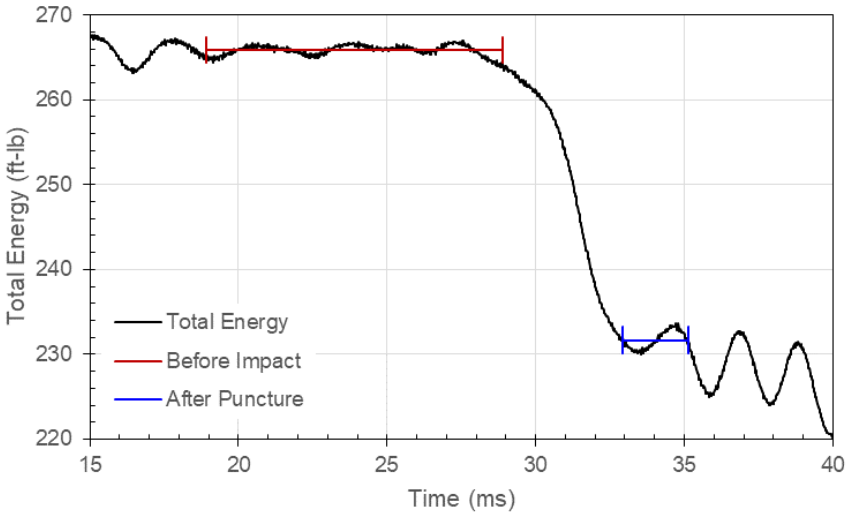

Figure 56: Total Energy in Test 27 with Specimen 20

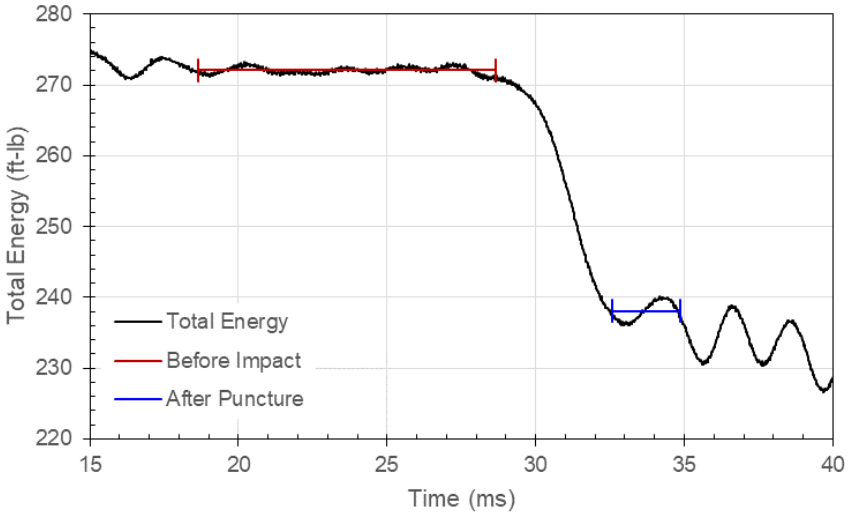

Figure 57: Total Energy in Test 28 with Specimen 21

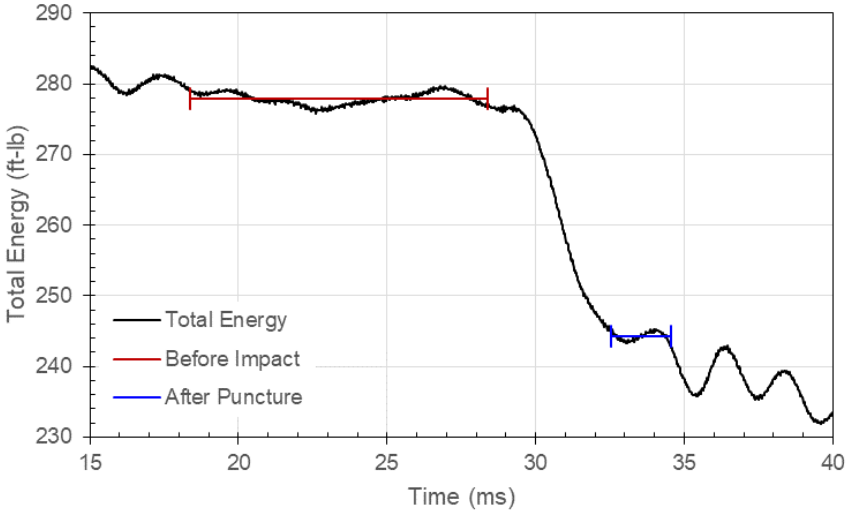

Figure 58: Total Energy in Test 29 with Specimen 22

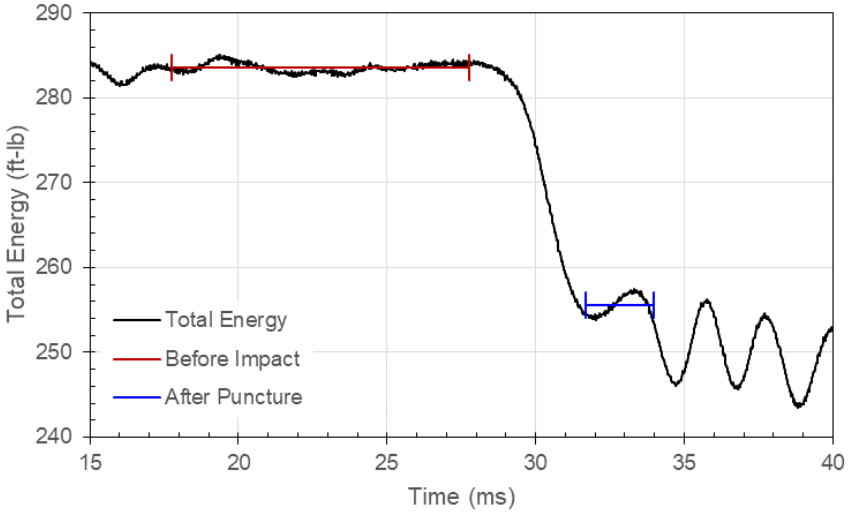

Figure 59: Total Energy in Test 30 with Specimen 23

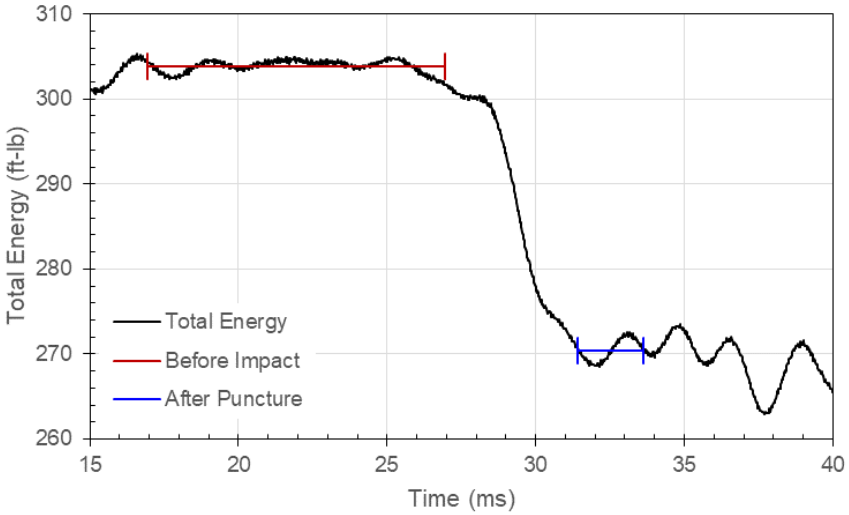

Figure 60: Total Energy in Test 31 with Specimen 24

Appendix C: Velocity

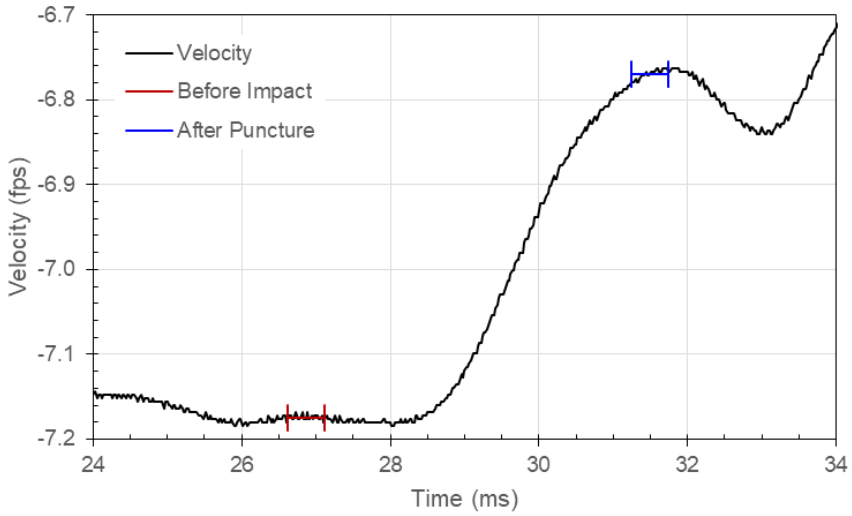

Figure 61: Carriage Velocity in Test 7 with Specimen 1

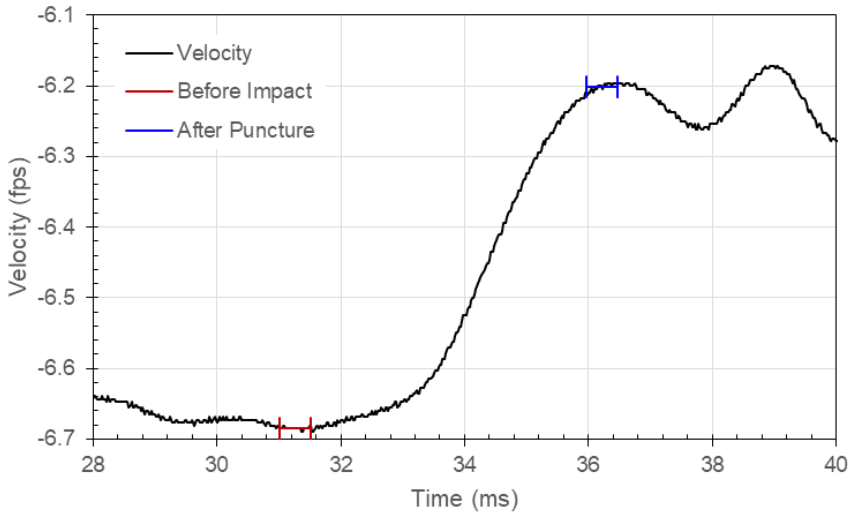

Figure 62: Carriage Velocity in Test 10 with Specimen 2

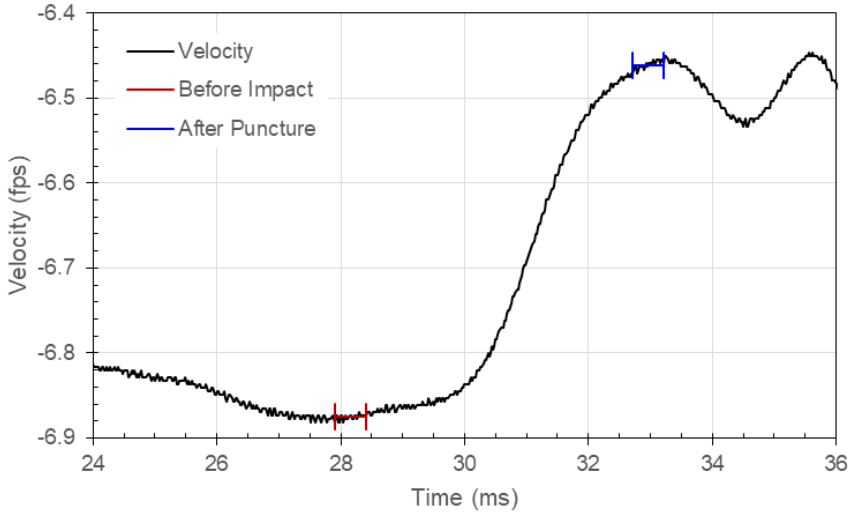

Figure 63: Carriage Velocity in Test 8 with Specimen 3

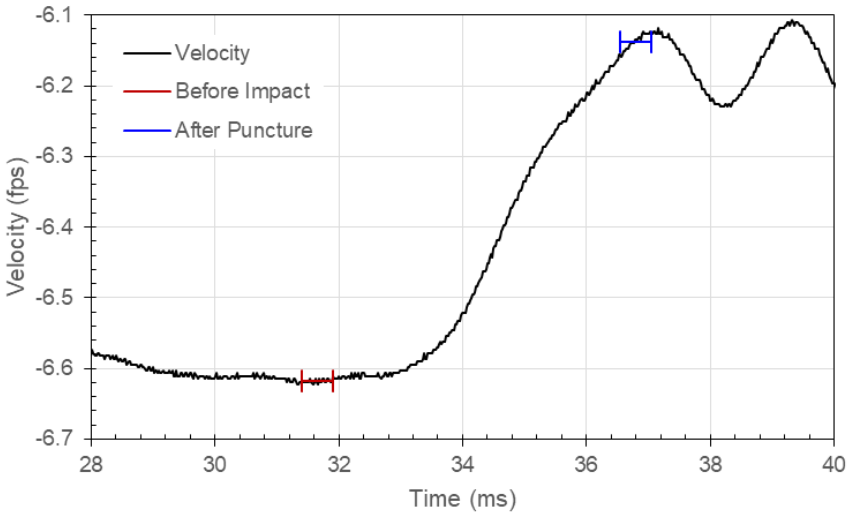

Figure 64: Carriage Velocity in Test 11 with Specimen 4

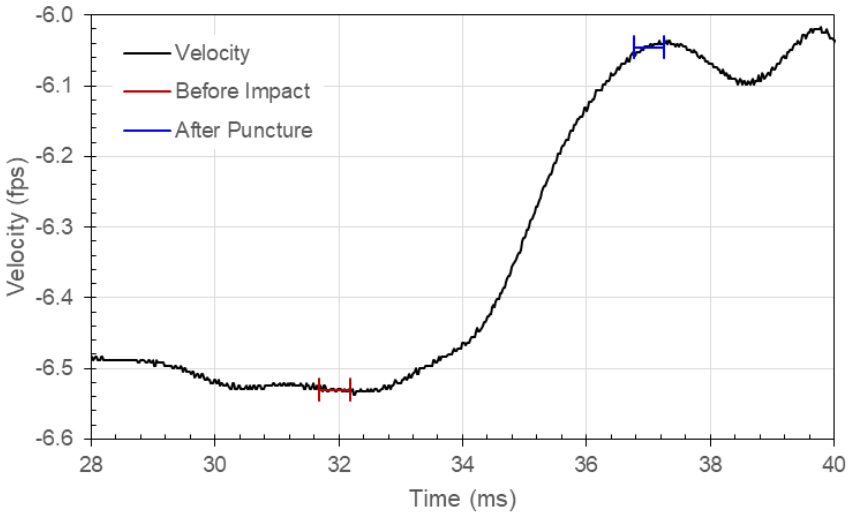

Figure 65: Carriage Velocity in Test 12 with Specimen 5

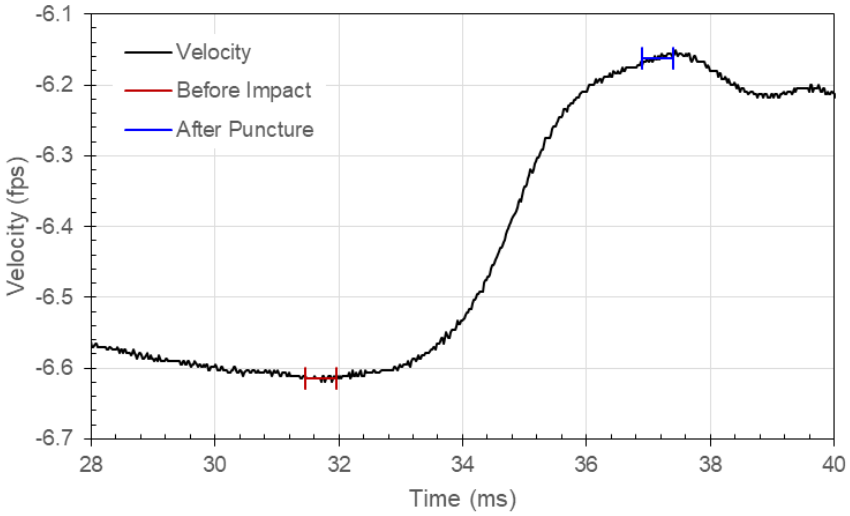

Figure 66: Carriage Velocity in Test 13 with Specimen 6

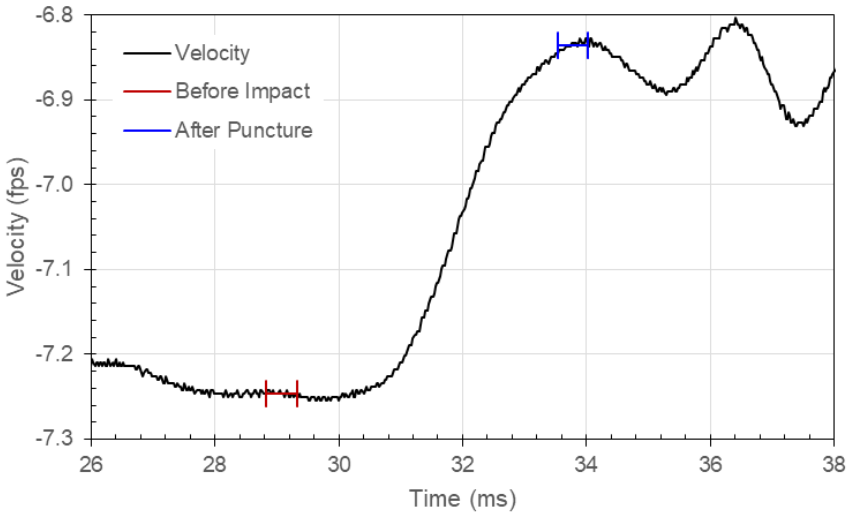

Figure 67: Carriage Velocity in Test 14 with Specimen 7

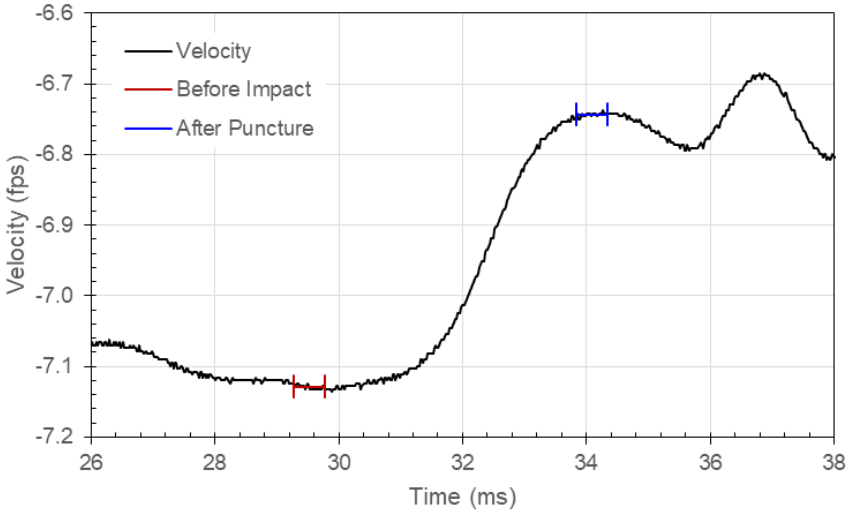

Figure 68: Carriage Velocity in Test 15 with Specimen 8

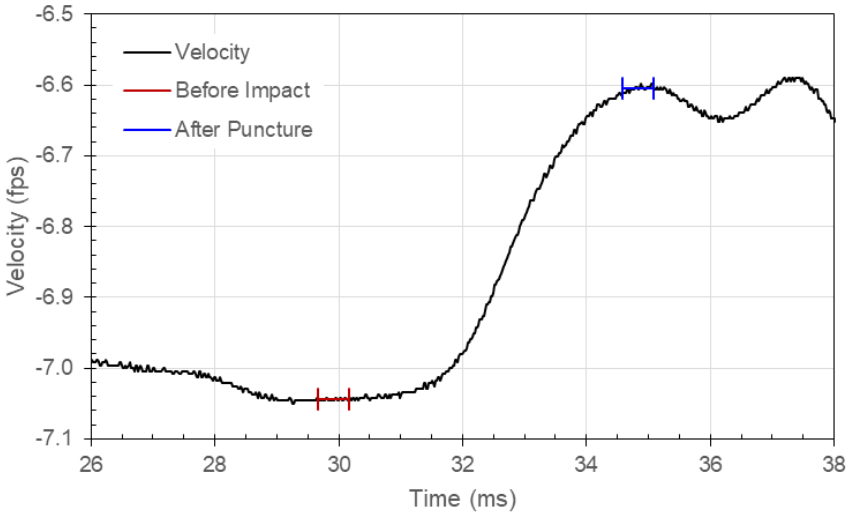

Figure 69: Carriage Velocity in Test 16 with Specimen 9

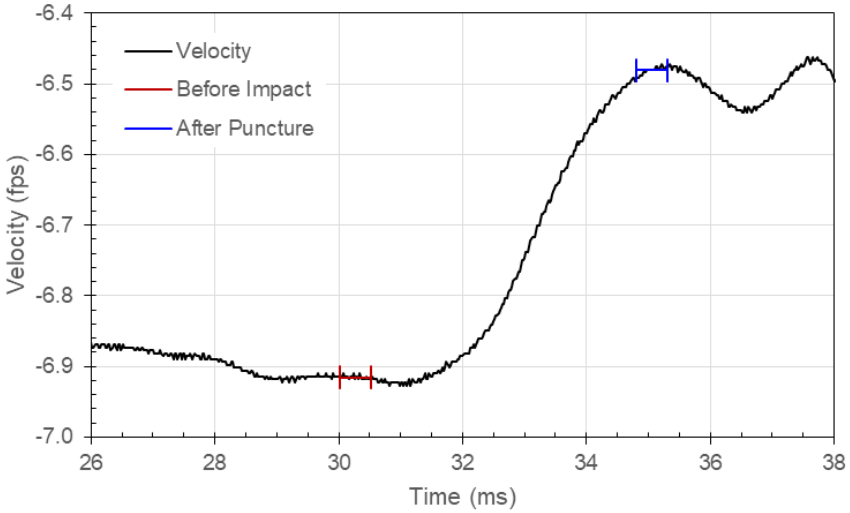

Figure 70: Carriage Velocity in Test 17 with Specimen 10

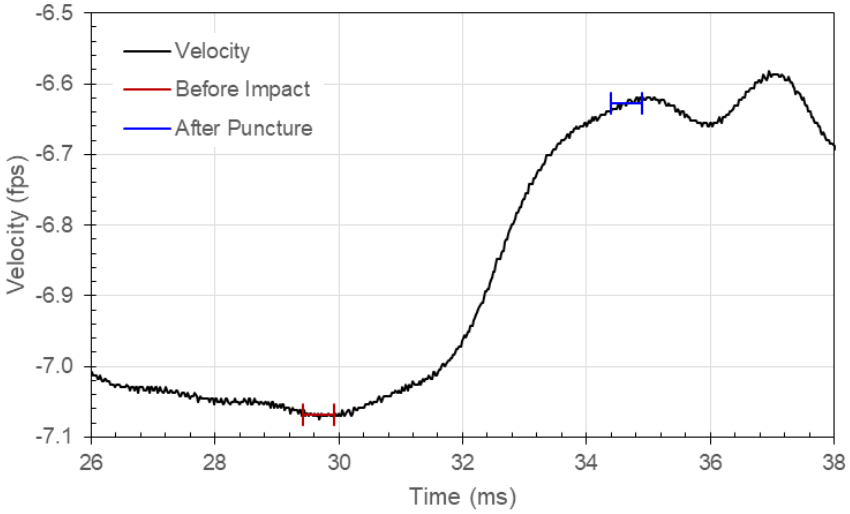

Figure 71: Carriage Velocity in Test 18 with Specimen 11

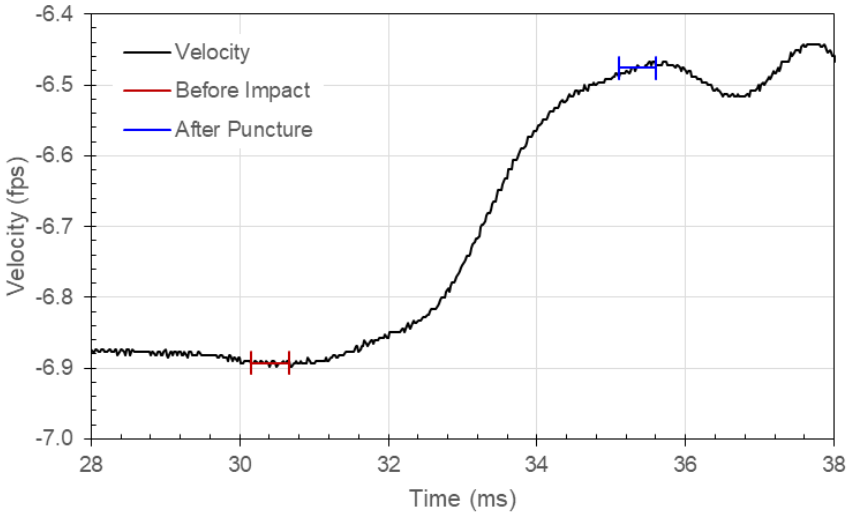

Figure 72: Carriage Velocity in Test 19 with Specimen 12

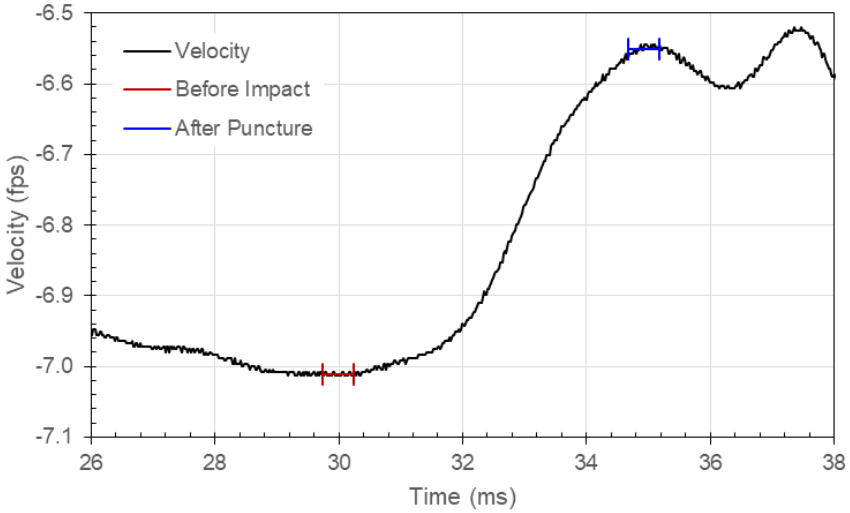

Figure 73: Carriage Velocity in Test 20 with Specimen 13

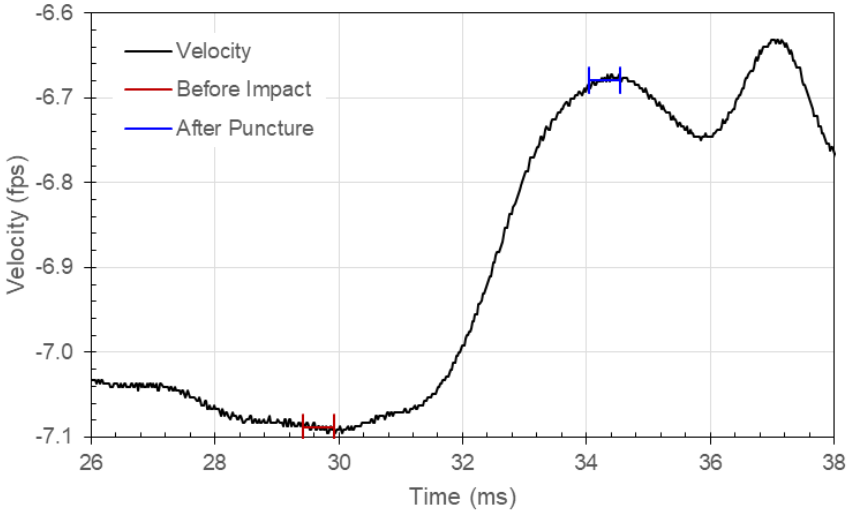

Figure 74: Carriage Velocity in Test 21 with Specimen 14

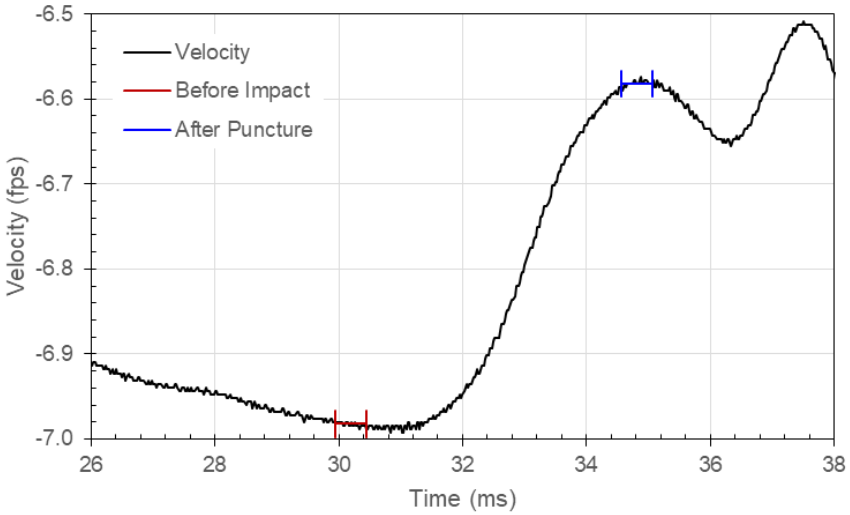

Figure 75: Carriage Velocity in Test 22 with Specimen 15

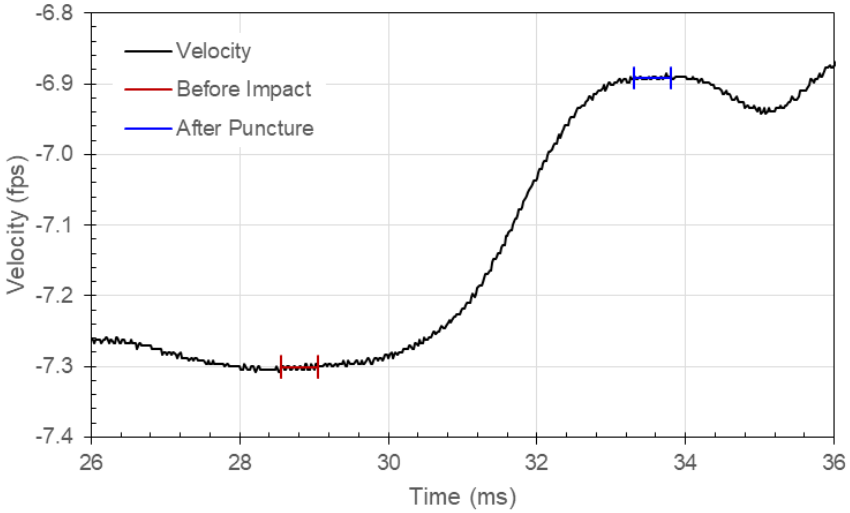

Figure 76: Carriage Velocity in Test 23 with Specimen 16

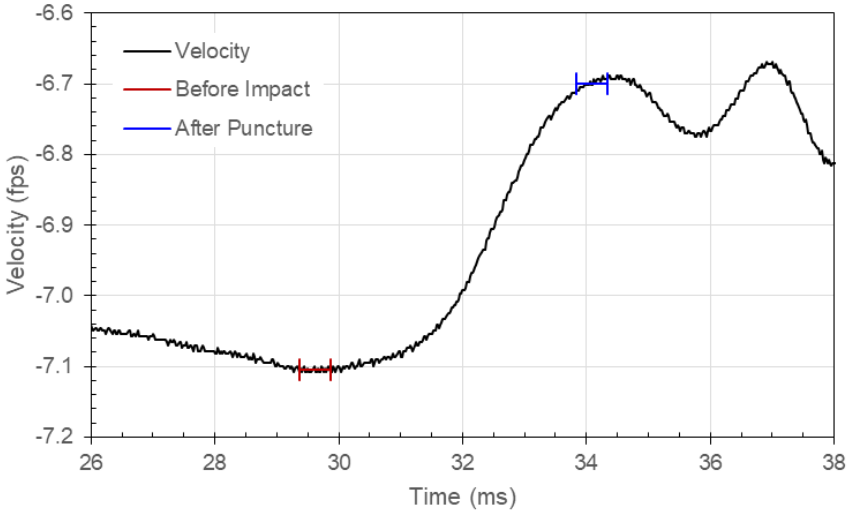

Figure 77: Carriage Velocity in Test 24 with Specimen 17

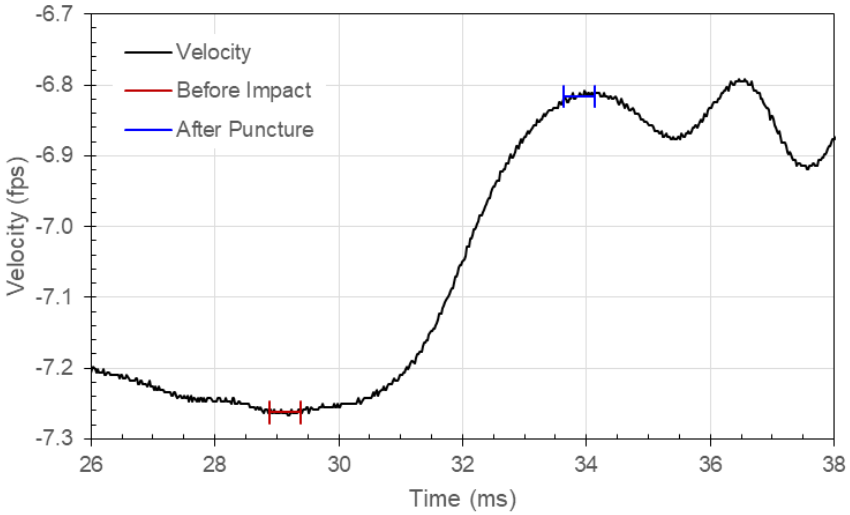

Figure 78: Carriage Velocity in Test 25 with Specimen 18

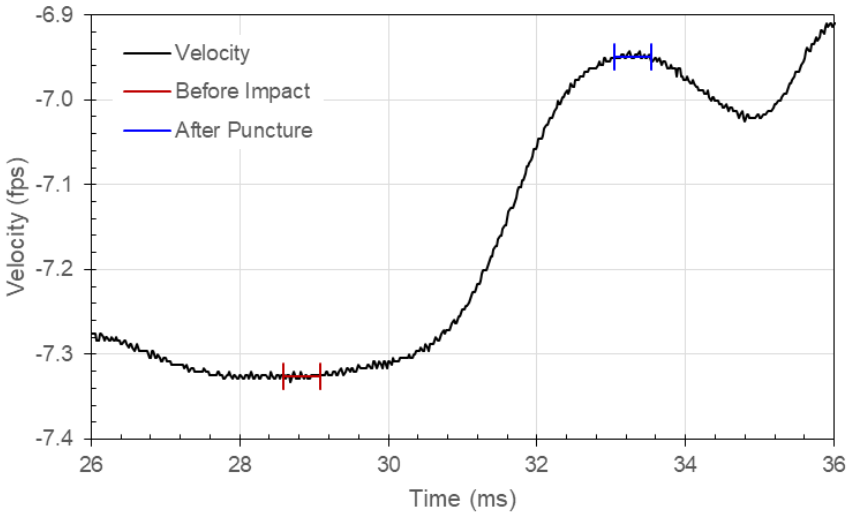

Figure 79: Carriage Velocity in Test 26 with Specimen 19

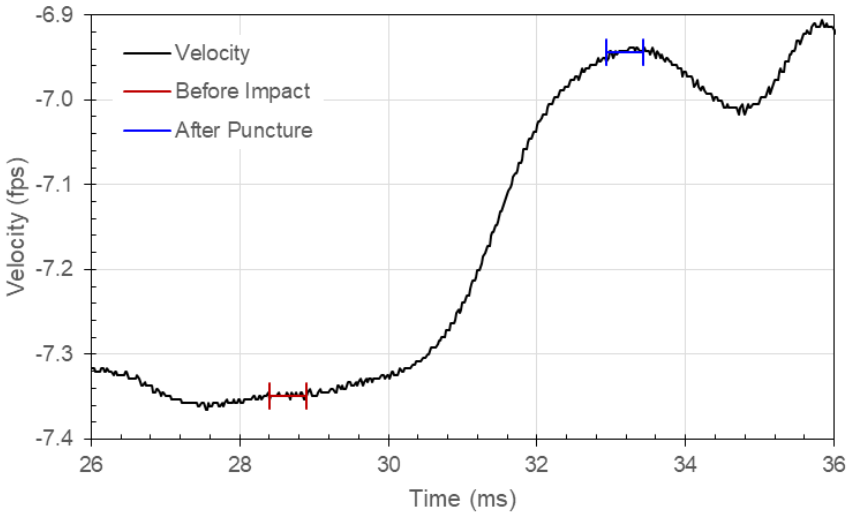

Figure 80: Carriage Velocity in Test 27 with Specimen 20

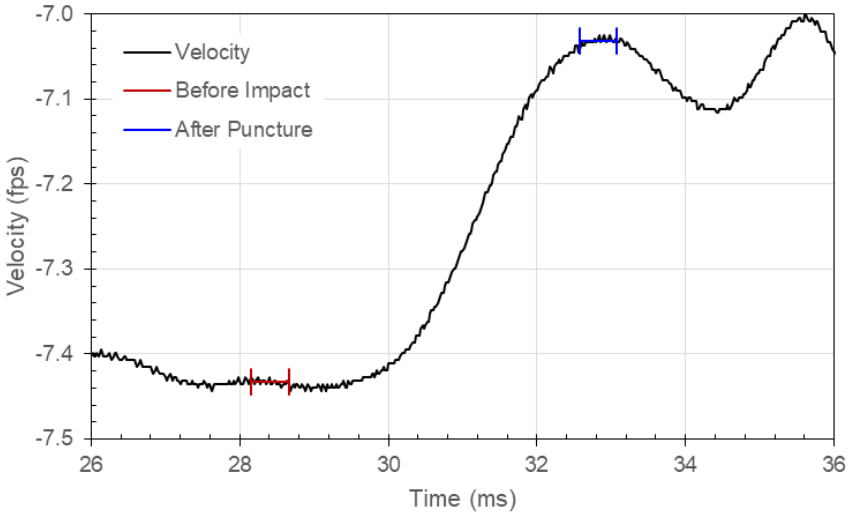

Figure 81: Carriage Velocity in Test 28 with Specimen 21

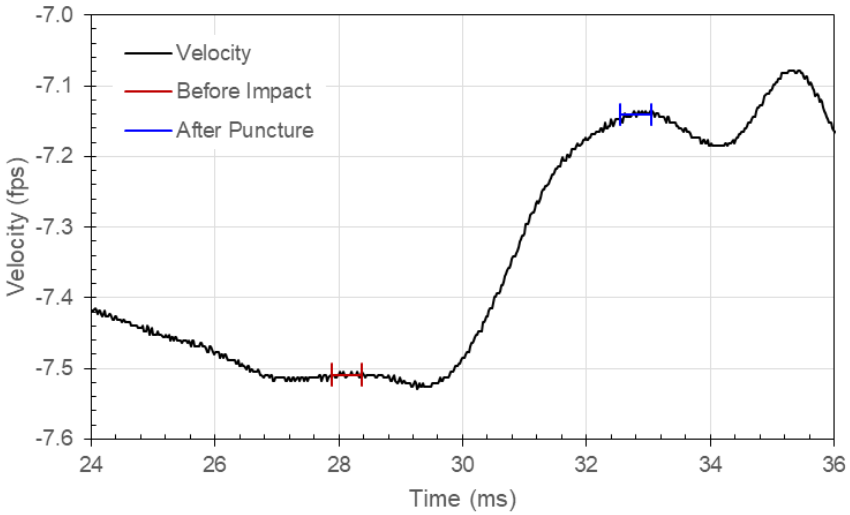

Figure 82: Carriage Velocity in Test 29 with Specimen 22

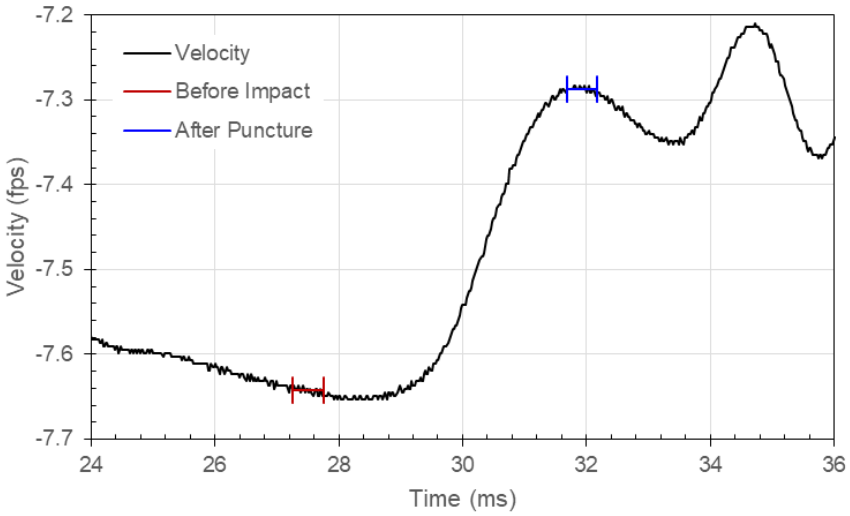

Figure 83: Carriage Velocity in Test 30 with Specimen 23

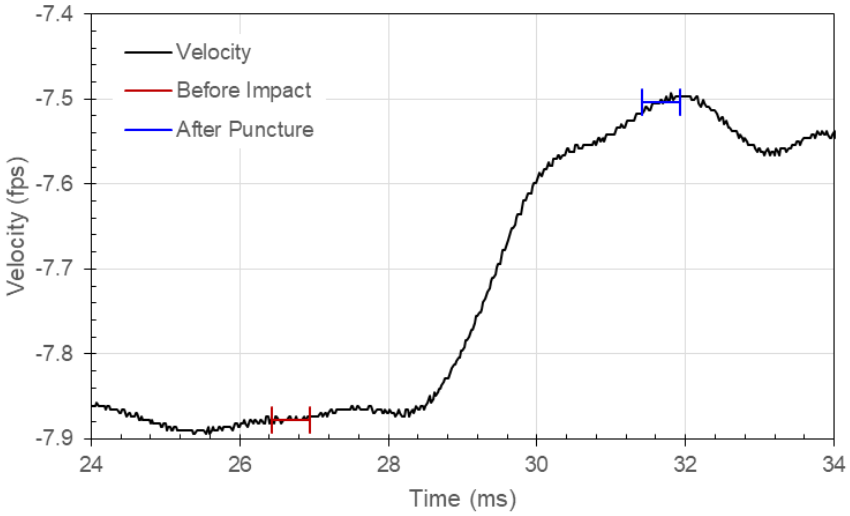

Figure 84: Carriage Velocity in Test 31 with Specimen 24

Sandia National Laboratories is a multimission laboratory managed and operated by National Technology and Engineering Solutions of Sandia, LLC, a wholly owned subsidiary of Honeywell International, Inc., for the U.S. Department of Energy's National Nuclear Security Administration under contract DE-NA0003525.